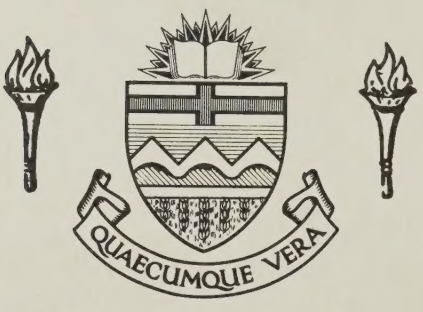

THE UNIVERSITY OF ALBERTA

AN ELECTROSTATIC SOLID COLLOID THRUSTER

A THESIS

SUBMITTED TO THE FACULTY OF GRADUATE STUDIES AND RESEARCH

IN PARTIAL FULFILMENT OF THE REQUIREMENTS FOR THE DEGREE

OF MASTER OF SCIENCE

DEPARTMENT OF ELECTRICAL ENGINEERING

EDMONTON, ALBERTA

SPRING 1972

ABSTRACT

This thesis discusses the concept of electric propulsion. Particular importance is placed on mission analysis and the various schemes for electric propulsion. A brief comparison of chemical, nuclear and electric regimes is included. Finally, the physics of solid colloid propulsion is discussed. Development of time of flight apparatus for the purpose of measuring the various propulsion parameters is described. Suggestions are presented for further necessary work in the field of solid colloid thrusters.

Books, and Dishes have this Common Fate; there was never any One, of Either of them, that pleas'd All Palates. And, in Truth, it is a Thing as little to be Wish'd for, as Expected; For an Universal Applause is at least Two Thirds of a Scandal. So that though I deliver up these Papers to the Press, I invite no Man to the Reading of them: And, whosoever Reads, and Repents, it is his Own Fault. To Conclude, as I made this Composition Principally for my Self, so it agrees exceedingly Well with My Constitution; and yet, if any Man has a Mind to take part with me, he has Free Leave, and Welcome. But, let him Carry this Consideration along with him, that He's a very Unmannerly Guest, that presses upon another Bodies Table, and then Quarrels with his Dinner.

Seneca

Letters from a Stoic

Sir Roger L'Estrange

1673

Penguin Books 1969

ACKNOWLEDGEMENTS

The author acknowledges his supervisors Dr. C.R. James, Dr. F.E. Vermeulen and Dr. F.S. Chute, without whom this thesis would not be what it is. In addition, the author is grateful to the National Research Council for financial assistance. Finally, the author would like to express his thanks to the members of the Phi Upsilon Kappa Society, in particular Dr. Frederick Stein, for encouragement during the course of this study.

TABLE OF CONTENTS

		Page
1.	INTRODUCTION	1
1.1	Statement of the Problem	1
1.2	Historical Development	2
1.3	The Principle of Propulsion	4
1.4	Types of Propulsion	6
1.4.1	Chemical Propulsion	7
1.4.2	Nuclear Propulsion	8
1.4.3	Electric Propulsion	8
1.4.4	Relative Merits of the Propulsive Schemes	9
2.	LOW THRUST PROPULSION	11
2.1	Performance Parameters	11
2.2	Optimization of Specific Impulse and Payload Capability	14
2.3	Types of Electric Propulsion	37
2.3.1	Electrothermal Thrusters	37
2.3.2	Electromagnetic Thrusters	41
2.3.2.1	MPD (Magnetoplasmadynamic) Thruster	42
2.3.2.2	Travelling Wave Thruster	44
2.3.2.3	Plasma Guns	44
2.3.3	Electrostatic Thrusters	45
2.3.3.1	Contact Ionization Thruster	45
2.3.3.2	Electron Bombardment Thruster	48
2.3.3.3	Colloid Thruster	51

2.3.4 Additional Forms of Electric Propulsion 52

3. COLLOID PROPULSION 54

3.1 Contemporary Colloid Thrusters 54

3.2 Liquid Colloid Thrusters 54

3.3 The Physics of Solid Colloid Thrusters 58

3.4 Theoretical Basis for Time of Flight Analysis of Colloid Thruster Parameters 66

4. THE EXPERIMENTAL THRUSTER AND DETECTOR 77

4.1 High Vacuum System 77

4.2 The Thruster 77

4.3 Switching Circuitry 81

4.4 The Detector 83

4.5 Presentation and Discussion of Experimental Results 87

5. SUGGESTIONS FOR FUTURE RESEARCH 97

5.1 The Thruster 97

5.2 Parametric Analysis 98

5.3 Propellant Size and Composition 99

BIBLIOGRAPHY 100

LIST OF TABLES

Table		Page
2.1	Optimized Parameters for Electric Flight	13
2.2	Flyby Electric Propulsion Missions	36

LIST OF ILLUSTRATIONS

Figure		Page
2.1	Payload Ratio versus y	19
2.2	Payload Ratio versus Mission Time	25
2.3	Payload Ratio versus Mission Time	26
2.4	Mission Time versus Interplanetary Distance	28
2.5	Mission Time versus Interplanetary Distance	29
2.6	Normalized Initial Acceleration versus Payload Ratio	31
2.7	Normalized Final Acceleration versus Payload Ratio	32
2.8	Normalized Average Acceleration versus Payload Ratio	33
2.9	Conceptual Model of Electrothermal Thruster	39
2.10	Accelerating Portion of MPD Thruster	43
2.11	Contact Ionization Thruster	46
2.12	Electron Bombardment Thruster	50
3.1	Liquid Colloid Thruster Concept	55
3.2	Contact Potential Charge per Volt versus Particle Radius	61
3.3	Charge-to-Mass Ratio versus Particle Radius	63
3.4	Specific Impulse versus Particle Radius	64
3.5	Particle Detection Scheme	67
3.6	Schematic of the Spatial Distribution of Various Subbeams Over the Distance Between the Accelerator and the Collector at Times $t = 0$ and $t = \Delta t$	68
3.7	Conceptual Sketch of TOF Trace of a Beam Having a Discrete Number of Subbeams	70

4.1	Photograph of Vacuum System	78
4.2	Sketch of Thruster and Components	79
4.3	Photograph of Thruster and Components	80
4.4	Schematic of Switching Circuit	82
4.5	Sketch of Detector	84
4.6	Photograph of Detector	85
4.7	Oscillogram of Time of Flight Trace	88
4.8	Oscillogram of Time of Flight Trace	89
4.9	Oscillogram of Time of Flight Trace	91
4.10	Oscillogram of Time of Flight Trace	92
4.11	Oscillogram of Time of Flight Trace	93
4.12	Oscillogram of Time of Flight Trace	94
4.13	Oscillogram of Time of Flight Trace	95

1. INTRODUCTION

1.1 Statement of the Problem

That method of rocket propulsion whereby electrical energy is transformed into directed kinetic energy of motion shall be termed electrical propulsion in this thesis. The possibility of electrical propulsion and the inherent advantages of the associated high exhaust velocities were recognized early in the century by Goddard [1] and Oberth. [2] It was not until the theoretical and experimental work of the late fifties and early sixties, however, that researchers discovered that the efficiency of the various types of electric engines varied with exhaust velocity. The efficiency of existing experimental electric engines decreases markedly in the exhaust velocity range of 10,000 to 50,000 m/sec. To fill this gap the colloidal thruster has been developed.

The approach taken in this thesis will be to discuss the principles of rocket propulsion and the parameters involved in a propulsion system. Thereafter, the three main types of rocket propulsion, namely chemical, nuclear and electric, will be discussed, followed by a description of the various types of electric propulsion devices. Electrostatic engines, both ion and colloid types, will then be examined. Colloid propulsion will then be discussed thoroughly and its place amongst other types of propulsion stressed with reference to its advantages and disadvantages.

Finally, an experimental electrostatic solid colloid thruster will be described. A theoretical analysis of the time of flight technique employed to obtain the various rocket parameters will be included. A description of the equipment and experimental setup will be followed

by experimental results, discussion of results, conclusions, implications and suggestions for future research.

1.2 Historical Development

A brief account of the history of propulsion is presented here in order that the reader obtain some perspective of how the science of propulsion has progressed over the ages to its present state of sophistication.

Most authorities attribute the invention of the rocket to the Chinese. The first rocket probably took the form of a firecracker and appeared as early as 206 B.C., during the Han Dynasty[3]. The reaction principle of propulsion was employed as early as 100 B.C. by Hero, a Greek resident of Alexandria, in his concept of what was a primitive steam engine. Nonetheless, it was not until 1898, two hundred years after Newton's laws of action and reaction had been formulated, that a Russian school teacher, Konstantin Tsiolkovsky, demonstrated mathematically by means of the rocket equation that a reaction device could enable man to escape from the planet Earth[4]. The two other pioneers of rocket propulsion were Robert H. Goddard who contributed most substantially to experimental and theoretical rocketry, and Hermann Oberth, whose contribution was largely theoretical. These three men may rightfully be termed "The Fathers of Rocketry".

Both Goddard and Oberth mentioned the possibility of electric propulsion. Oberth, in fact, allotted an entire chapter to it in a book in 1929 and recommended the simultaneous expulsion of positive and negative particles in order to maintain charge neutrallity[5]. Two world wars watched rocketry progress and become incorporated into the

military. Post World War II years brought a surge of interest in rocketry. In 1947 Seifert et al published a series of three articles on the physics of rockets[6]. In the fifties a large amount of theoretical work was done on electrical propulsion, low thrust dynamics and trajectories. The late fifties witnessed the beginning of many experimental electric propulsion projects. The first space test of an electric engine, SERT I (SPACE ELECTRIC ROCKET TEST), was not carried out until 1964[7]. On this occasion a mercury electron bombardment thruster on a ballistic trajectory operated for over thirty-one minutes, thereby qualifying as the first successful electric space thruster of any kind. Since that time other experiments have been successful[8], [9]. On February 3, 1970 a significant step forward was taken in the field of electric propulsion with the launching of SERT II. The thruster (a 15 cm. diameter mercury electron bombardment ion thruster) operated successfully for six months without failure. This experiment represents the transformation of the electric propulsion concept from the laboratory experimental stage to candidature for deep space missions[10]-[12].

It should be emphasized that more theoretical and experimental knowledge and more accumulated ground test time are available on electric thrusters today than were available for any one of the chemical rocket engines at the time it was first decided to use that type of engine for the first time on a flight project. There are two principal reasons for this long delay. The first is that it is only recently that sufficiently light, efficient and reliable power supplies, as are required for electric propulsion systems, have become available in the form of solar electric supplies[13]-[15]. The second reason for the

delay is that electric thrusters are limited to applications which involve long propulsion periods such as altitude control, station keeping, orbit correction of satellites and planetary and interplanetary probes with large payloads. As such systems are to be used over extended periods of time, reliability tests of such components as thrusters of course require a large amount of time. Now that the space program is in its second decade, emphasis on precision control of satellites and planetary spacecraft should provide many opportunities for electric thrusters.

During the last two decades much serious thought and theoretical analysis has been devoted to nuclear propulsion. The mechanism of propulsion of the nuclear rocket is similar to that of the chemical rocket; that is, expansion of hot gases through a supersonic nozzle. The hot gases expelled are heated by nuclear fission energy and their exhaust velocity is limited by the refractory properties of the exhaust nozzle, a much more severe constraint than that set by the energy per gram released by the nuclear reaction.

Rockets of the near future will, in all likelihood, be a hybrid nuclear-electric type. This type of vehicle will make use of the advantages of the nuclear and the electric rocket. The reliable energy supplied by the nuclear rocket will be converted to electric energy and the fuel will be accelerated electrically, resulting in a long range vehicle capable of large exhaust velocities.

1.3 The Principle of Propulsion

The fundamental principle of propulsion may be considered to be expressed in Sir Isaac Newton's third law of motion; namely that

to every action there is an equal and opposite reaction. By expelling mass from a body in one direction and thereby effecting a change in momentum, an equal but opposite change in momentum is imparted to the body and it is accelerated in the opposite direction.

Consider a rocket of mass M executing rectilinear motion at velocity u. As the rocket progresses, fuel is ejected in the backward direction at constant velocity u_{ex} relative to the rocket. Should an external force F, along the line of motion, be exerted upon the vehicle for a short time dt, during which a fuel mass $\dot{M}dt$ (where $\dot{M}$ is the total mass flow rate and is assumed constant) is ejected, the corresponding change in momentum will be given by Fdt. The rocket will experience a corresponding change in velocity du so that the equation of motion becomes

$$Fdt = (M - \dot{M}dt)(u + du) + \dot{M}dt\ (u - u_{ex}) - Mu \qquad (1.1)$$

Neglecting second order terms and rearranging

$$F + u_{ex}\dot{M} = M\ du/dt \qquad (1.2)$$

This is the rocket equation. Throughout the remainder of this thesis it shall be assumed that no external forces are present; that is, the rocket is travelling in gravity-free space. As stated above u_{ex} and $\dot{M}$ are constant and consequently all missions analyzed will be those of constant thrust. For convenience equation (1.2) may now be rewritten as

$$\begin{aligned} u_{ex}\dot{M} &= M\ du/dt \\ &= T \end{aligned} \qquad (1.3)$$

The term $u_{ex}\dot{M}$ is referred to as the thrust T and is equal to the mass times the acceleration of the vehicle. Since the mass flow rate is constant and equal to $\dot{M}$

$$M(t) = M_o - \dot{M}t \tag{1.4}$$

where $M(t)$ is the instantaneous rocket mass and $M_o = M(o)$. Employing equation (1.4) the rocket equation may be integrated once and cast in one of the two forms:

$$\Delta u = u_{ex} \ln\left[M_o/M(t)\right] \tag{1.5}$$

or

$$M(t) = M_o\, e^{-\Delta u/u_{ex}} \tag{1.6}$$

where Δu is the change in velocity of the vehicle over the time interval t. Equation (1.5) demonstrates the limitations placed upon the final rocket velocity by the ratio of initial to final mass and the exhaust velocity. In order to attain a significant velocity increment a large value of exhaust velocity is necessary. Obviously a large value of exhaust velocity is not sufficient. A large ratio of initial to final mass must accompany it. For example, a ratio of $M_o/M(t) = e$ (e is the base of the Naperian logarithms) would be required if the velocity increment at time t were to equal the exhaust velocity of the propellant. In this case 63% of the rocket would have to be fuel. Equation (1.6) reveals, as expected, that the mass of the rocket decreases with time.

1.4 Types of Propulsion

To the present date prime rocket propulsion has always been accomplished by chemical means. However, in the next few decades it is not unreasonable to anticipate the introduction of nuclear and electric thrusters as prime propulsion devices. For the sake of completeness a brief description of each type of device and the energy conversion process it employs is presented.

1.4.1 Chemical Propulsion

When one speaks of rocket propulsion today, one normally thinks of the conventional chemical propulsion system. Chemical propulsion is characterized by high thrust and low exhaust velocity and is considered to be the simplest of the three basic types of propulsion systems. The two necessary ingredients for a chemical propulsion system are the fuel and the reactant (frequently referred to as the oxidant). During the chemical reaction that takes place, heat is released and propellant is produced. The thermal energy is then converted to directed kinetic energy by expansion of the propellant through a convergent-divergent supersonic nozzle. The reaction energy requirement depends upon the heat of formation of the reactants and their products and thus upon their bond energies[16].

The principal shortcoming of this type of propulsion is the low exhaust velocity and consequent exorbitant mass flow rate necessary to produce thrusts capable of lifting a rocket from the surface of the earth. Unfortunately the problem of low exhaust velocity of a chemical rocket is fundamental. The two factors limiting the exhaust velocity of the fuel are

i) the low energy content of the fuel, and

ii) the thermal resistance of the combustion chamber and nozzle materials.

It has been found that the low energy content of the fuel (for example 2 kcal/gm burning hydrogen and oxygen[17]) is much more severe than the thermal resistance constraint. Current nozzle materials cannot withstand temperatures in excess of 4000°C[18]. These two constraints

set the maximum exhaust velocity of chemical propellants to less than 5 km/sec. In many cases one seeks a form of propulsion in which the exhaust velocity is greater and hence the fuel expenditure less. An excellent discussion of the physics of chemical rockets can be found in reference (19).

1.4.2 Nuclear Propulsion

Like chemical propulsion, nuclear propulsion is capable of producing thrusts greater than the earth weight of the vehicle to be propelled. Conversion of nuclear energy into thrust may be accomplished either indirectly by heat transfer to the propellant or directly by using the nuclear fuel as either the propellant itself or as part of the propellant mixture.

The most frequently discussed nuclear rocket is the nuclear fission, heat transfer rocket. The energy per unit mass released in a nuclear reaction is many orders of magnitude greater than that released in a chemical reaction and the inability of nozzle and chamber materials (in the case of the heat exchange type nuclear engines) to withstand the resulting high temperatures places an upper limit on the exhaust velocity. In the case of solid core rockets this limit is about 9 km/sec while in the case of gaseous core rockets about 25 km/sec. (20)-(23).

1.4.3 Electric Propulsion

The task of an "electric rocket engine" is to convert electrical energy into directed kinetic energy of the propellant beam. The

energy conversion is effected through the interaction of the electrically charged constituents of the beam with an electric and/or magnetic field.

If the nature of the energy transfer from applied field to propellant is considered, it can be shown that for some types of thrusters extremely large exhaust velocities are possible. In fact, it is quite within reason to conceive of an electric thruster capable of an exhaust velocity of 100 km/sec. Since very large exhaust velocities are possible, correspondingly smaller quantity of fuel will be necessary. Of course, it is well to observe that an electric thruster requires a separate electrical power supply as will be mentioned in the following section. As will be discussed in Chapter 2, many different types of "electric engines" have been developed, all of which must eject electrically neutral beams.

1.4.4 Relative Merits of the Propulsive Schemes

One of the most conspicuous differences between the three propulsive methods is the operable range of exhaust velocity. Chemical rockets are restricted to exhaust velocities below 5 km/sec, nuclear rockets to below 25 km/sec, while electric rockets may possess exhaust velocities greater than either. For this reason, chemical and nuclear vehicles have been termed exhaust velocity limited. While chemical and nuclear systems are capable of thrust to earth weight ratios in excess of one, electric systems will be hard pressed to achieve this value. As will be shown in the following chapter, a maximum thrust to weight ratio of 10^{-3} is representative of an electric propulsion device at this time. It will be shown in Chapter 2 that electric pro-

pulsion offers significant reduction in trip time for distant interplanetary journeys as well as a substantial increase in payload capability when compared to chemical and nuclear systems.

It would be an oversight to assume electric propulsion superior on all accounts. Since the thrust to weight ratio is typically of the order of 10^{-3}, at present electric propulsion devices are incapable of unassisted liftoff from the surface of the earth and are therefore restricted to launchings from earth orbit. While it is clear that an electric rocket must carry its own power supply, it is also clear that since all rockets require electrical power of some sort, the disadvantage of a need for a separate power supply is not as serious as might be imagined.

Finally, electric propulsion will certainly prove its versatility in precise rocket trajectory control and in precision control of satellites for purposes of attitude control and station-keeping[24]-[28].

2. LOW THRUST PROPULSION

2.1 Performance Parameters

In order to discuss low thrust propulsion in a meaningful fashion, it is first necessary to put forth a set of parameters which will characterize the system. The set of parameters was selected on the basis of conciseness (i.e. use of a minimum number of parameters) and the large degree of physical insight afforded. The method of analysis was chosen because it is exact (ie, no approximations are used).

With the above in mind, consider the total initial mass of the rocket, M_o, to be made up of three components: the mass of the power supply and power conversion equipment M_p, the mass of the propellant or fuel M_f, and the mass of the payload plus structure M_l. Structure refers to the non-productive portion of the terminal mass and includes such items as empty fuel tanks and true structural members of the spacecraft. The equation relating these components is

$$M_o = M_l + M_p + M_f \tag{2.1}$$

Furthermore since $\dot{M}$ is assumed constant the instantaneous mass is given by $M(t) = M_o - \dot{M}t$ (2.2)

Three important relations linking beam power and electric power to other parameters are next in order. The assumption is made that the mass of the power supply is directly proportional to the electric power output P_e. Thus

$$M_p = \alpha P_e \tag{2.3}$$

where α is the specific mass of the power supply. The beam power, P, may be obtained by considering the energy change in the rocket-propellant

system in the time interval dt. Applying conservation of energy yields

$$\tfrac{1}{2}(M - \dot{M}dt)(u + du)^2 + \tfrac{1}{2}\dot{M}dt\,(u - u_{ex})^2 - \tfrac{1}{2}Mu^2 = Pdt \qquad (2.4)$$

Neglecting second order terms $\tfrac{1}{2}\dot{M}u_{ex}^2 = P$ (2.5)

Finally, the beam power is related to the electrical power by an efficiency factor η such that $P = \eta P_e$

$$= \frac{\eta}{\alpha} M_p \qquad (2.6)$$

Employing equations (1.3) and (2.5) the power to thrust ratio is given by $P/T = u_{ex}/2$ (2.7)

It is clear from equation (2.7) that once the power level and exhaust velocity are fixed, the thrust is determined regardless of the propellant used or the method of acceleration. For fixed power, provided there are no restrictions on $\dot{M}$ and u_{ex} other than those implied by equation (2.5), there is no fundamental limitation on the magnitude of the thrust that can be produced. Although electric thrusters are often conceived of as low thrust devices, it is obvious that by increasing $\dot{M}$ and decreasing u_{ex}, while maintaining constant beam power, the thrust may be made arbitrarily large. Vehicle acceleration, however, will be limited to the order of 10^{-3}g or less (g is the acceleration of gravity at the Earth's surface). The maximum possible acceleration for an electric rocket occurs when no payload is carried and the fuel supply is just depleted. Then, neglecting structure, the maximum acceleration of the vehicle is

$$a_{max} \doteq \frac{2P}{u_{ex}M_p}$$

$$= \frac{2\eta}{\alpha u_{ex}} \qquad (2.8)$$

For some time to come even the most advanced power generating systems will have specific masses in the range $1 < \alpha < 100$ kg/kw[29],[30]. Choosing $\alpha = 20$ kg/kw, $u_{ex} = 50$ km/sec and $\eta = 0.80$ results in $a_{max} = 1.6 \times 10^{-4}$g.

It is also interesting to examine the thrust-to-weight ratio of the vehicle. It is simply

$$\frac{T}{W} = \frac{Ma}{Mg}$$

$$= \frac{a}{g}$$

A ratio of $\frac{a}{g} = 10^{-4}$ is characteristic of an electric vehicle. In the terms of rocket analysts a low thrust-to-weight ratio device is referred to as a low thrust device. It is not practical to achieve high acceleration by using very small exhaust velocities because, as will be seen in the following section, this usually implies small payload capabilities. Until some dramatic improvement in power system design occurs, electric rockets will be unable to take off unassisted from the surface of the earth. Their usefulness begins only after they have been placed in earth orbit by a chemical booster. Once in orbit, even very small thrusts can influence the spacecraft. For example, an acceleration as small as $10^{-4}g$ can cause a space vehicle to spiral slowly away from earth reaching escape velocity in approximately ninety days[31].

The rocket velocity as a function of time may be expressed by combining equations (1.5) and (2.2) to yield

$$u - u_o = u_{ex} \ln \left[\frac{M_o}{M_o - \dot{M}t} \right] \qquad (2.10)$$

for $t \leq \tau$, where u_o is the initial velocity of the vehicle and τ is the thrust duration or the time at which all propellant has been consumed. At $t = \tau$, u reaches its maximum value and the total change in rocket velocity is

$$\Delta u = u_{ex} \ln \left[\frac{M_o}{M_1 + M_p} \right] \qquad (2.11)$$

Finally, equation (2.10) may be integrated to give the position of the rocket for t with the result

$$X - u_o t = u_{ex}\left[t + \left(t - \frac{M_o}{\dot{M}}\right)\ln\left(\frac{M_o}{M_o - \dot{M}t}\right)\right] \qquad (2.12)$$

Exhaust velocity is often considered to be a measure of fuel economy since, for a constant thrust, if the exhaust velocity is increased the mass flow rate and hence fuel consumption will be decreased by the same factor. A frequent measure of exhaust velocity and hence fuel economy is specific impulse I_{sp}. It is defined as the ratio of total impulse to earth weight of fuel. For a thrust duration of seconds

$$I_{sp} = \frac{T}{\dot{M}_f g}$$

$$= \frac{u_{ex}}{g} \qquad (2.13)$$

Upon examination one can see that specific impulse may be interpreted as the time in seconds for which a propellant mass of 1/9.8 kilograms can maintain a constant thrust of one newton. Thus specific impulse may be regarded as a "miles per gallon" figure for a rocket and in fact its reciprocal is often referred to as specific propellant consumption. As may be inferred from Chapter 1, chemical rockets are restricted to specific impulses of less than 500 seconds and nuclear rockets to less than 2500 seconds while electric rockets are capable of providing specific impulses well in excess of 10,000 seconds and are consequently very attractive from a fuel economy point of view.

2.2 Optimization of Specific Impulse and Payload Capability

Mission analysis of the low thrust, separately powered rocket proceeds in a manner rather different from that of the conventional

chemical rocket. The chemical rocket operates at high thrust for a duration of time much, much smaller than the total journey time and coasts to its destination for the remainder of the time. An electric rocket, on the other hand, operates at low thrust for perhaps the entire mission time. The objective of mission analysis is to maximize the payload capability subject to existing constraints. Typical constraints are the time permitted for the mission, the specific mass, the distance to be travelled and the overall change in rocket velocity. Such limitations are usually dependent upon the reliability, lifetime, or availability of various components and subsystems of the space vechicle.

In practice many types of missions are possible. Two simple types are orbital transfer of earth satellites and interplanetary flyby. Mission analysis involves the manipulation of a large number parameters, for example $\Delta u, \tau, P, \alpha, \eta, u_{ex}$ and the distance travelled X. Consequently some must be selected quite arbitrarily. The choice usually affects the ratio of payload mass to total initial mass. In principle this payload ratio may approach unity. However, accompanying this benefit is the penalty of zero velocity increment or infinite mission time.

If $\Delta u, \alpha, \eta$ and τ are suitably specified, as would be the case in an orbital transfer mission, the payload ratio is a maximum for some value of exhaust velocity. Thus an arbitrarily high specific impulse is not necessarily a desirable aim for an electrically propelled vechicle. The remainder of this section shall be devoted to the optimization of such missions. As well it will be shown that the procedures can be extended to provide a useful description of interplanetary missions in which X, α, η, and τ may be fixed.

Consider the payload fraction $\frac{M_1}{M_o} = 1 - \frac{M_p}{M_o} - \frac{M_f}{M_o}$ (2.14)

From equations (2.5), (2.6), (2.11) and (2.13) and since $M_f = \dot{M}\tau$

$$\frac{M_f}{M_o} = 1 - e^{-\Delta u/u_{ex}} \tag{2.15}$$

and $$\frac{M_p}{M_o} = \frac{M_f}{M_o}\frac{u_{ex}^2}{u_c^2} \tag{2.16}$$

where $$u_c^2 = \frac{2\eta\tau}{\alpha} \tag{2.17}$$

u_c is referred to as the "characteristic velocity" for the mission. Combining equations (2.14), (2.15) and (2.16), the payload ratio may be expressed as a function of the two ratios u_{ex}/u_c and $\Delta u/u_c$

$$\frac{M_1}{M_o} = e^{-\Delta u/u_{ex}} - \frac{u_{ex}^2}{u_c^2}\left(1 - e^{-\Delta u/u_{ex}}\right) \tag{2.18}$$

Equation (2.18) demonstrates that for a specified value of $\Delta u/u_c$, a maximum payload ratio exists for some particular value of u_{ex}/u_c.

Although equation (2.18) appears indeed formidable, it is possible to determine the equation which is the locus of maxima of payload ratio as a function of u_{ex}/u_c while $\Delta u/u_c$ is a running parameter. For convenience define

$$\frac{u_{ex}}{u_c} = y \tag{2.19}$$

and $$\frac{\Delta u}{u_c} = z \tag{2.20}$$

Equation (2.18) now becomes

$$\frac{M_1}{M_o} = e^{-z/y} - y^2\left(1 - e^{-z/y}\right) \tag{2.21}$$

In order to maximize the payload ratio with respect to y it is necessary that

$$\frac{\partial \frac{M_1}{M_o}}{\partial y} = 0 \tag{2.22}$$

Accordingly $z(1 + \frac{1}{y^2})e^{-z/y} - 2y(1 - e^{-z/y}) = 0$

or $$(1 - e^{-z/y}) = \frac{z}{2y}(1 + \frac{1}{y^2})e^{-z/y} \qquad (2.23)$$

For a given z_o, a corresponding y_o can be found by solving equation (2.23). If this pair, (y_o, z_o) is substituted in equation (2.21), the result is the equation of the locus of maxima of $\frac{M_1}{M_o}$. The results are displayed in Table 2.1.

The existence of an optimum payload ratio reflects a compromise between the mass of the power supply and that of the propellant. Examination of equations (2.15) and (2.16) reveals that below the optimum exhaust velocity the required fuel mass becomes excessively high while above the optimum exhaust velocity the power plant mass increases.

Further physical insight into the interrelationship between the various parameters may be gained through investigation of equation (2.23). By multiplying through by $e^{z/y}$, expanding $e^{z/y}$ and solving for u_{ex}, one finds that if the series is truncated after the term z/y, the result is

$$u_{exopt} = u_c \qquad (2.24)$$

and if the series is truncated after the term $\frac{1}{6}(\frac{z}{y})^3$, the result is

$$u_{exopt} \doteq u_c \left[1 - \frac{1}{2}\frac{\Delta u}{u_c} - \frac{1}{24}\left(\frac{\Delta u}{u_c}\right)^2\right] \qquad (2.25)$$

This result is accurate to within 3% for $\frac{\Delta u}{u_{ex}} < 1$ which in turn implies $\frac{M_1}{M_o}_{opt} > 0.1$ as indicated in Table 2.1. It is interesting to note that for optimized missions where $z \ll 1$ equations (2.16) and (2.25) demonstrate that the mass of the power supply is approximately equal to the mass of the fuel.

In Fig. 2.1 payload ratio as expressed by equation (2.21) is plotted against y for several values of z. Included is the locus of maxima. Observe that as z increases, the payload fraction rapidly decreases

TABLE 2.1

OPTIMIZED PARAMETERS FOR ELECTRIC FLIGHT

y_o	z_o	$\frac{M_1}{M_{o\ opt}}$	$\frac{M_f}{M_o}$	$\frac{M_p}{M_o}$	K_1
.50	.81	0	.80	.20	.59
.55	.76	.03	.75	.22	.53
.60	.70	.07	.69	.24	.47
.65	.63	.12	.62	.26	.41
.70	.56	.19	.55	.26	.35
.75	.52	.23	.50	.27	.31
.80	.38	.38	.38	.24	.22
.85	.29	.50	.29	.21	.16
.90	.18	.66	.18	.16	.10
.95	.07	.86	.07	.07	.06
1.00	0	1.00	0	0	0

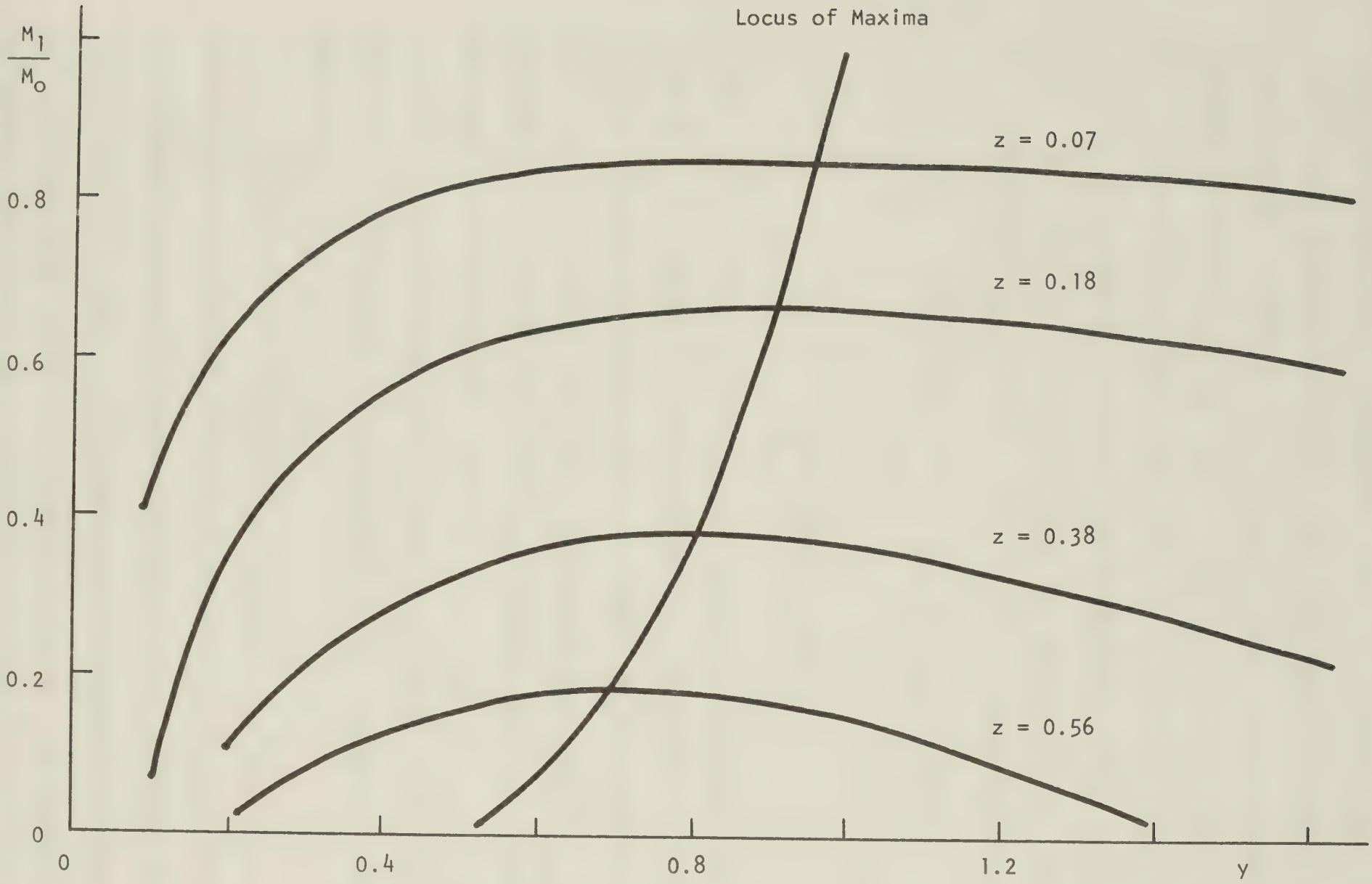

Fig. 2.1 Payload Ratio versus y

along the optimum curve. Increasing values of z represent more difficult missions either because the velocity increment is large or the time allowed for flight is small. When $z_o = 0.81$ the payload ratio is reduced to zero and $y_o = 0.50$. At this point the fuel carried is capable only of propelling the power supply itself. It remains to determine y_o as $M_1/M_{o\ opt}$ approaches unity or z_o approaches zero. This may be done simply with the aid of L'Hospital's rule and equation (2.23). Rearranging this equation and passing to the limit as z_o approaches zero

$$\lim_{z_o \to o} \frac{e^{z_o/y_o} - 1}{z_o} = \lim_{z_o \to o} \frac{1}{2y_o}\left(1 + \frac{1}{y_o^2}\right) e^{-z_o/y_o}$$

$$\frac{1}{y_o} = \frac{1}{2y_o}\left(1 + \frac{1}{y_o^2}\right)$$

Thus $y_o^2 = 1$ or $y_o = 1$ since u_{ex} is positive in this analysis. The range of y_o is therefore between 0.50 and 1.0. Thus on an optimized journey, the exhaust velocity will never exceed the characteristic velocity. It is reasonable, too, that z_o approaches zero as $M_1/M_{o\ opt}$ approaches unity since the latter condition implies lack of fuel and power supply and of course Δu should be zero. When $M_1/M_{o\ opt} = 0$ then $M_p + M_f = M_o$ or just enough fuel has been taken along to transport the power supply. By equation (2.16) $M_p/M_f = u_{ex}^2/u_c^2 \doteq \frac{1}{4}$ or approximately 80% of the vehicle must be fuel.

It is worthwhile to examine the characteristic velocity to determine how it influences the mission and what significance it has. As mentioned previously z_o varies from zero to 0.81. In other words, the characteristic velocity is a measure of the maximum attainable velocity increment of an electrically propelled vehicle. The importance of the specific mass of the power supply and the efficiency with which

electrical energy is converted into directed kinetic energy is now clarified. Since $\Delta u/u_c$ is proportional to $(\frac{\alpha}{\eta\tau})^{\frac{1}{2}}$, larger payloads or shorter travel times are possible as α is decreased or η is increased. It is possible to incorporate $\frac{\alpha}{\eta}$ into one parameter and define an effective specific mass which includes η. This, however, is not desirable since η is a function of the type of thruster employed more than any other factor. Specific mass and time play complementary roles. In gravity-free space they are exactly equivalent and one may be traded off against the other. A similar role is played between α and η.

A more thorough understanding of the interrelationship between the parameters involved in electrically propelled flight can be obtained by scrutinizing the equations already presented. For example, it is possible to arrive at useful estimates of flight times and deliverable payloads even though gravitational effects are neglected. By means of judicious manipulation of equations (2.11) and (2.12) a minimum mission time may be found in addition to useful relationships between Δu, τ, X and u_{ex}. For $t = \tau$ and $u_o = 0$ equations (2.11) and (2.12) become

$$\Delta u = -u_{ex} \ln\left[1 - \frac{M_f}{M_o}\right] \tag{2.26}$$

and

$$X = u_{ex}\tau\left[1 - (1 - \frac{M_o}{M_f}) \ln\left[1 - \frac{M_f}{M_o}\right]\right] \tag{2.27}$$

Inserting equation (2.26) in (2.27) one discovers

$$X - u_{ex}\tau = \Delta u\tau\left[1 - \frac{M_o}{M_f}\right] \tag{2.28}$$

A very interesting result follows from this equation. Since X, τ, Δu and u_{ex} are all positive quantities and $M_o/M_f \geq 1$ it follows that $X - u_{ex}\tau < 0$

or $$\tau > \frac{X}{u_{ex}} \qquad (2.29)$$

Relation (2.29) defines a minimum travel time for interplanetary journeys. This minimum mission time exists purely because the mass of the fuel carried is at most the total mass of the rocket. Note that the concept of a minimum mission time is not restricted to electrically propelled craft, but only to continually accelerating devices. For this reason, it is preferable to conceive of a minimum mission time rather than a minimum exhaust velocity specified by rearranging equation (2.29). In travelling to a given planet, once the exhaust velocity has been specified, there exists a minimum time, τ_{min}, which is required to reach the planet in question. For example, if the planet to be visited were Pluto ($X = 5.7 \times 10^{12}$m.) and the optimum specific impulse were 8000 sec. then τ_{min} = 27 months assuming a flyby mission (i.e. continually accelerating for the entire flight time and no deceleration). Equation (2.29) reveals an obvious advantage of electric propulsion as opposed to nuclear and chemical types. The minimum mission time is considerably less for electric vehicles since u_{ex} (chemical) $<<$ u_{ex} (electric).

On an interplanetary mission one has a destination and hence X is fixed. As above, α and η may be assumed fixed by state of the art developments. The following two equations are sufficient to completely specify the mission if gravity is ignored:

$$\frac{M_1}{M_o} = e^{-z/y} - y^2(1 - e^{-z/y}) \qquad (2.21)$$

$$X = u_c \tau \left(y + z - \frac{z}{1 - e^{-z/y}}\right) \qquad (2.30)$$

where equation (2.30) is merely a rearrangement of equation (2.27). With X, α and η fixed there remain y, z, τ and $\frac{M_1}{M_o}$ to be found that

satisfy these two equations. It is obviously possible to fix two of these parameters arbitrarily and solve for the others. Thus, for example, $\frac{M_1}{M_o}$ may be set to any value between zero and unity. There is no optimum solution to this problem in the sense of the preceding analysis.

One very informative set of solutions is obtained by setting y and z and solving for τ and $\frac{M_1}{M_o}$. Such a calculation would provide the reader with the time necessary and the payload deliverable to the destination X for fixed y and z. Even in this case there are an infinite number of possible choices - one for every pair of y and z. How then is one to select y and z such that useful values of payload and travel times are obtained?

An interesting approach to this problem is to select y and z such that $\frac{\partial}{\partial y}\frac{M_1}{M_o} = 0$

Although this approach does not yield an absolute maximum value of $\frac{M_1}{M_o}$ (which does not exist), it provides typical values of all parameters and is a convenient means of obtaining simple comparisons between chemical and electrical systems. Values of y and z satisfying this relationship are listed in Table 2.1 and are designated (y_o, z_o). For every pair (y_o, z_o) there is a distinct value of payload ratio $\frac{M_1}{M_o}$ opt.

Thus in terms of (y_o, z_o) the expression for X becomes

$$X = u_c \tau \, y_o \left[K_1 (y_o, z_o) \right]$$

where $$K_1(y_o, z_o) = \left[1 + \frac{z_o}{y_o} - \frac{z_o}{y_o} \frac{1}{1 - e^{-y_o/z_o}} \right]$$

Values of $K_1(y_o, z_o)$ are given in Table 2.1. Thus

$$X = \left(\frac{2\eta}{\alpha}\right)^{\frac{1}{2}} y_o \, K_1(y_o, z_o) \, \tau^{3/2} \qquad (2.31)$$

In other words, for each set of coordinates $\left(\frac{M_1}{M_o}_{opt}, y_o, z_o\right)$, τ may be calculated for a flyby mission between planets, provided propellant is ejected uniformly throughout the flight, according to

$$\tau = \left(\frac{\alpha}{2\eta}\right)^{\frac{1}{2}} \left[\frac{X}{y_o K_1(y_o, z_o)}\right]^{\frac{2}{3}} \tag{2.32}$$

where X is chosen as the average distance between planets and the total mission time is assumed equal to the thrust duration τ. Fig. 2.2 and 2.3 display payload ratio as a function of mission time. In order to plot these curves values of (y_o, z_o) and $\frac{M_1}{M_o}_{opt}$ were selected and τ determined as described above. Note that for each pair (y_o, z_o) the corresponding u_{ex} and Δu depend on the mission time τ. Thus each point on the curve has distinct values of exhaust velocity and velocity increment. Fig. 2.2 provides one basis of comparison of electric with chemical propulsion systems. The chemical rocket is credited with an $I_{sp} = 450$ sec. and the electric rocket with an $\alpha = 10$ kg/kw and an $\eta = 0.8$; all state of the art figures. One can see that there exists a "crossover point" at which both systems carry equal payload in equal time. The payload ratio at crossover is, however, so small as to make the journey rather uninteresting (18% for Venus and 11% for Mars). Above the crossover point electric systems are obviously superior. While the electric rocket can deliver 65% payload to Venus in 4.2 months, the chemical rocket can deliver only 41%. To Mars the electric system will deliver 65% payload in 6.4 months while a chemical system will deliver 33%. Actually the net payload delivered by a chemical system would be even less since it must carry its own electrical power supply which is, of course, an integral portion of the electric system. The superiority

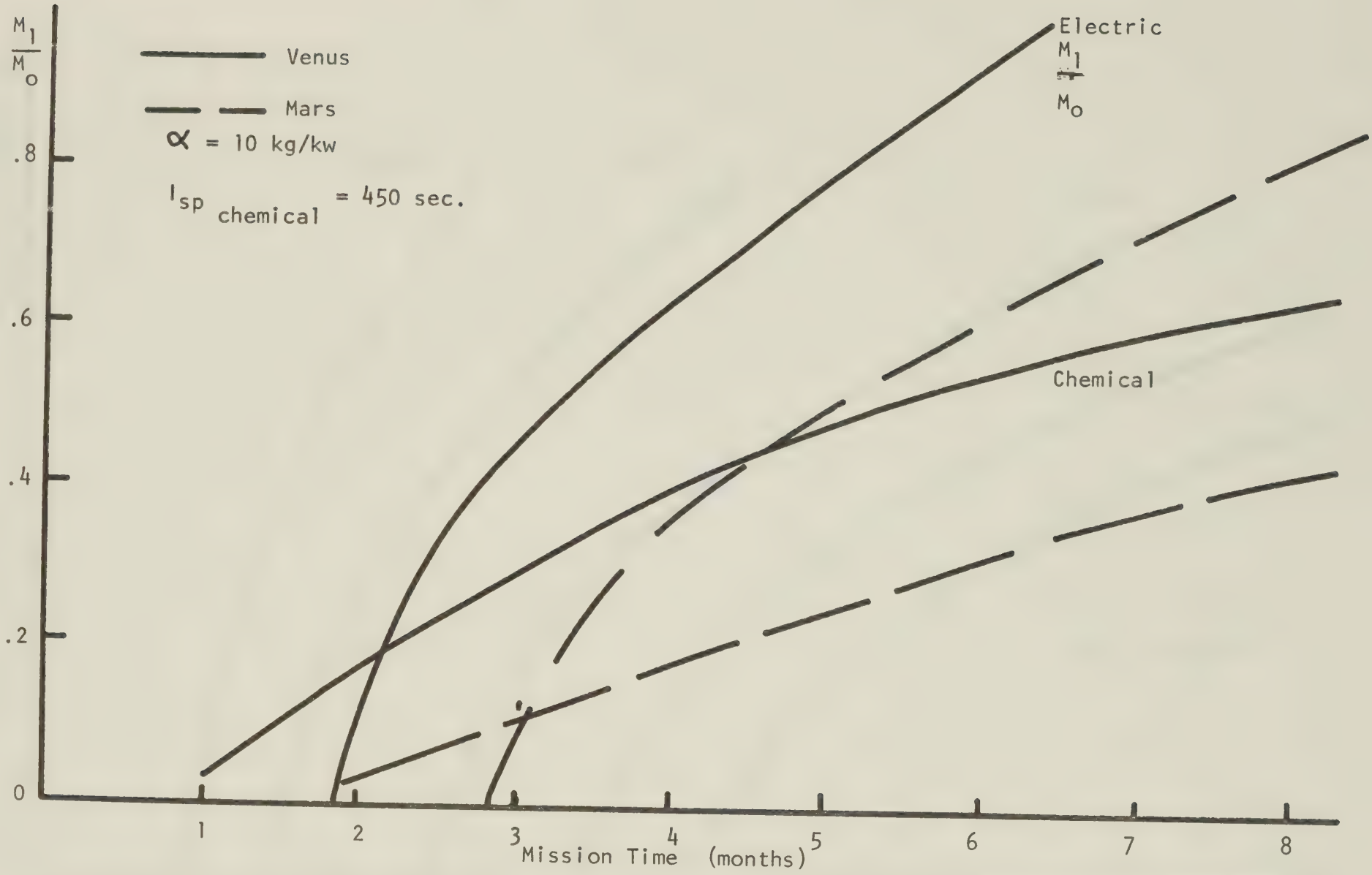

Fig. 2.2 Payload Ratio versus Mission Time

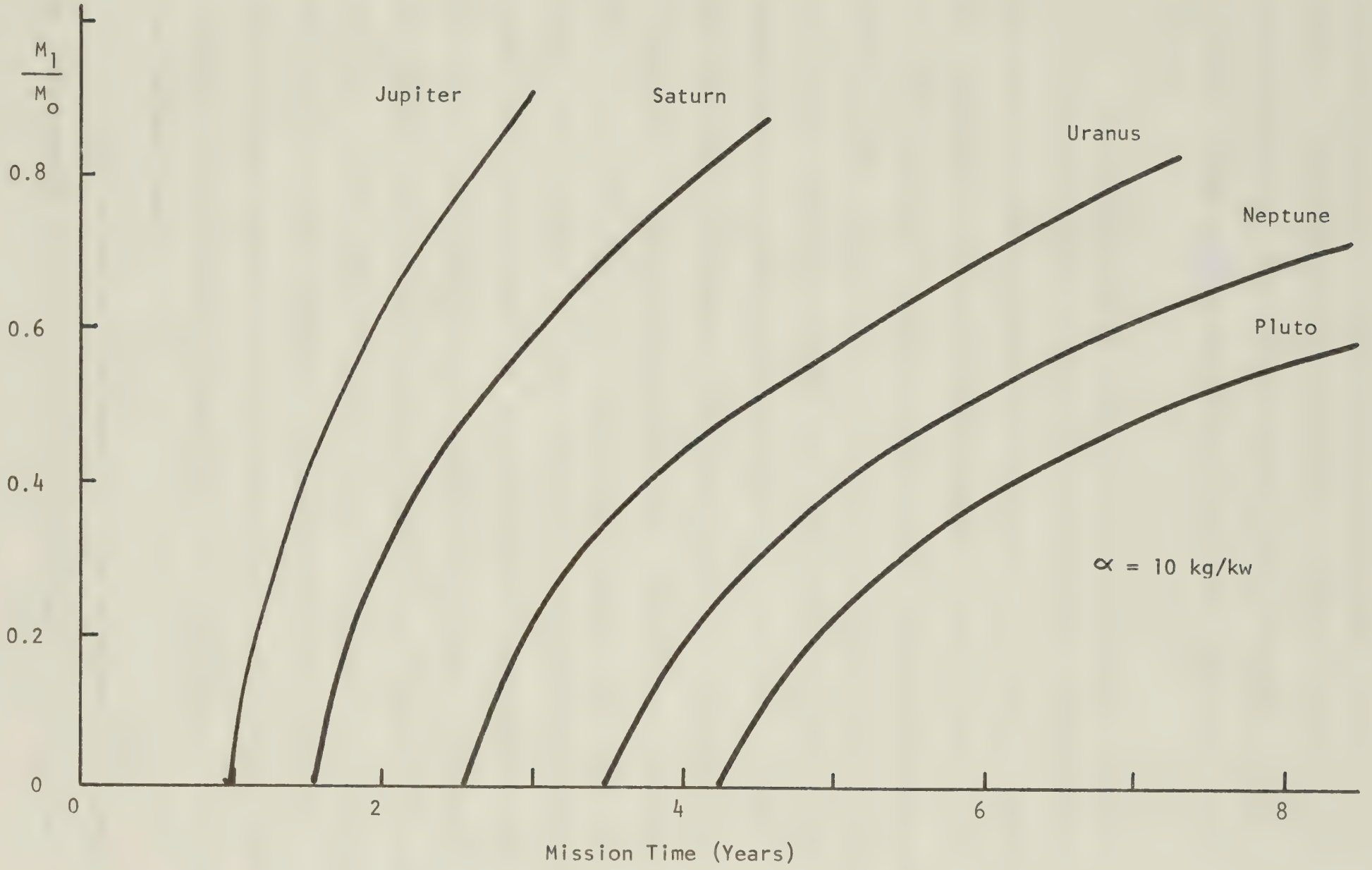

Fig. 2.3 Payload Ratio versus Mission Time

of electric propulsion is even more evident on longer missions. For example, a 50% payload could be delivered to Jupiter in 1.7 years or Pluto in 7.2 years. For the same payload, the corresponding times for a chemical system would be approximately 6.5 years and 60 years respectively.

The advantages of electric propulsion may be seen in another light by considering the variation in interplanetary distance with mission time for a given payload ratio and hence (y_o, z_o) and K_1. Equation (2.31) elucidates the three-halves dependence of position on mission time. The advantage of electric propulsion over the short-impulse type chemical system is obvious since for the latter system $X = \Delta u \tau$ (2.33) or X varies linearly with mission time. Fig. 2.4 and 2.5 display the distance-time relationship for both systems. In Fig. 2.4 the scale is expanded so that the crossover point may be seen. It can be seen that the crossover time decreases as payload ratio increases. Of course, this is to be expected. It is interesting to observe that for a small payload ratio (18.5%), electrical and chemical systems would reach Venus in about the same time while for a substantially larger payload (50%) the electric rocket would arrive 2.2 months earlier than its chemical counterpart. Fig. 2.5 demonstrates the superiority of electric systems over larger interplanetary distances. Fig. 2.3 and 2.5 are an extremely useful pair of graphs for estimating interplanetary missions. While Fig. 2.3 displays payload ratio as a function of mission time for fixed distances, Fig. 2.5 displays distance as a function of mission time for fixed payload ratio.

The last parameter to be examined is the acceleration. Since the instantaneous mass and acceleration are related to the thrust as

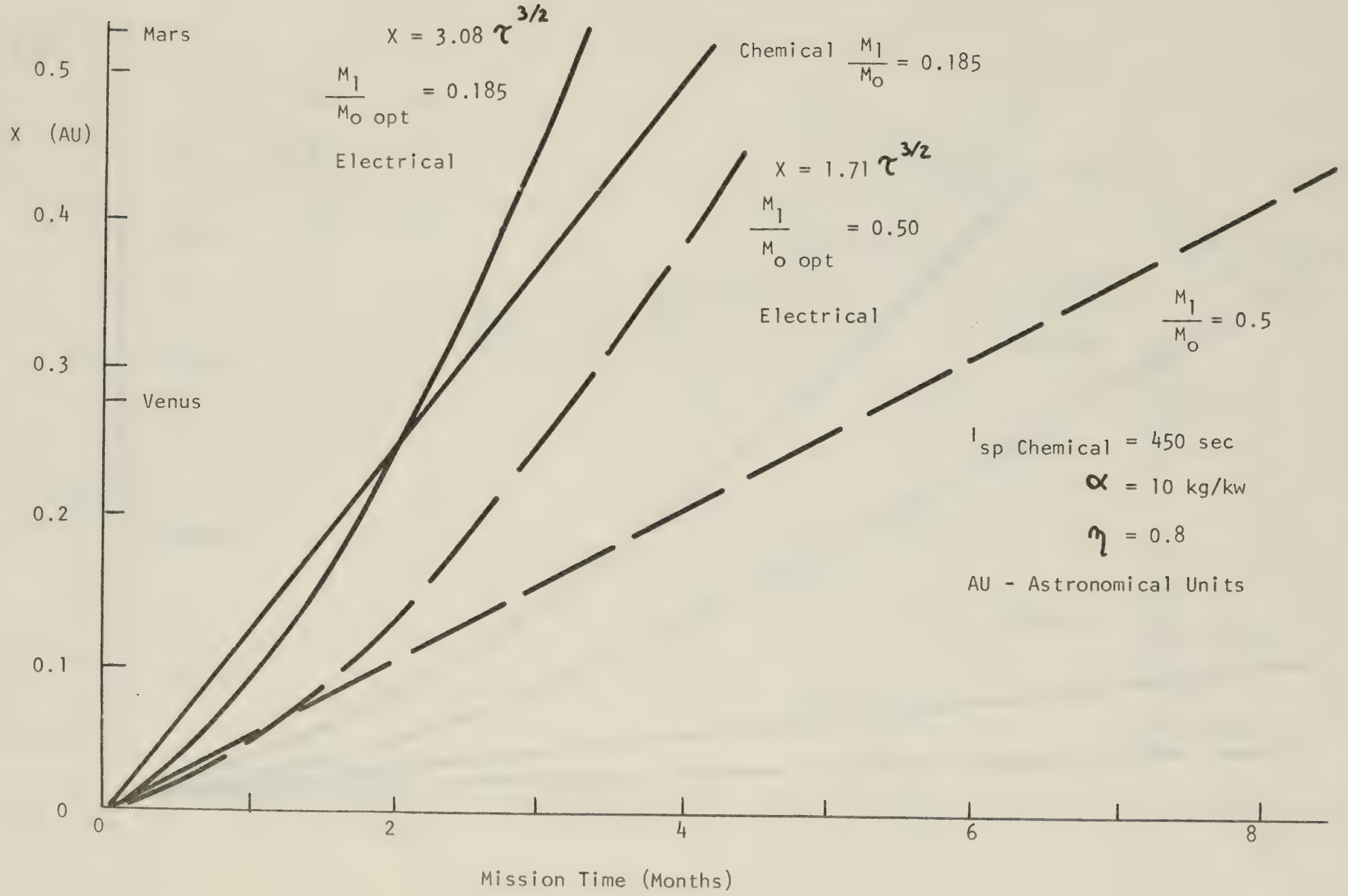

Fig. 2.4 Interplanetary Distance versus Mission Time

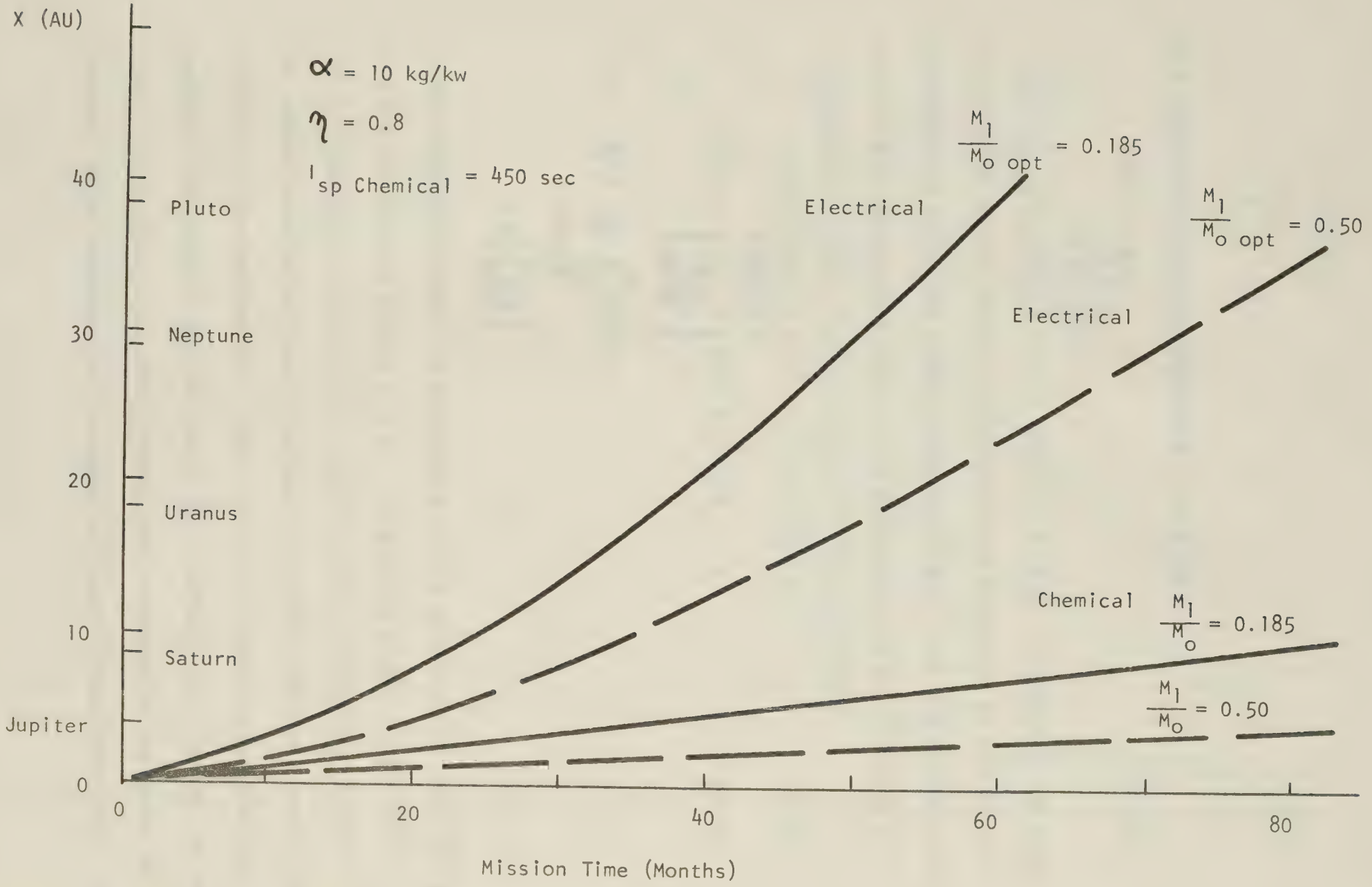

Fig. 2.5 Interplanetary Distance versus Mission Time

$$T = M(t)\, a(t)$$

$$= \frac{2P}{u_{ex}}$$

the acceleration can be expressed in the form

$$a(t) = \frac{2\eta M_p}{\alpha u_{ex} M(t)} \tag{2.34}$$

according to equations (1.3), (2.6), and (2.7). Employing the above equation it is now possible to examine the behaviour of the initial acceleration $a(0)$, the final acceleration $a(\tau)$, and the average acceleration $\langle a \rangle$ noting particularly the dependence on α. With the aid of equations (2.15), (2.16), (2.17), (2.19) and (2.20)

$$a(0) = \left(\frac{2\eta y_o^2}{\alpha\tau}\right)^{1/2} \left(1 - e^{-z_o/y_o}\right) \tag{2.35}$$

$$a(\tau) = \left(\frac{2\eta y_o^2}{\alpha\tau}\right)^{1/2} \left(e^{z_o/y_o} - 1\right) \tag{2.36}$$

and

$$\langle a \rangle = \frac{1}{\tau} \int_0^\tau a(t)dt$$

$$= \Delta u/\tau$$

$$= z_o \left(\frac{2\eta}{\alpha\tau}\right)^{1/2} \tag{2.37}$$

These equations reveal the dependence of the acceleration on α, τ, η and the coordinates M_1/M_o, y_o, z_o. To achieve higher acceleration it is necessary to decrease the specific mass of the power supply or to reduce the mission time. The need for highly efficient energy conversion is also emphasized. Figs. 2.6 to 2.8 show acceleration normalized with respect to g at the Earth's surface, on a journey to Jupiter. It is clear from these graphs that acceleration decreases as payload ratio increases and increases as specific mass decreases. For

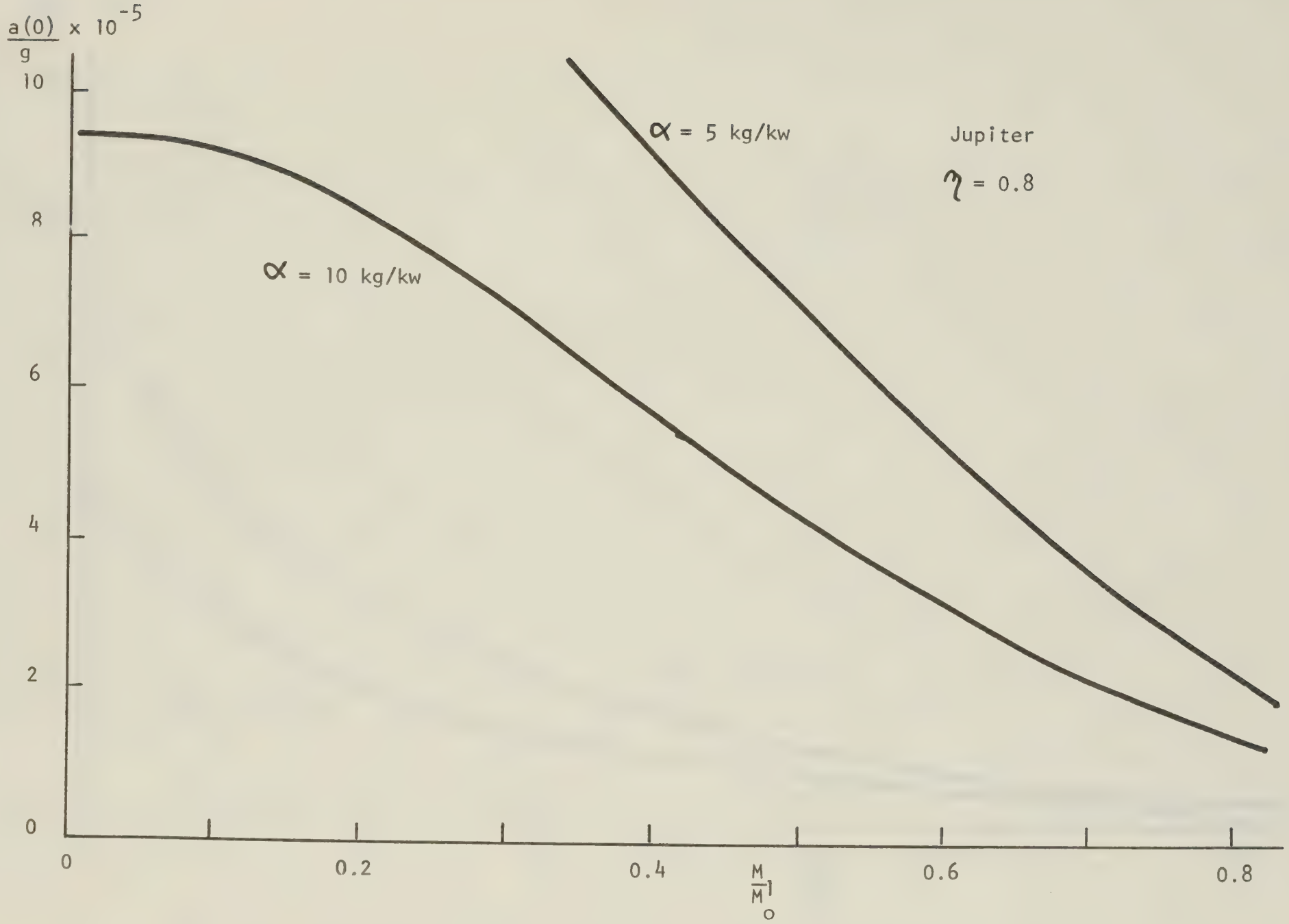

Fig. 2.6 Normalized Initial Acceleration versus Payload Ratio

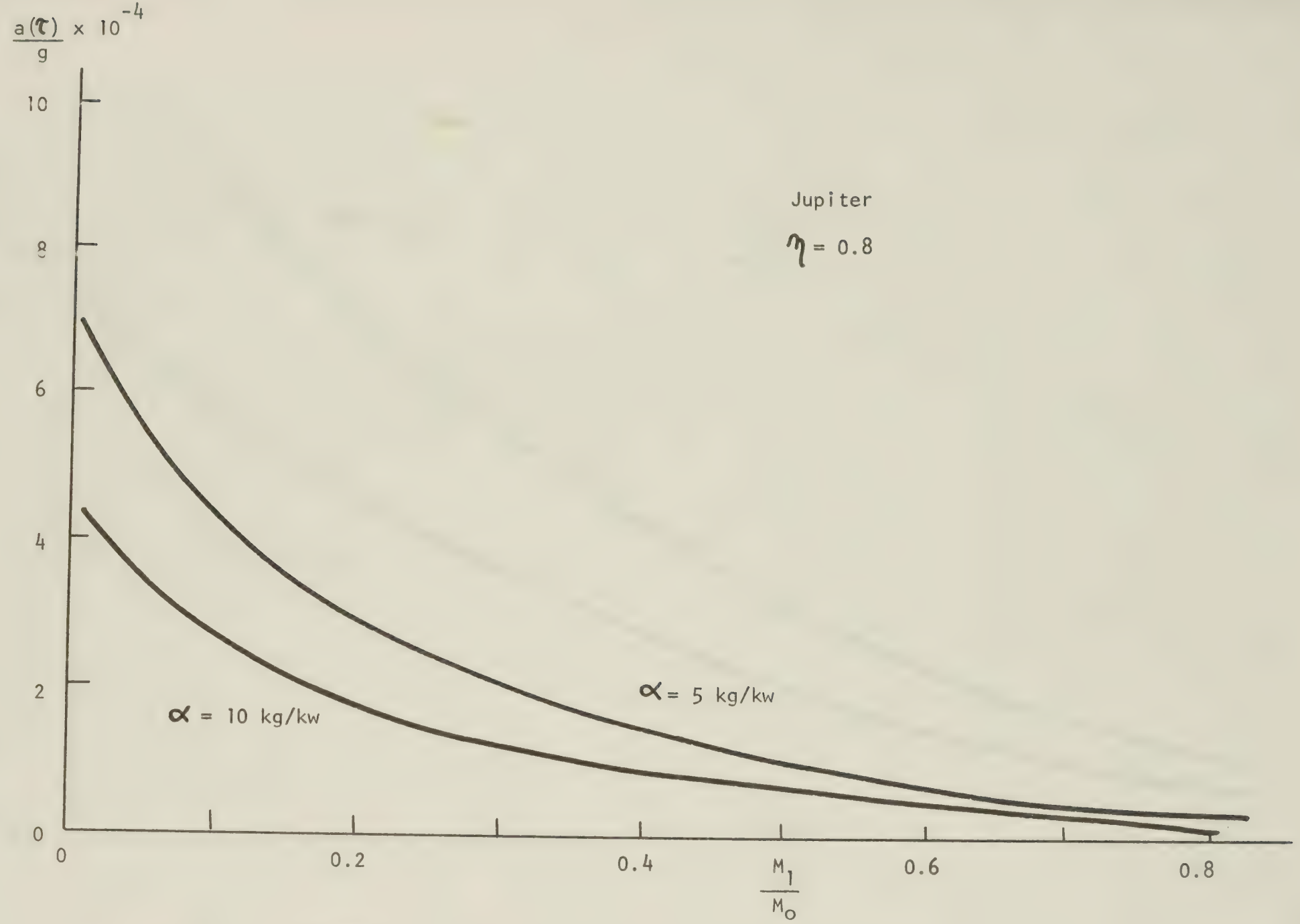

Fig. 2.7 Normalized Final Acceleration versus Payload Ratio

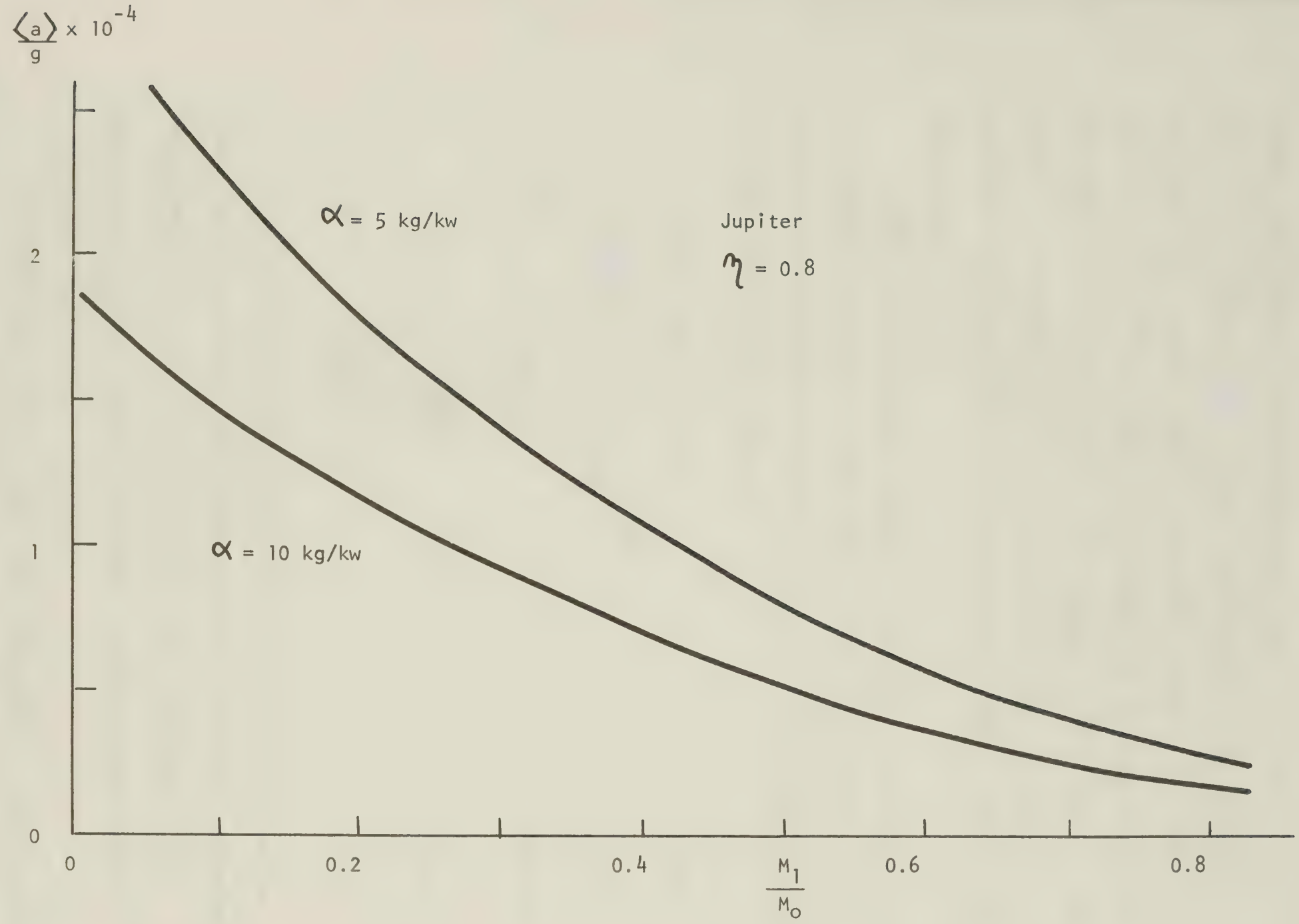

Fig. 2.8 Normalized Average Acceleration versus Payload Ratio

example, on a mission with α = 10 kg/kw, $a(0) = 5 \times 10^{-5}g$, $a(\tau) = 6 \times 10^{-5}g$ and $\langle a \rangle = 5.03 \times 10^{-5}g$ while on the same mission with α = 5 kg/kw, $a(0) = 7.3 \times 10^{-5}g$, $a(\tau) = 11 \times 10^{-5}g$, and $\langle a \rangle = 8 \times 10^{-5}g$. These three figures also indicate one of the weaknesses of electric propulsion; the extremely low a/g ratio. This ratio is of the order of 10^{-4} and will prevent electric propulsion from unassisted Earth launching until a major breakthrough in power sources takes place.

Before concluding this section, a summary is presented of mission analysis procedures for the cases where y and z are arbitrarily selected to satisfy equation (2.23). Five equations are repeated here in a form similar to the original

$$f(y_o, z_o) = 0 \tag{2.23}$$

$$X = \left(\frac{2\eta}{\alpha}\right)^{\frac{1}{2}} y_o \; K_1(y_o, z_o) \, \tau^{3/2} \tag{2.31}$$

$$\left(\frac{M_1}{M_o}\right)_{opt} = g(y_o, z_o) \tag{2.21}$$

$$u_{exopt} = y_o \left(\frac{2\eta\tau}{\alpha}\right)^{\frac{1}{2}} \tag{2.19}$$

$$\Delta u = z_o \left(\frac{2\eta\tau}{\alpha}\right)^{\frac{1}{2}} \tag{2.20}$$

In planning a mission, one can see with the aid of equations (2.21), (2.23) and (2.31) that selection of X, τ, α and η determines the parameters u_{exopt}, Δu, $a(0)$, $a(\tau)$, $\langle a \rangle$, M_f/M_o and M_p/M_o. Observe that all the parameters are simply related through functions of y_o, z_o, α, η and τ.

Alternatively, one can select Δu, X, α and η. Equation (2.20) can then be substituted into (2.31) to eliminate τ and the resulting

equation solved simultaneously with (2.23) for (y_o, z_o). Equations (2.21) and (2.20) will then yield $M_1/M_{o\ opt}$ and τ respectively. Another possibility is the design of a mission around a given thruster. In this case u_{ex} may be selected along with α, η and X. The procedure for calculation of the other parameters is the same as in the case in which Δu is selected. Of course, there is no reason why $M_1/M_{o\ opt}$ cannot be chosen along with α, η and X. In this case also, τ may be calculated.

In other words, there are four types of missions possible when α, η and X are fixed. (X is assumed fixed since it represents the distance to a given planet in space). Depending upon the purpose of the mission and the equipment available (i.e. power supply and type of thruster), one may choose one of either Δu, u_{ex}, $M_1/M_{o\ opt}$ or τ.

In order to calculate the masses of the individual components M_f, M_1, M_p, it is necessary to specify either P_e, T or $\dot{M}$. Since P_e is determined by the type of energy source available, it is usually selected and T, $\dot{M}$ and individual masses calculated subsequently.

Table 2.2 lists two flyby missions analyzed by the method presented. The parameters selected for these missions are X, α, η and $M_1/M_{o\ opt}$. Both vehicles have been credited with the same payload ratio, available power, engine specific mass and efficiency. The result is that each vehicle has the same set of M_o, M_1, M_p and M_f while the remainder of the corresponding parameters of the two missions are quite different. Of course, the thrust, mass flow rate and acceleration of the Mars vehicle are larger.

TABLE 2.2

FLYBY ELECTRIC PROPULSION MISSIONS

X	Jupiter	Mars
$\frac{M_1}{M_o}$	.50	.50
y_o	.85	.85
z_o	.29	.29
η	0.8	0.8
α	10 kg/kw	10 kg/kw
$\frac{M_p}{M_o}$	.21	.21
$\frac{M_f}{M_o}$	.29	.29
τ	1.65 years	4.9 months
u_c	91.5 km/sec.	45.4 km/sec.
u_{ex}	77.6 km/sec.	38.6 km/sec.
I_{sp}	7910 sec.	3940 sec.
Δu	26.5 km/sec.	13.2 km/sec.
P_e	100 kw	100 kw
T	2.06 nt	4.15 nt
$\dot{M}$	2.66×10^{-5} kgm/sec.	1.07×10^{-4} kg/sec.
M_f	1390 kgm.	1390
M_1	2400 kgm.	2400
M_p	1000 kgm	1000
M_o	4790 kgm.	4790
a(o)	5×10^{-5} g	8.8×10^{-5} g
$a(\tau)$	6×10^{-5} g	4.28×10^{-4} g
$\langle a \rangle$	5.03×10^{-5} g	1.04×10^{-4} g

2.3 Types of Electric Propulsion

Most of the electric propulsion systems currently under development fall into one of three categories: electrothermal, electromagnetic or electrostatic. Electrothermal devices produce thrust by heating a propellant electrically and then exhausting it through a convergent-divergent supersonic nozzle. Electromagnetic propulsion refers to the acceleration of a propellant beam via the interaction of magnetic fields with electric currents in the beam. As the fuel is often "highly" ionized gas, electromagnetic devices are often termed "plasma engines". Electrostatic thrusters, as the name implies, employ electrostatic fields to accelerate the propellant. Possible propellants range from heavy ions to charged multimolecular solid and liquid particles.

When comparing various propulsion systems it should be born in mind that the thrust is determined by the beam power and exhaust velocity, regardless of the method of acceleration. Thus the power efficiency is of prime concern in evaluating an electric thruster. Of particular importance is the manner in which specific impulse varies with power efficiency, for this phenomenon has a great influence on the applicability of a particular electric propulsion system. Reliability, lifetime and total system weight are also major considerations.

2.3.1 Electrothermal Thrusters

Basically there are two different types of electrothermal thrusters. The first of these two devices, the resistojet, consists of an electrically heated solid surface over which propellant passes while the second, the arc-jet, derives its thrust from the passage of propellant through an arc-discharge and subsequent expansion through a nozzle.

In each case the attainable exhaust velocity is determined primarily by the maximum temperature that the chamber and nozzle surfaces can tolerate and by the kinetic and thermodynamic properties of the propellant gas.

A conceptual model of an electrothermal thruster is presented in Fig. 2.9. With the simplifying assumption of one dimensional adiabatic expansion through a nozzle, the exhaust velocity u_{ex} may be obtained from an energy balance.

$$\tfrac{1}{2} u_{ex}^2 = \tfrac{1}{2} u_m^2 + (h_m - h_{ex}) \qquad (2.39)$$

where h_{ex} is the specific enthalpy of the propellant in the exhaust, h_m is the specific enthalpy of the propellant in the chamber and u_m is the velocity of the propellant in the chamber.[32] The electrically heated gas is then allowed to expand through a supersonic nozzle to a low pressure determined by the nozzle area ratio and by the chamber pressure P_m.

The thrust that such a propulsion system can provide clearly depends upon the mass flow which can be heated and expanded and hence upon the size of the device and on the chamber pressure level. In reality, a more fundamental limit is set by the available electric power supply which drives the unit. For example, perfect conversion of a 30 kw source into kinetic energy of a 1000 second exhaust beam limits the mass flow to $\dot{M} = \frac{2P}{u_{ex}^2} = 6 \times 10^{-4}$ kgm/sec with a corresponding thrust of 6 nt. (1.35 lbs.). A practical electrothermal thruster departs from the one dimensional model in at least two important respects. Firstly, flow is not one dimensional due to temperature and density gradients set up in the chamber. Secondly, radiant heat loss from the thrusters further complicates the problem. A third factor involved is the strong

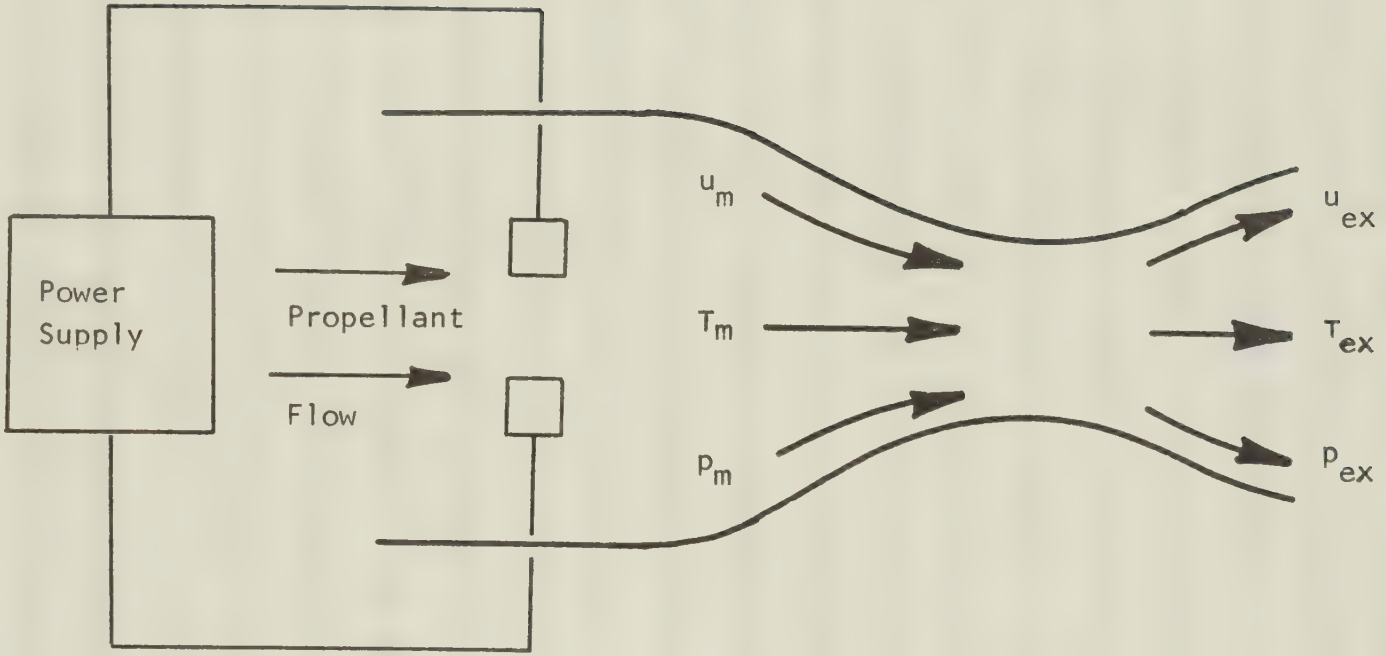

Fig. 2.9 Conceptual Model of Electrothermal Thruster

dependence of the properties of the propellant on temperature.

Possibly the simplest of all electric propulsion devices is the resistojet. This device provides a rugged, constructionally simple, very reliable propulsion system. No complex power or control circuitry is required since the heating element can be operated directly from the output of a solar array. When hydrogen is used as the propellant, specific impulses of approximately 1000 seconds can be obtained[33]. Hydrogen, however, must be stored in a liquified state because of its low density. The cryogenic equipment necessary imposes a severe weight penalty on the thruster system. A more practical fuel is ammonia, which combines ease of storage with specific impulses between 200 and 500 seconds[34]. It does, nevertheless, introduce the problem that its chemical activity tends to enhance nozzle and heater erosion. Other possible propellants include nitrogen, carbon dioxide, lithium and hydrazine. Although resistojets are simple, compact and adaptable to a variety of power supplies, they are fundamentally temperature limited by the available structural materials which at present constrain them to a range of specific impulse below 1000 seconds. As a point of interest, the first space test of an electrothermal thruster took place in September 1965 and was a resistojet which developed a thrust of .042 lb. at a specific impulse of 123 seconds[35]. More recently, the use of biowaste as propellant in electrothermal thrusters has become of interest. A common propellant is carbon dioxide, delivering a specific impulse in the 180 second range at efficiencies of 60%[36] [37].

In order to improve upon the specific impulse attainable from the resistojet, it becomes necessary for an electrothermal device to produce a gas flow in its chamber such that the average temperature is higher than that of the chamber walls. One method of overcoming this

difficulty is by heating the central gaseous stream by passing an electric arc through it within a geometry suitable to radiative and conductive energy transport such that the device is not damaged.

Many arcjet thrusters have been constructed. The two most common propellants are hydrogen and ammonia. Input power has ranged from 1 watt to 200 kw while the mode of operation has been either pulsed, AC or DC. Typical efficiencies lie in the 40% range while specific impulse varies from 1000 to 2000 seconds[38]. An excellent introduction to electrothermal acceleration may be found in reference (33).

2.3.2 Electromagnetic Thrusters

Electromagnetic propulsion is a second major and perhaps the most complex form of the electric propulsion concepts. This form of thruster is comprised of a body of ionized gas accelerated by the interaction of currents driven through the gas with magnetic fields established either by those currents or by external means. Basically, there are two modes of operation within the class; steady and pulsed. A good deal of research has been devoted to each mode with only a limited degree of success. Progress has been largely of an empirical nature with fundamental understanding of the detailed acceleration and loss mechanisms lagging far behind. Most of these devices have proved unsuitable for space propulsion because of low efficiency, inadequate specific impulse or unrealistic power supply requirements.

Electromagnetic thrusters offer the advantages of high thrust density along with high beam power density, higher in fact than electrostatic thrusters which must face the problem of space charge limitation of currents. Furthermore, no need for a neutralizer exists as the propellant is a quasi-neutral plasma. In many forms of so-called "plasma

thrusters" the required operating potential is only some tens of volts, adding a further advantage of direct operation from solar cells. The principal drawbacks of this type of device are its low efficiency, its stringent demands placed upon power supplies and its phenomenological complexity.

A veritable host of schemes for electromagnetic propulsion may be found in the literature[39]-[42]. A few of the more promising ones shall now be briefly described.

2.3.2.1 MPD (Magnetoplasmadynamic) Thruster

The MPD arc thruster is an offshoot of the electrothermal thruster. It was accidentally discovered that by reducing the mass flow of the propellant and hence the chamber pressure (to the mm. Hg. range), the arc could be caused to diffuse over the cathode surface and to extend far out into the gas stream. In this mode arc currents of 3000 amps could be drawn with no serious erosion, resulting in Isp's of the order of 10,000 seconds at overall efficiencies of 50%[43]. At higher currents (up to 100,000 amps) this device has been operated in a pulsed regime[44]. The MPD thruster offers the possibility of high thrust density at high specific impulse and is receiving much attention for these reasons. A sketch of the accelerating region of this thruster is presented in Fig. 2.10. The wealth of literature available on this device is an indication of the degree of optimism held for its future[45]-[51].

The precise mechanism of propellant acceleration in the MPD thruster is not known. It has not been possible to describe accurately the gaseous acceleration in terms of a body force or on a particle basis alone. That is to say, it has not been possible to describe accurately

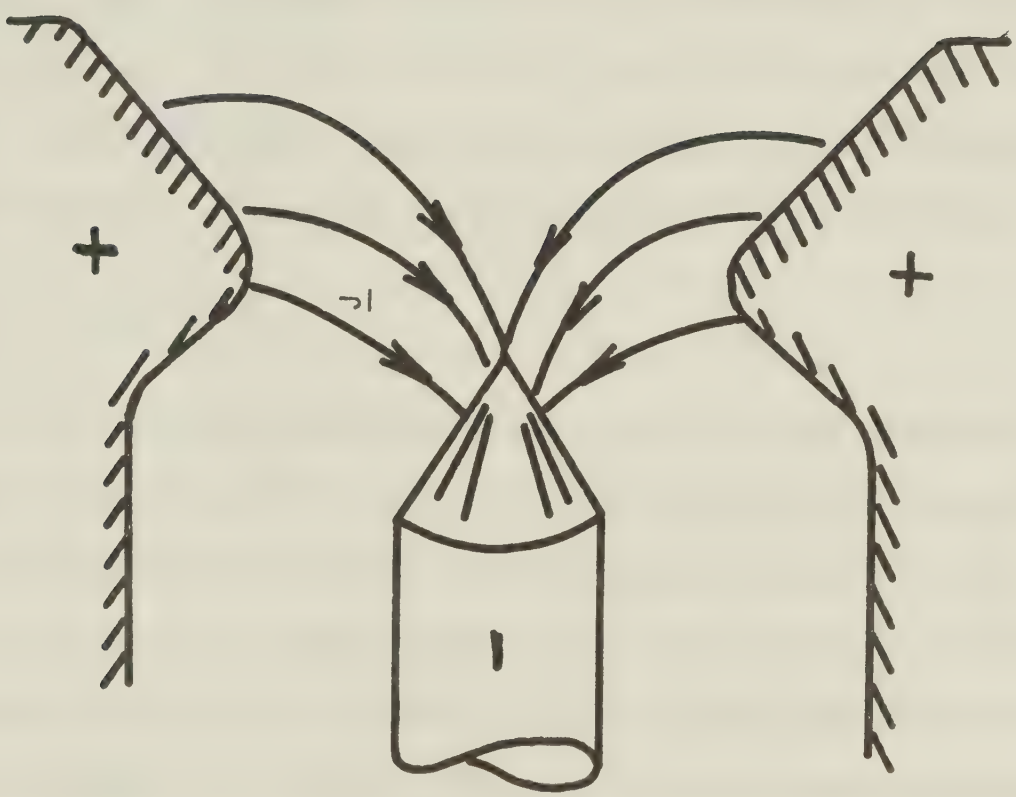

Fig. 2.10 Accelerating Portion of an MPD Thruster

the acceleration by treating the gas as a continuous fluid or as a statistical number of particles alone.

2.3.2.2 Travelling Wave Thruster

In a travelling wave accelerator a series of phased coils driven from a radio-frequency source are arranged to produce a continuous electromagnetic wave that propagates through the ionized propellant. Frequencies of the order of 100 khz are typical. Acceleration results from interaction of the wave train with currents induced in the plasma. Since the process is essentially independent of electrodes, the lifetime of this type of device is expected to be higher than for other plasma thrusters. Experiments indicate that efficiencies of 40% can be achieved at specific impulses between 2000 and 3000 sec.[52].

2.3.2.3 Plasma Guns

A plasma gun consists of two long electrodes arranged either coaxially or as parallel rails. The gun is fired by discharging a high energy capacitor bank between the electrodes in such a way as to initiate an arc at one end of the electrode pair. The propellant in the inter-electrode region is ionized and a current flows from the capacitor through the electrodes and the arc. This loop current produces a magnetic field that interacts with the current in the arc, resulting in a $\underline{J} \times \underline{B}$ body force that drives the plasma along the electrodes. Electrode life and incomplete ionization of the propellant are major problems with this type of thruster. Specific impulses range from about to 1200 to 5000 sec. with efficiencies to date less than 30%[53].

2.3.3 Electrostatic Thrusters

Electrostatic propulsion is the most highly developed of the electric propulsion concepts. Members of this group are the so-called "ion engines" - the electron bombardment and contact ionization type and the colloid engine. In fact, it is the electron bombardment or Kaufman thruster that has been recently tested on board SERT II for a six month reliability experiment. A wealth of information on electrostatic propulsion exists in the literature[54]-[58].

2.3.3.1 Contact-Ionization Thruster

As the name implies, propellant atoms (usually alkali atoms such as cesium) are ionized through contact with a metal of high work function (for example, tungsten) at a high temperature (1300 to 1500^{o}k). The contact ionization probability is usually as high as 99% with the most common type of ionizer consisting of tungsten powder composed of tungsten spheroids two to four microns in diameter. By virtue of its own vapor pressure, cesium diffuses through the pores of the ionizer and is ionized predominantly by contact on the "downstream" face of the ionizer as in Fig. 2-11. As cesium has the lowest ionization potential of all acceptable propellants and tungsten the highest work function, this combination seems to be the best. Thermal radiation from the ionizer is the major power loss in this class of thruster.

Subsequent to ionization the particles are accelerated by an intense electrostatic field and finally neutralized by a stream of electrons injected from a hot filament at the exhaust exit. Without such neutralization the thrust would be substantially reduced by the increasing space charge behind the vehicle. To prevent electron back-

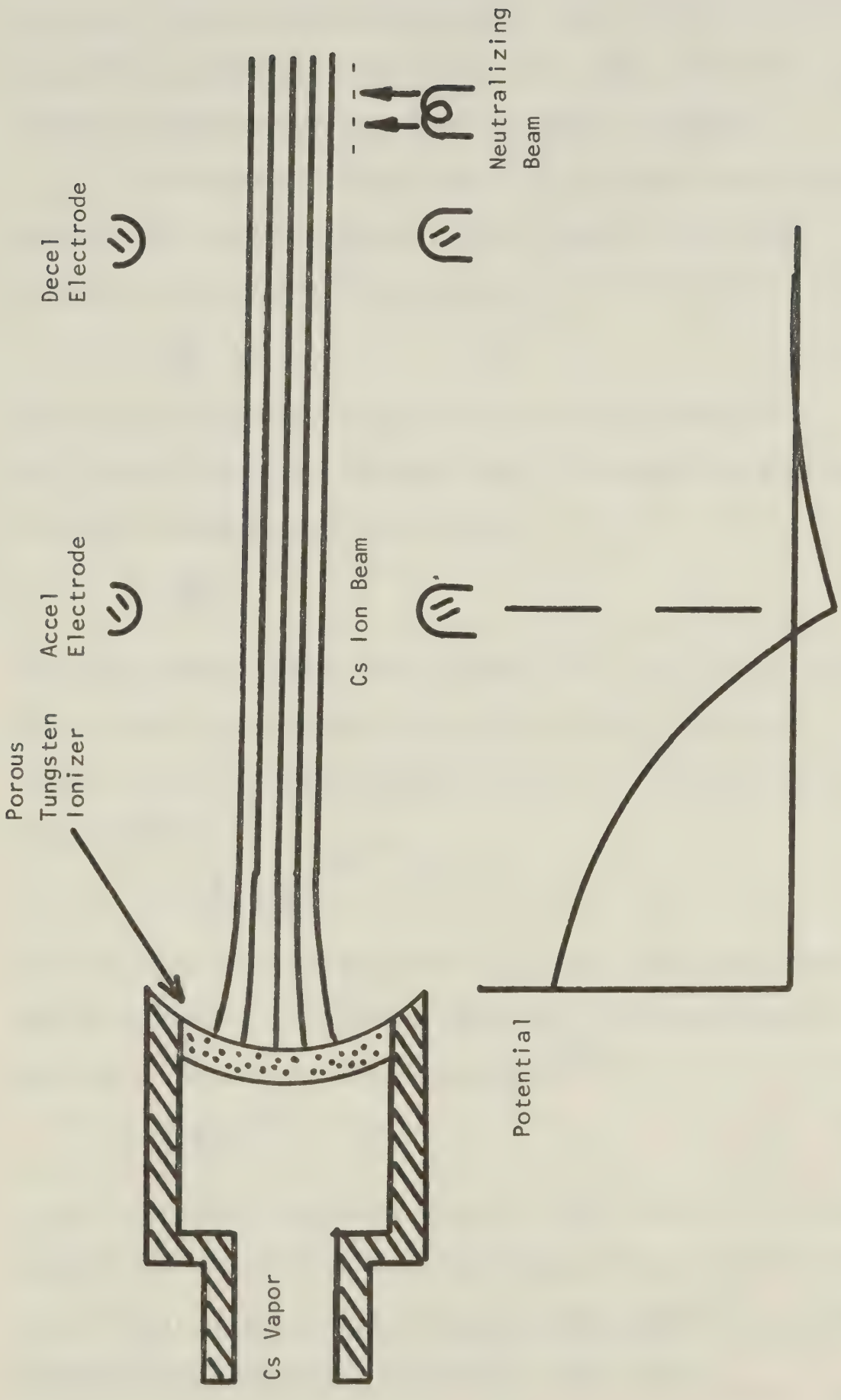

Fig. 2.11 Contact Ionization Thruster

streaming from the neutralized exhaust beam a "decel electrode" is situated as indicated in Fig. 2.11. This decel electrode is at a potential negative with respect to spacecraft potential.

If one chooses a simple parallel plate configuration for the accelerator, the thrust density may be readily calculated. If the cross-sectional area of the thruster is A then the thrust density is

$$\frac{T}{A} = \frac{\dot{M}}{A} u_{ex} \tag{2.40}$$

assuming all propellant particles have the same velocity u_{ex}. Furthermore the mass flow rate per unit area is related to the current density J and the charge to mass ratio q/m by

$$\frac{\dot{M}}{A} = J\left(\frac{m}{q}\right) \tag{2.41}$$

Assuming paraxial space charge limited flow, the current density may be expressed in terms of the interelectrode spacing d, the charge to mass ratio and the applied potential V according to the Langmuir-Child relation[59]

$$J = \frac{4}{9} \frac{\varepsilon_o}{d^2} \left(\frac{2q}{m}\right)^{1/2} V^{3/2} \tag{2.42}$$

where ε_o is the permittivity of free space. The thrust density may now be calculated by inserting equations (2.41) and (2.42) in (2.40). Upon manipulation[60] the thrust density is

$$\frac{T}{A} = \frac{8}{9}\varepsilon_o\left(\frac{V}{d}\right)^2 \tag{2.43}$$

It is interesting to observe that the thrust density is directly proportional to the square of the average electric field, inversely proportional to the square of the electrode spacing for a fixed potential and independent of charge to mass ratio.

Hence as small an electrode separation as is physically possible is desirable. The separation, however, is constrained by electric breakdown[61]. Practical accel lengths are a few millimeters. Whereas the thrust density is independent of the charge to mass ratio of the propellant, such is not the case for the beam power density. Mickelsen has shown that the beam power density has two constraints imposed upon it. One is due to space charge limitation and the other to electric breakdown[62]. In the space charge limited regime, the power density varies inversely as the square of the charge to mass ratio while in the breakdown limited mode the power density varies directly as the square. These facts illustrate some of the considerations necessary in the design of an ion engine.

Most ion engines are capable of operating at any desired value of specific impulse in the range 3000 to 12,000 seconds merely by adjusting the accelerating voltage. Unfortunately the power efficiency decreases with decreasing specific impulse. The losses in an ion engine which include the power to vaporize the cesium, to heat the neutralizer filament and maintain the tungsten at 1150° C. are independent of specific impulse. Since beam power decreases with decreasing specific impulse, the ratio of beam power to total expended electrical power decreases with decreasing specific impulse. At present, efficiencies approach 80 to 90% for $I_{sp} > 8000$ sec. but drop to about 50% in the 4000 second range[63].

2.3.3.2 Electron-Bombardment Thruster

The propellant in an electron-bombardment thruster is first vaporized and passed through the distributor into the ion chamber as

in Fig. 2-12. Electrons are emitted from a thermal filament which forms the cathode on the axis of the cylindrical chamber. They are attracted to the anode which is concentric with the ionization chamber. Application of a weak axial magnetic field increases their flight time from cathode to anode and hence increases the probability of a collision with a propellant atom and ionization. Electrons are prevented from striking the ends of the chamber by maintaining the latter at the same potential as the cathode. Thus a portion of the propellant is ionized by electron bombardment and a portion of these ionized particles reach the screen and are accelerated into the ion beam. Of course an electron source is required to neutralize the beam. An acceleration system similar to that discussed for contact type thrusters is employed and indeed the relations concerning thrust density and beam power density are identical.

The two propellants most frequently used have been mercury and cesium. Propellant is selected for its combination of low ionization potential, high atomic weight and handling and storage properties. Of the two above propellants mercury has the higher atomic weight and is easier to handle while cesium has the lower ionization potential. In early work mercury caused serious sputtering problems, however, various new cathode geometries seem to have solved the problem.

Efficiency of electron-bombardment thrusters like contact thrusters decreases with decreasing specific impulse. Energy loss in this device may be attributed to two main sources:

(1) energy necessary for propellant ionization

(2) energy necessary to provide electron current to the cathode

Typical ion production costs are less than 500 eV. per ion. The fact that this figure is much larger than the ionization potentials of the

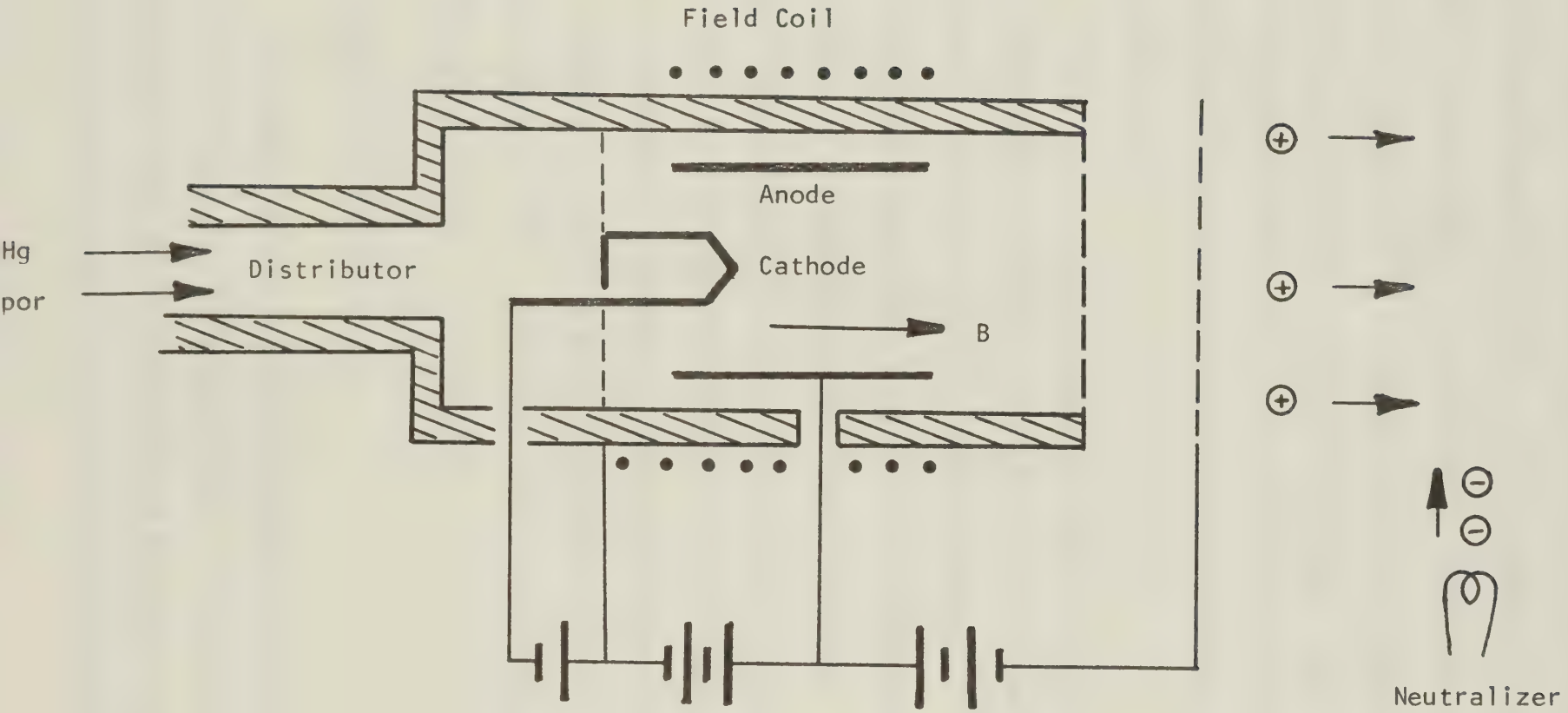

Fig. 2.12 Electron Bombardment Thruster

propellant candidates (3.89 eV for cesium and 10.4 eV for mercury) may be attributed to neutralization of some of the ionized propellant and the subsequent need for reionization. Bombardment thrusters are now capable of 70% efficiency at a specific impulse of 4000 seconds. Specifically, SERT II, a 15 cm diameter thruster, operated at 68% efficiency with I_{sp} = 4200 sec., input power of 850 watts and at a thrust of 28 mN[64]. Recently, King has reported an efficiency of 69% at I_{sp} = 2750 sec. and a nominal input power of 2.5 kw.[65]. Typical operating potentials are in the two to three kilovolt range. The problem of high voltage power conditioning may require up to 1000 extra parts.

A variation on the electron bombardment thruster is the radio frequency ion thruster. This type of thruster has been developed almost exclusively by H.W. Loeb in Germany[66]-[68]. The essential difference between this type and the conventional bombardment source lies in the method of propellant ionization. Whereas the conventional source operates in a D.C. mode, this source couples sufficient energy to the propellant for ionization by means of a radio frequency transmitter. Typically, the optimum length of the discharge chamber is between 2.5 and 3.5 cm., the diameter 10 cm. and the operating frequency 3.2 Mhz[69]. Efficiency of a 10 cm. engine operating at 309 W. input power is 71%.

2.3.3.3 Colloid Thruster

The propellant of a colloid thruster consists of submicron sized multi-electronic charged particles. These particles are accelerated through a potential difference of several kilovolts producing a thrust in the same manner as the ion engines previously discussed.

Both liquid and solid particles have received attention although success has only been attained with the former. Thrusts of approximately 0.4 millinewtons have been achieved at I_{sp} = 800 sec. and an efficiency of 70% employing sodium iodide doped glycerol as the propellant. As considerable emphasis is placed upon colloidal propulsion in this thesis; an entire chapter, the one to follow, is allotted to the discussion of this topic.

2.3.4 Additional Forms of Electric Propulsion

Other forms of electric propulsion exist, two of which are sputtering propulsion and photon propulsion. Thrust is generated by sputtering of neutral particles from a solid target. Specific impulses in the 1000 second range at thrusts of 100 μN/ma of ion current are possible[(70)-(72)]. A magnification of thrust is achieved through the multiple yield of ejected atoms per incident ion. Three main advantages of sputtering propulsion are obvious. Firstly, the problem of propellant storage is eliminated since propellant atoms may be stored in their natural state as solids. Secondly, a major portion of the propellant may be obtained from structural members such as a booster stage. Thirdly, the ion source for a sputtering engine does not require the precision components as in the case of an ion engine. Although much data is available in the sputtering field, more thorough scrutinization of this data and further experimentation is warranted in order to ascertain whether this form of propulsion will prove fruitful.

The other form of electric propulsion to be considered here is photon propulsion. A photon thruster offers the highest specific impulse attainable, namely c/g where c is the velocity of light. Of

course, since the specific impulse is the highest attainable, the price that must be paid is the highest power-to-thrust ratio necessary. The power-to-thrust ratio is easily computed for a photon thruster since it is merely the ratio of the energy per unit time E in the photon beam to the momentum transfer R per unit time. Accordingly, the beam of radiation of frequency f and wavelength λ has

$$\begin{aligned} \frac{P}{T} &= \frac{E}{R} \\ &= \frac{hf}{h/\lambda} \\ &= c \end{aligned} \qquad (2.44)$$

where h is Planck's constant. This relationship clearly illustrates the tremendous amounts of power necessary to propel a photon rocket. For example, an ion engine of I_{sp} = 6000 sec. has a power-to-thrust ratio of 30,000 watts per newton. Hence if the photon and ion rockets are to produce the same thrust, the photon rocket requires 10,000 times as much power.

The central favorable feature of photon propulsion is that at present it is the only conceivable means of accomplishing interstellar travel. The nearest stars are of the order of ten light years away[73]. If one wishes to traverse interstellar distances, one must necessarily take advantage of the time dilatation of relativity theory[74]-[76]. Unfortunately, due to the colossal amount of energy required it appears that photon propulsion is far from realizable in the near future.

3. COLLOID PROPULSION

3.1 Contemporary Colloid Thrusters

In the very early stages of electric propulsion development it was discovered that thruster efficiency varied with specific impulse. Arcjet thrusters were capable of efficient operation below I_{sp}=1000 sec. while electrostatic ion engines could hold their own above I_{sp}=5000 sec. The so-called specific impulse gap between 1000 and 5000 seconds was to be filled by the colloid thruster. This device promised extremely efficient operation over this gap. Basically two types of colloid thrusters exist: those expelling liquid particles and those expelling solid particles. As most of the research on microparticle propulsion has been devoted to liquid particle thrusters, the liquid thruster now awaits space testing. Solid particle thrusters have presented formidable problems such as particle feeding, agglomeration and manufacture, to mention only a few. Consequently, this device is relatively underdeveloped.

3.2 Liquid Colloid Thrusters

Development of liquid particles as an electrostatic propellant began seriously around 1960[77],[78]. Figure 3.1 is a sketch of the basic thruster. The propellant consists of glycerol doped with sodium iodide to increase the electrical conductivity. The liquid is forced through a capillary needle (typically 14 mil O.D. by 4 mil I.D.) and extracted by a potential V. The charged particles in the spray attain some equilibrium radius r. The equilibrium exists between the surface electrostatic forces $\frac{1}{2}\varepsilon_0 E_s^2$ per unit area (E_s is the surface electric field) and the forces $2\gamma/r$ per unit area due to the surface tension γ in the liquid. The force per unit area ΔP due to the surface tension

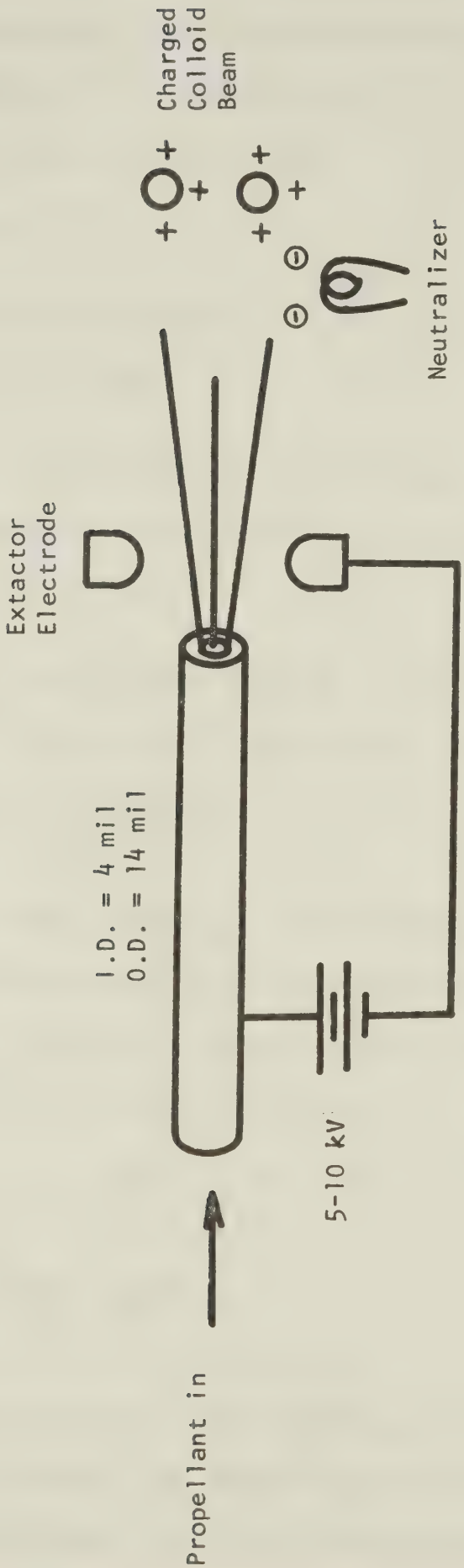

Fig. 3.1 Liquid colloid Thruster Concept

is readily calculated by considering the forces binding two hemispheres of liquid together. The equation describing the equilibrium of an uncharged droplet is $\pi r^2 \Delta P = 2\pi r \gamma$

which yields upon solving for ΔP

$$\Delta P = \frac{2\gamma}{r} \tag{3.1}$$

To maintain particle stability

$$\tfrac{1}{2} \varepsilon_o E_s^2 \leq \frac{2\gamma}{r} \tag{3.2}$$

where ε_o is the permittivity of free space.

Since the charge q on the particle is related to the surface field E_s by [79] $q = 4\pi \varepsilon_o r^2 E_s$ (3.3)

the maximum charge-to-mass ratio of a stable particle having average mass density ρ_m and mass m is obtained from the relation

$$\frac{q}{m} \leq \frac{6}{\rho_m} \left(\frac{\gamma \varepsilon_o}{r^3} \right)^{\frac{1}{2}} \tag{3.4}$$

The charge-to-mass ratio is a very important parameter of colloid thrusters and consequently has received much attention [80]-[83]. Application of conservation of energy leads to an expression for exhaust velocity and hence specific impulse.

$$u_{ex} = \left(2 \frac{q}{m} V \right)^{\frac{1}{2}} \tag{3.5}$$

or $$I_{sp} = \left(\frac{2}{g^2} \frac{q}{m} V \right)^{\frac{1}{2}} \tag{3.6}$$

From the above equations, the importance of the charge-to-mass ratio is glaringly obvious. To obtain high specific impulse it is clear that particles should display low mass density, have very small radii

(submicron) and a large surface tension coefficient. For example, an exhaust beam composed of particles for which $r = 10^{-8}$m., $\gamma = 72.7$ dyne/cm., $\rho_m = 1.44$ gm/cm^3 being accelerated through a potential difference of 5.6 kilovolts will exhibit a specific impulse of 625 seconds[84]. Of all types of colloid thrusters, the liquid type has definitely received the most attention[85]-[103]. Present modules develop thrusts of about 100 μlb. at I_{sp}'s ranging from 500 to 1000 sec. at a minimal accelerating voltage of six kilovolts[104]. In addition to needle thrusters, slit and annular types have been developed[105]-[107]. Schemes such as bipolar operation to eliminate the necessity for neutralization and operation from AC sources have been investigated in various laboratories[108],[109]. Thus it can be truthfully said that liquid colloid thrusters are ready for space testing the moment some group decides to incorporate them in a space test.

Another type of colloid thruster not to be excluded is the condensation thruster. The desire in constructing a colloid source is to create particles having a charge-to-mass ratio ranging from about 100 to 10^5 coulombs per kilogram. This desire may be fulfilled by a condensation thruster. The first process involved in such a device is the vaporization of the propellant and subsequent ionization of a portion of the vapor. This vapor is expanded through a nozzle and stable charged condensation nuclei are formed. Growth of the nuclei is collisionally dependent and may be controlled by adjusting ion velocities with an electrostatic field. Research on this device has been conducted; however, development remains at the initial level[110]-[115].

3.3 The Physics of Solid Colloid Thrusters

Although much research has been devoted to liquid as a colloidal propellant, much less attention has been paid to solids. A few researchers have proposed microparticle charging by ion or electron bombardment[116]-[118]. It has been shown that such techniques are very inefficient[119]. Experiments have been conducted in which particles are charged by contact with a metal surface at some potential, the metal surface being the plates of a parallel plate capacitor. In one case the applied field was 10^5 volts per meter and the resulting average charge-to-mass ratio about 0.1 coul/kg.[120]. Analysis was accomplished by means of a quadrupole mass spectrometer[121]. This thesis discusses contact charging only.

Since this type of thruster is purely electrostatic, equations (3.5) and (3.6) yield the beam exhaust velocity and specific impulse. Furthermore, with the aid of equation (3.3) and the assumption that each particle has uniform mass density ρ_m, the charge-to-mass ratio of a solid spherical particle is given by

$$\frac{q}{m} = \frac{3\epsilon_o E_s}{\rho_m r} \tag{3.7}$$

An upper limit is placed upon the charge-to-mass ratio of a particle of given radius and mass density by the fact that there exists a maximum theoretical value of surface field strength. The maximum surface field strength is determined by the field electron emission limit (approximately 10^9 v/m for iron[122]) in the case of negatively charged particles and by the field ion emission limit (approximately 10^{10} v/m for tungsten[123]) in the case of positively charged particles.

In practice it has been found that the maximum value of charge-to-mass ratio as described by equation (3.7) is rarely attained in a collection of particles. The following reasons are suggested to explain this discrepancy between theory and experiment:

i) Particles and agglomerates tend to be aspherical.

ii) Particle chargeability may be a strong function of the contact area during charging and of the time interval of contact[124].

iii) The surface conditions of the particle may strongly influence the chargeability. For example, some particles are charged by contact with a layer of particles while others are charged via direct contact with the metal surface.

The maximum surface field and hence maximum charge-to-mass ratio possible were not attained in the experiments described in this thesis since idealized particle surface conditions (perfectly smooth spheres) and idealized charging techniques were absent.

A slightly more subtle factor influencing the charge-to-mass ratio is the material from which electrodes and propellant are constructed. Since the propellant particles are extremely small (micron-sized), the contact potential charge developed due to the difference in materials of propellant and electrodes can act in such a manner as to increase or decrease q/m. Cho has discussed this effect[125]. If Ve is the contact potential difference (i.e. difference in work functions of the metals) and C is the capacitance between the microparticle and electrode, then the contact potential charge Q_c is given by

$$Q_c = CV_c \qquad (3.8)$$

For particles of radius r and spacing D between particle centre and plane it can be shown that[125]

$$C = 4\pi\varepsilon_o r \sinh \xi \sum_{n=1}^{\infty} \operatorname{csch} n\xi \qquad (3.9)$$

where ξ is obtained from

$$D = r \cosh \xi \qquad (3.10)$$

The contact potential charge per volt is plotted as a function of particle radius in Fig. 3.2. The distance between particle circumference and plane is assumed to be 10^{-10}m. Q_c is positive if the particle has a lower work function than the charging plate and negative if the particle has a higher work function. Fig. 3.2 demonstrates that over the region indicated Q_c varies directly as the particle radius. Accordingly in this region Q_c/m varies inversely as the square of the particle radius. Since the charge-to-mass ratio of a particle, when contact potential charging is neglected, varies inversely as the first power of the particle radius, it is clear that the contribution to the charge-to-mass ratio from contact potential charging can be considerable for particles of very small radii. It should also be noted that conductive materials likely make better candidates for propellants than do semiconductors or insulators. The reason for this is simply that conductors contain more free electrons per unit volume than do insulators or semiconductors. While it is true that researchers claim to have charged individual particles of glass and latex to near their theoretical maximum limit[127], attempts by the author to charge a collection of particles of insulators such as aluminum oxide proved unsuccessful.

It is obvious from equation (3.7) that since the charge-to-mass

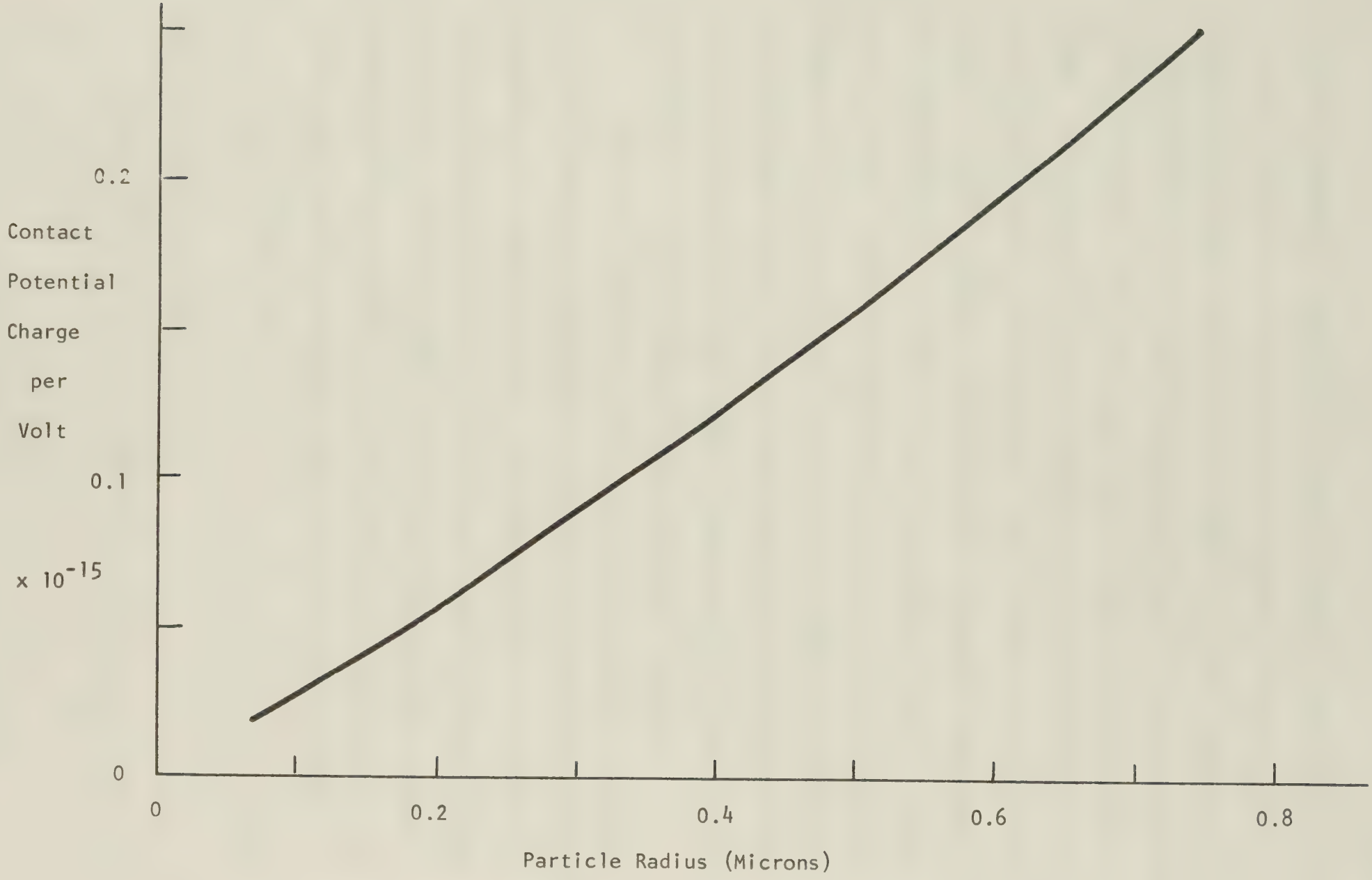

Fig. 3.2 Contact Potential Charge per Volt versus Particle Radius

ratio is inversely proportional to particle radius, particles having as small a radius as possible are most desirable. Figure 3.3 displays q/m as a function of particle radius for a field strength of 10^{10} v/m (approximately the field ion emission limit[128]) for aluminum and iron propellants. The importance of mass density is readily apparent here. Not apparent is the complimentary role played by mass density and surface electric field strength. Fig. 3.4 illustrates the dependence of specific impulse on particle size and accelerating potential. This graph demonstrates that only particles smaller than 0.1 micron radius are of interest if accelerating potentials are to be kept beneath 45 Kv. In other words, if the colloid thruster is to fill the specific impulse gap of 1000 to 5000 seconds, at an accelerating potential of 45 Kv, the largest particle acceptable will have a radius just under 0.1 microns assuming the propellant is aluminum.

The other important considerations in the physics of solid colloid thrusters are the forces on the particles and their functional dependence upon particle radius. The forces acting on a particle are the gravitational force of the earth, the electric force due to the applied field and the London - Van der Waals interparticle forces. Interparticle gravitational and coulomb forces are negligible. The gravitational force exerted on a particle by the earth is simply

$$F_g = \frac{4}{3}\pi \rho_m g r^3 \qquad (3.11)$$

For iron carbonyl particles

$\rho_m = 7800$ kg/m^3 and therefore

$F_g = 3.2 \times 10^5 r^3$

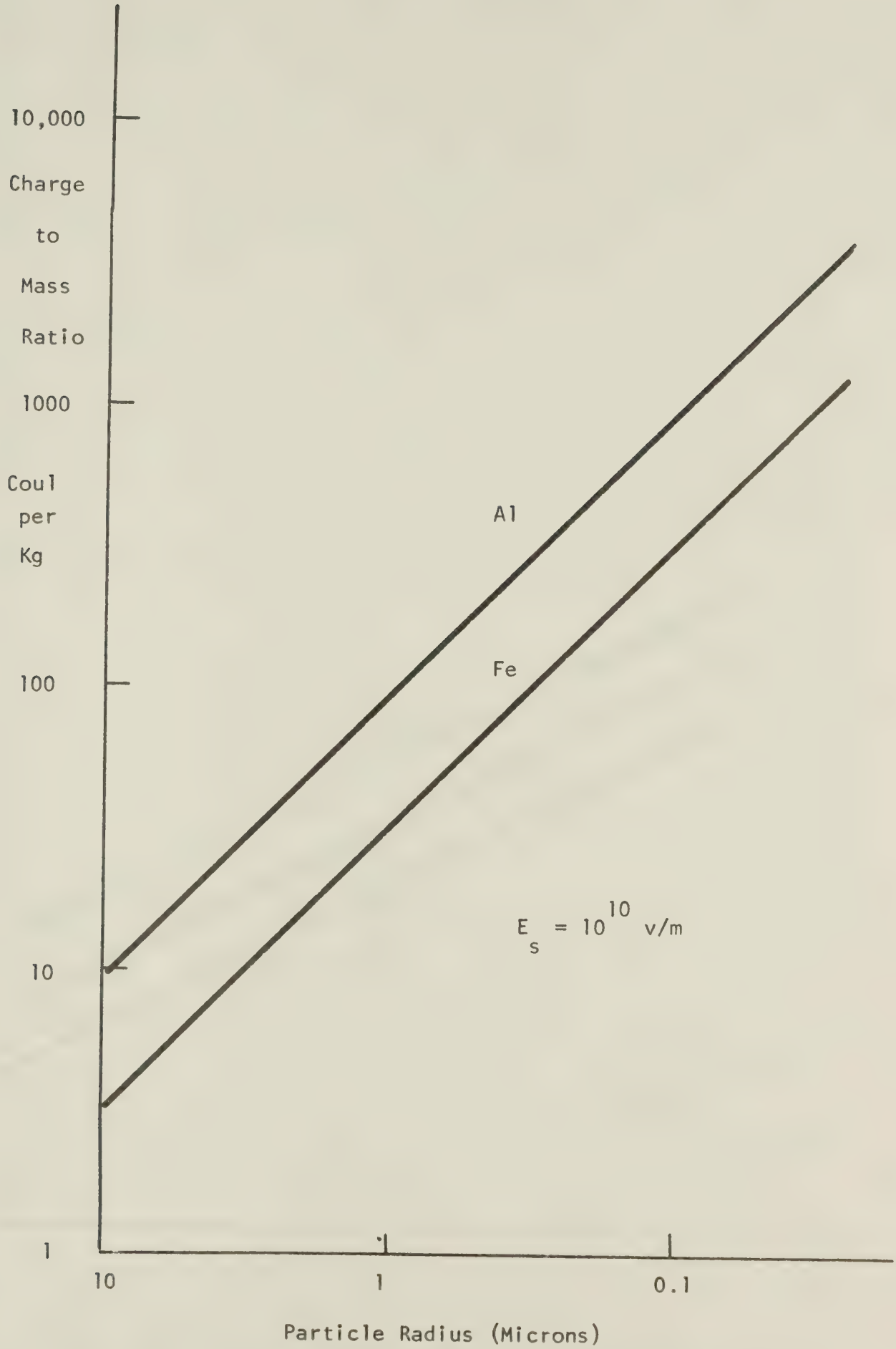

Fig. 3.3 Charge to Mass Ratio versus Particle Radius

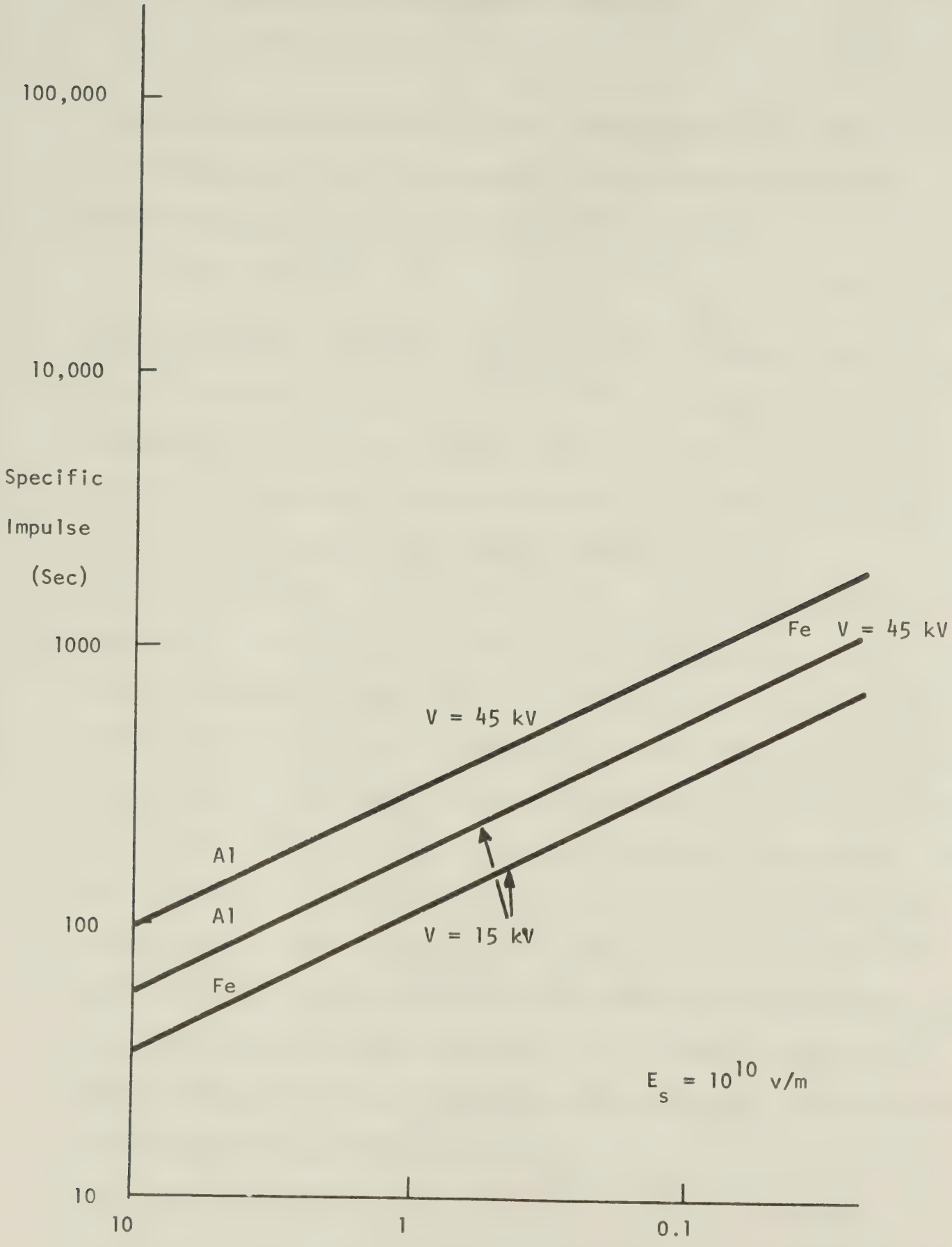

Fig. 3.4 Specific Impulse versus Particle Radius

The force due to the applied electric field is

$$F_e = 4\pi \varepsilon_o z E_a^2 r^2 \qquad (3.12)$$

where z is the proportionality factor relating particle surface field and applied field. The London - Van der Waals interparticle force between two spheres is given by[129]

$$F_l = + \frac{H}{12} \frac{r}{s^2} \qquad (3.13)$$

where H is termed the Hamaker constant and has an average value (to within one order of magnitude) of 7×10^{20} joules, and s is the circumference to circumference particle spacing chosen here as 10^{-10}m.

For three micron diameter particles it is interesting to calculate the magnitude of these forces. The results are

$F_g = 1.08 \times 10^{-12}$nt. $F_e = 1.52 \times 10^{-8}$nt. $F_l = 8.75 \times 10^{-7}$nt.

assuming $z = 1.65$ and $E_a = 6 \times 10^6$ v/m corresponding to a parallel plate configuration. (Actually F_l could fall within the range 8.75×10^{-6}nt. to 8.75×10^{-3}nt.). Examination of these three types of forces illustrates that the force of gravity is overcome by the electric field so that particles may be accelerated against gravity while London - Van der Waals forces are approximately within the same order of magnitude as the electric field forces and hence some agglomeration will still take place. Of course these formulae are based upon the assumption that all particles are spherical and charge is distributed uniformly over their surface. For order of magnitude calculations and for the purpose of comparison they certainly suffice.

3.4 Theoretical Basis for Time of Flight Analysis of Colloid Thruster Parameters

By means of time-of-flight (TOF) techniques it is possible to measure indirectly the various thruster performance parameters. The technique consists of measuring beam current decay upon the removal of the accelerating potential at some prescribed time t_o. A schematic of the detection system is shown in Fig. 3.5. A detailed description of the system is given in Chapter 5. The collecting plate is situated in a Faraday Cage a distance L from the source. Under steady state conditions the beam current i(t) has the value I_o amperes. Since particles comprising the beam have a distribution in radius it is reasonable to assume that they shall also possess a distribution in charge-to-mass ratio. The fact that these particles may attain different charge-to-mass ratios for different mass densities and different field charging conditions also contributes to this distribution in charge-to-mass ratio. Assume that all particles in the beam may be placed in discrete groups or subbeams. Now consider all particles of the n th subbeam having charge-to-mass ratio $(q/m)n$ to contribute current $(\Delta i)_n$ and mass flow rate $(\Delta\dot{M})n$ to the beam. The amount of current of the n th subbeam contributing mass flow rate $(\Delta\dot{M})n$ is

$$(\Delta i)n = \left(\frac{q}{m}\right)_n \quad (\Delta \dot{M})n \tag{3.14}$$

The particles in the n th subbeam all have the same velocity $u_{ex\ n}$. At time t_o the accelerating voltage is removed. For convenience, t_o is assigned the value of zero. Fig. 3.6 a and 3.6 b illustrate schematically the spatial distribution of the various subbeams over the distance between the accelerating electrode and the collector at times

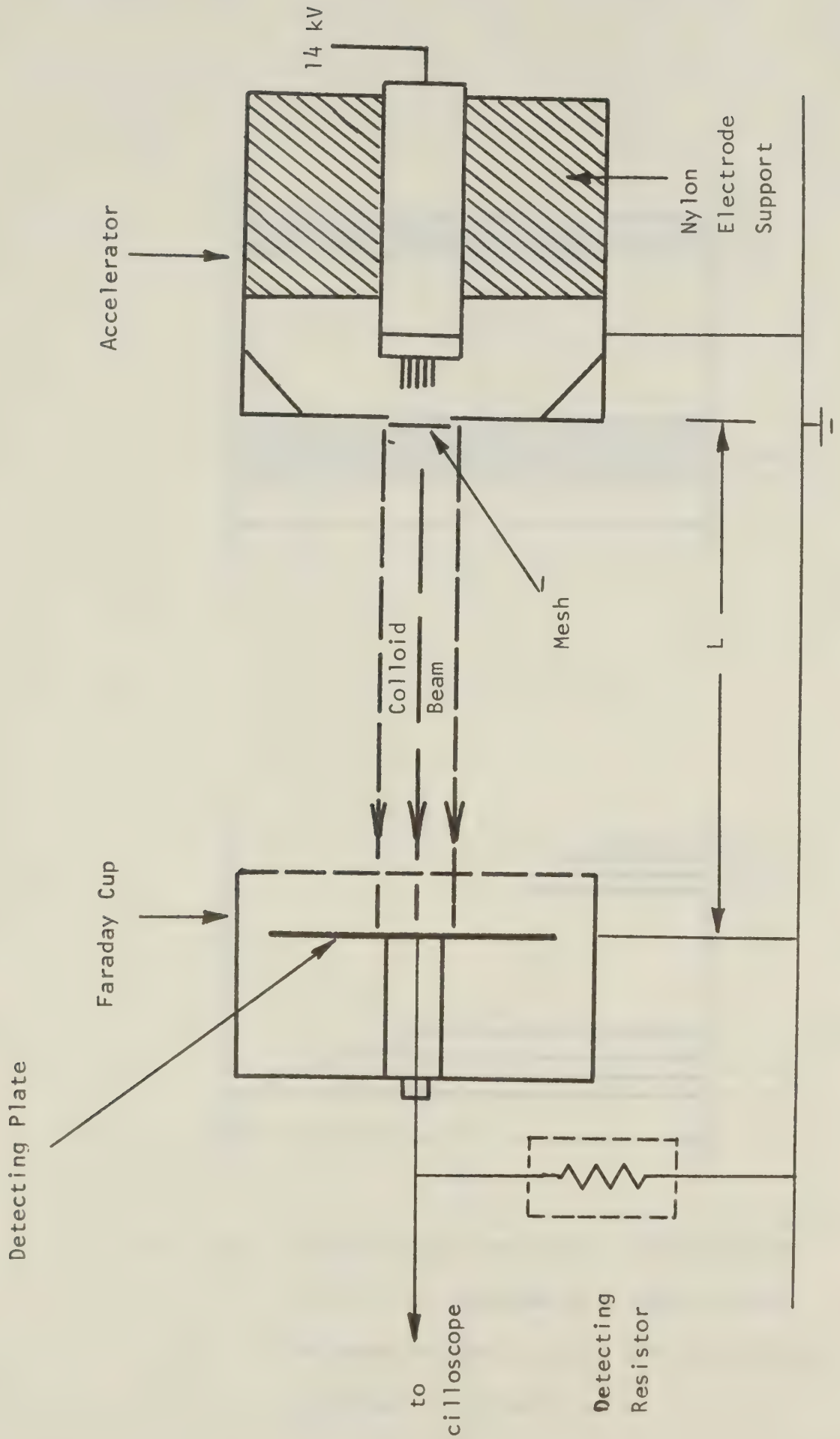

Fig. 3.5 Particle Detection Scheme

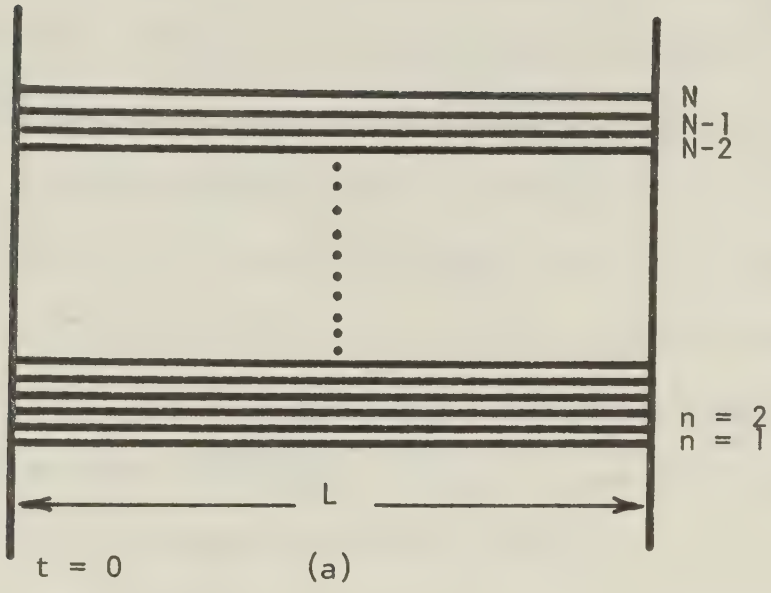

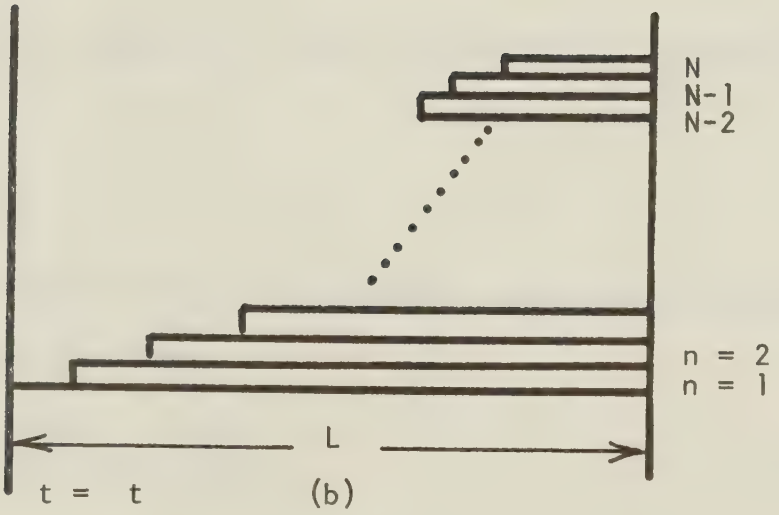

Fig. 3.6 Schematic of the Spatial Distribution of Various Subbeams Over the Distance Between the Accelerator and the Collector at Times t = 0 and t = t

$t = 0$ and $t = \Delta t$. The current remains at I_o until time t_m at which point it begins to decrease. This time t_m represents the time necessary for the trailing edge of the fastest subbeam (highest $\frac{q}{m}$) to traverse the distance L since it is travelling at constant velocity. The current is monitored by observing the voltage, on an oscilloscope, measured across a resistor placed from the detecting plate to ground. Finally after time t_f the current has decayed to zero. From the resulting trace of current versus time it is possible to determine all thruster parameters as shall be seen by the following computations.

In principle the TOF (time of flight) trace would appear as in Fig. 3.7. The n th subbeam contributes thrust

$$(\Delta T)n = u_{ex\ n}(\Delta \dot{M})_n \tag{3.15}$$

Inserting equations (3.5) and (3.14) in (3.15)

$$(\Delta T)_n = \frac{2V}{u_{exn}} \ (\Delta i)_n$$

The exhaust velocity of the n th subbeam is constant and is given by

$$u_{exn} = \frac{L}{t_n} \tag{3.16}$$

where t_n is the time at which the trailing edge of the nth subbeam reaches the collector. Thus

$$(\Delta T)_n = \frac{2V}{L} \ t_n \ (\Delta i)_n$$

The total thrust is the sum of all the incremental contributions from the various subbeams. Therefore

$$T = \sum_{n=1}^{N} (\Delta T)_n$$

$$= \sum_{n=1}^{N} \frac{2V}{L} t_n \ (\Delta i)_n \tag{3.17}$$

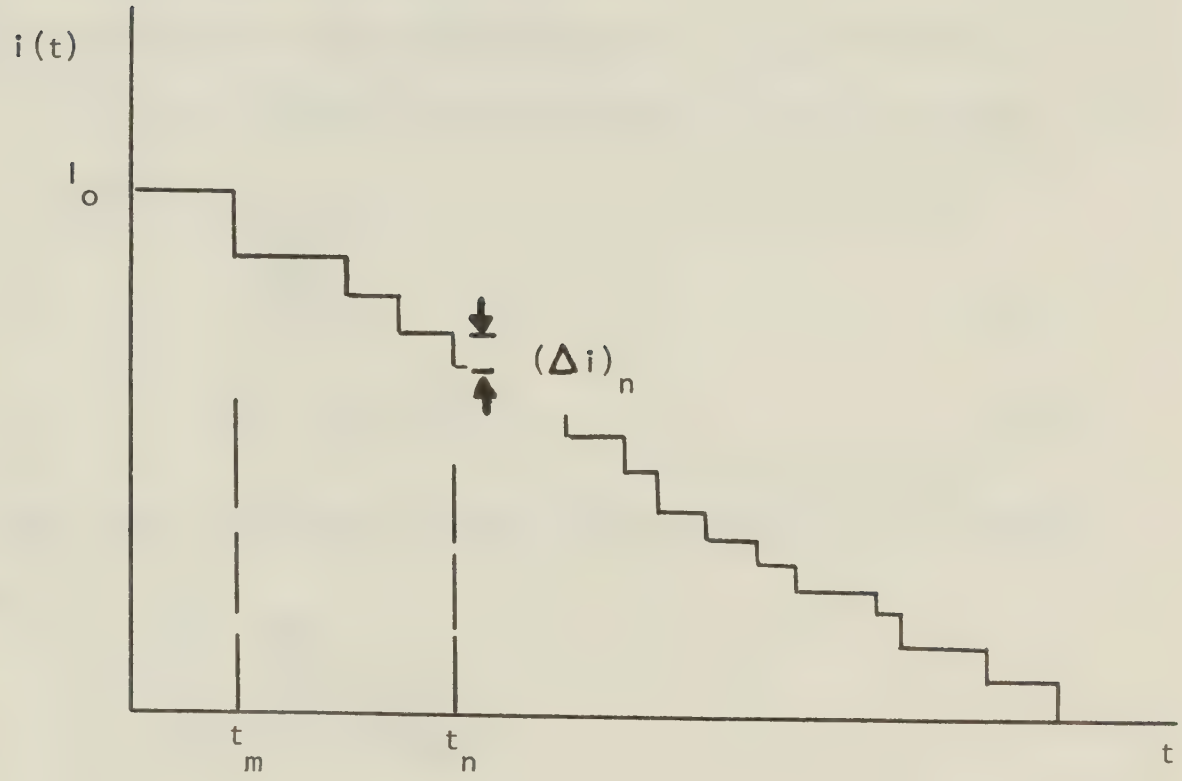

Fig. 3.7 Conceptual Sketch of TOF Trace of a Beam Having a Discrete Number of Subbeams

In practice the number of subbeams (N) is very large and the finite differences $(\Delta \dot{M})_n$, $(\Delta i)_n$, and $(\Delta T)_n$ approach zero. The discrete approach may then be replaced by a continuous approach and summation becomes integration. In this case

$$T = \frac{2V}{L} \int_{o}^{I_o} t\,di$$

$$= \frac{2V}{L} \int_{t_f}^{o} d(it) - \frac{2V}{L} \int_{t_f}^{o} i\,dt$$

Finally,

$$T = \frac{2V}{L} \int_{o}^{t_f} i\,dt \qquad (3.18)$$

This integral can be evaluated numerically from the TOF trace.

The mass flow rate may be evaluated in a similar manner. Thus

$$(\Delta \dot{M})_n = \frac{(\Delta i)_n}{\left(\frac{q}{m}\right)_n}$$

$$= \frac{2V}{L^2} t_n^2 (\Delta i)_n \qquad (3.19)$$

The total mass flow rate is obtained by summing over all subbeams. Hence,

$$\dot{M} = \sum_{n=1}^{N} (\Delta \dot{M})_n$$

$$= \sum_{n=1}^{N} \frac{2V}{L^2} t_n^2 (\Delta i)_n$$

As before the summation can be replaced by an integration when the number of subbeams is large and the finite differences approach zero. Therefore

$$\dot{M} = \int_{o}^{I_o} \frac{2V}{L^2} t^2\,di$$

$$= \frac{2V}{L^2} \int_{t_f}^{o} d(it^2) - \frac{4V}{L^2} \int_{t_f}^{o} it\,dt$$

or $$\dot{M} = \frac{4V}{L^2} \int_0^{t_f} it\, dt \qquad (3.20)$$

which again can be evaluated using TOF data.

It is possible to express all other parameters in terms of T, $\dot{M}$ and I_o. Since there exists a distribution in charge-to-mass ratio and hence velocity, all parameters computed shall be averaged. Averaging shall be done via the various mass flow rates. The average velocity of the particles in the beam is

$$\langle u_{ex} \rangle = \frac{\sum_{n=1}^{N} u_{exn} (\Delta \dot{M})_n}{\sum_{n=1}^{N} (\Delta \dot{M})_n}$$

$$= \frac{\sum_{n=1}^{N} (\Delta T)_n}{\sum_{n=1}^{N} (\Delta \dot{M})_n}$$

$$= \frac{T}{\dot{M}} \qquad (3.21)$$

The very interesting result is that the thrust is the product of the mass flow rate and the mass flow rate averaged velocity. The mean-square velocity is

$$\langle u_{ex}^2 \rangle = \frac{\sum_{n=1}^{N} u_{exn}^2 (\Delta \dot{M})_n}{\sum_{n=1}^{N} (\Delta \dot{M})_n}$$

$$= 2 \frac{\sum_{n=1}^{N} (\Delta P)_n}{(\Delta \dot{M})_n}$$

$$= 2 \frac{P}{\dot{M}} \qquad (3.22)$$

Thus the beam power is seen to be a function of the total mass flow rate and the mass flow rate averaged mean-square velocity of the beam.

The mass flow rate averaged charge-to-mass ratio is computed to be

$$\left\langle \frac{q}{m} \right\rangle = \frac{\sum_{n=1}^{N} \left(\frac{q}{m}\right)_n \ (\Delta \dot{M})_n}{\sum_{n=1}^{N} (\Delta \dot{M})_n}$$

$$= \frac{\sum_{n=1}^{N} (\Delta i)_n}{\sum_{n=1}^{N} (\Delta \dot{M})_n}$$

$$= \frac{I_o}{\dot{M}} \qquad (3.23)$$

The mass flow rate averaged charge-to-mass ratio can be computed in a different manner with the aid of equation (3.20)

$$\left\langle \frac{q}{m} \right\rangle = \left\langle \frac{u_{ex}^2}{2V} \right\rangle$$

$$= \frac{1}{2V} \frac{2P}{\dot{M}}$$

$$= \frac{I_o \ V}{V \ \dot{M}}$$

$$= \frac{I_o}{\dot{M}}$$

When a colloidal thruster has a distribution in q/m and hence in u_{ex}, the power required to produce a given thrust is

$$P_{distrib} = \tfrac{1}{2} \dot{M} \left\langle u_{ex}^2 \right\rangle$$

$$= \tfrac{1}{2} \frac{\left\langle u_{ex}^2 \right\rangle}{\left\langle u_{ex} \right\rangle} T$$

since $T = \dot{M} \langle u_{ex} \rangle$. An ideal device, one with no distribution in exhaust

velocity, and with exhaust velocity equal to the mass flow rate averaged exhaust velocity of the thruster producing the distribution, only requires the power

$$P_{ideal} = \tfrac{1}{2} \dot{M} \langle u_{ex} \rangle^2$$

$$= \tfrac{1}{2} \langle u_{ex} \rangle T$$

to produce the same thrust, T. Thus a distribution efficiency may be defined as

$$\eta_u = \frac{P_{ideal}}{P_{distrib}} = \frac{\langle u_{ex} \rangle^2}{\langle u_{ex}^2 \rangle} \tag{3.24}$$

Expressed in terms of charge-to-mass ratio

$$\eta_u = \frac{\langle \left(\frac{q}{m}\right)^{\frac{1}{2}} \rangle^2}{\langle \frac{q}{m} \rangle} \tag{3.25}$$

The last parameter to be discussed is the efficiency η_d which arises from the fact that all particles do not travel in the same direction but disperse throughout a cone of half angle ψ. As a result of this dispersion the thrust of the beam is decreased from the amount it would be, were all particle velocity vectors parallel. In the analysis following, it is assumed that the same charge-to-mass distribution exists in each element of solid angle $d\Omega$. Furthermore, the mass flow rate per unit solid angle $d\dot{M}/d\Omega$ is isotropic and therefore constant. It is readily calculated as below.

$$\frac{d\dot{M}}{d\Omega} = G \tag{3.26}$$

Integrating equation (3.26) to find G

$$\int d\dot{M} = G \int d\Omega$$

$$= G \int_0^{\psi} \int_0^{2\pi} \frac{r^2 \sin\theta \, d\theta \, d\phi}{r^2}$$

where (r, θ, ϕ) are the coordinates of a conventional spherical coordinate system. The apex of the cone of dispersion is located at the origin and the axis of the cone extends along the $\theta = 0$ axis. Evaluating the integral on the right and solving for G

$$G = \frac{\dot{M}}{2\pi (1 - \cos\psi)}$$

or

$$\frac{d\dot{M}}{d\Omega} = \frac{\dot{M}}{2\pi (1 - \cos\psi)} \tag{3.27}$$

The thrust of the dispersed beam may be calculated by a similar integration over the cone. The component of thrust per unit solid angle that contributes useful or axial thrust is

$$dT_{axial} = \frac{d\dot{M}}{d\Omega} \langle u_{ex} \rangle \cos\theta \, d\Omega \tag{3.28}$$

Employing equation (3.27) and integrating

$$T_{axial} = \frac{\dot{M}\langle u_{ex} \rangle}{2\pi (1 - \cos\psi)} \int_0^{2\pi} \int_0^{\psi} \frac{\cos\theta \, r^2 \sin\theta \, d\theta \, d\phi}{r^2}$$

or

$$T_{axial} = \dot{M}\langle u_{ex} \rangle \frac{(1 + \cos\psi)}{2} \tag{3.29}$$

Thus, when a beam is dispersive the power required to produce a given axial thrust is

$$P_{disp} = \tfrac{1}{2} \dot{M} \langle u_{ex}^2 \rangle \tag{3.30}$$

Substituting equation (3.24) in (3.30)

$$P_{disp} = \frac{1}{2} \frac{T_{axial}^2}{\dot{M} \eta_u} \frac{4}{(1 + \cos\psi)^2}$$

A device ejecting a paraxial beam having the same mass flow rate and having exhaust velocity equal to the mass flow rate averaged exhaust velocity of the dispersive device only requires the power

$$P_{axial} = \frac{1}{2} \dot{M} \langle u_{ex} \rangle^2$$

$$= \frac{1}{2} \frac{T^2}{\dot{M}}$$

since in this case $T = \dot{M} \langle u_{ex} \rangle$, to produce the thrust T such that $T = T_{axial}$. Hence a total efficiency may be defined as

$$\eta_t = \frac{P_{axial}}{P_{disp}}$$

$$= \eta_u \frac{(1 + \cos\psi)^2}{4}$$

Thus a dispersive efficiency may be defined as

$$\eta_d = \frac{(1 + \cos\psi)^2}{4}$$

Of course, all practical thrusters will have dispersion as well as distribution efficiencies.

4. THE EXPERIMENTAL THRUSTER AND DETECTOR

4.1 High Vacuum System

The high vacuum system used consisted of a six inch oil diffusion pump backed by a 13.7 cfm roughing pump. Fig. 4.1 is a photograph of the system. The experiment was carried out at a pressure of 10^{-7} torr in order to eliminate atmospheric drag on the particles and to allow use of higher electric field strengths without danger of breakdown. With this system it was possible to pump the experimental chamber from atmospheric pressure to 10^{-7} torr in approximately twenty minutes.

4.2 The Thruster

A sketch of the thruster appears in Fig. 4.2. The necessary component sizes are indicated. A photograph appears in Fig. 4.3. As may be seen from the sketch and photograph, the device is coaxial in construction, the central electrode being supported by a nylon dielectric into which the former is screwed. The aperture is covered by a 0.125" mesh grid. A conical insert is located around the front wall of the accelerator to enhance particle agitation. The particles are thought to scatter from the conical insert in such a manner as to produce a high density dust cloud in the proximity of the accelerating electrode. Indeed, it was found that removal of the insert reduced the beam current below the measureability of the detector used in this experiment. Several electrode configurations were devised consisting of either an arrangement of needles, razor blades or a flat plate. Needle electrodes were found to produce beam currents of less than

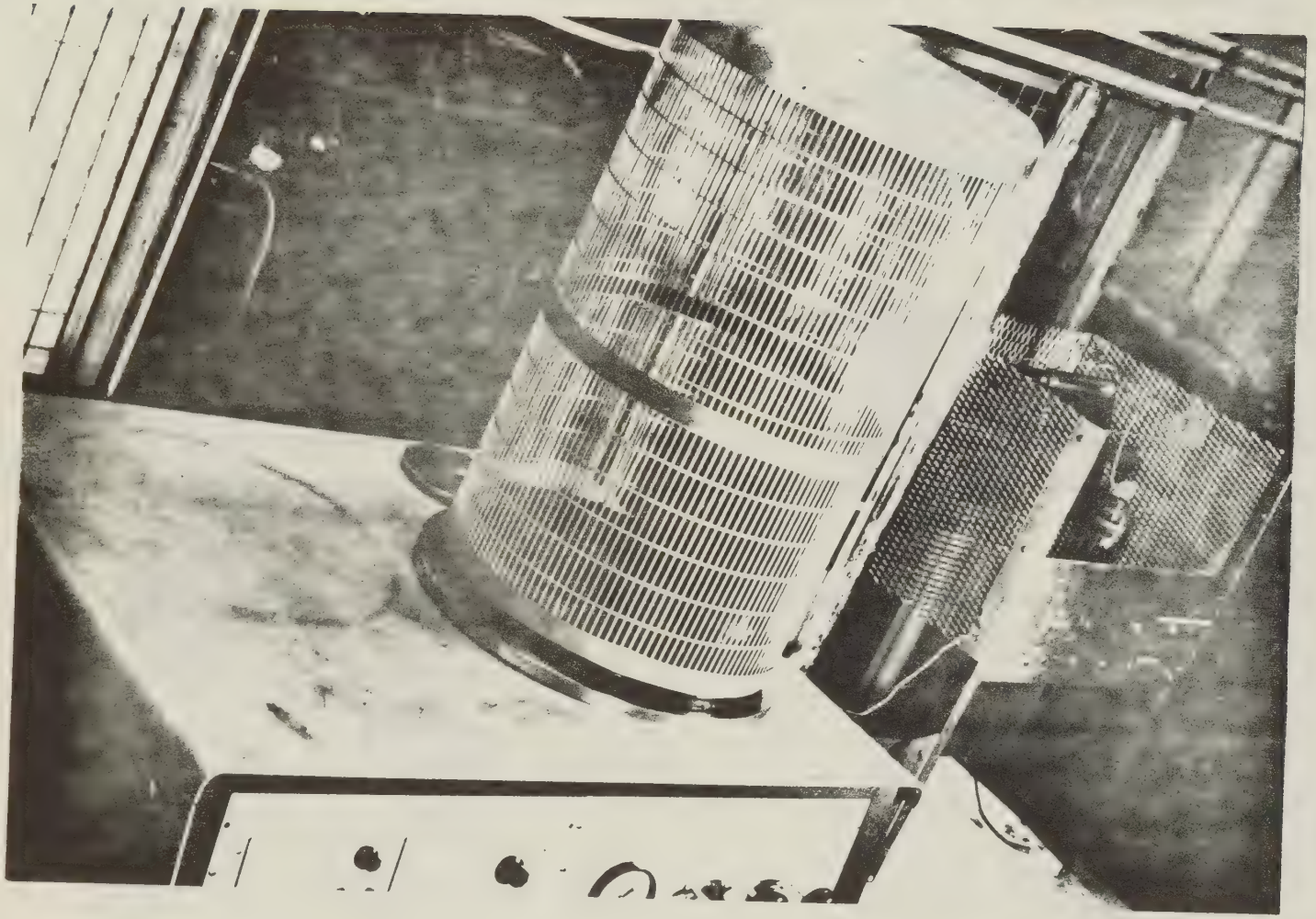

Fig. 4.1 Photograph of Vacuum System

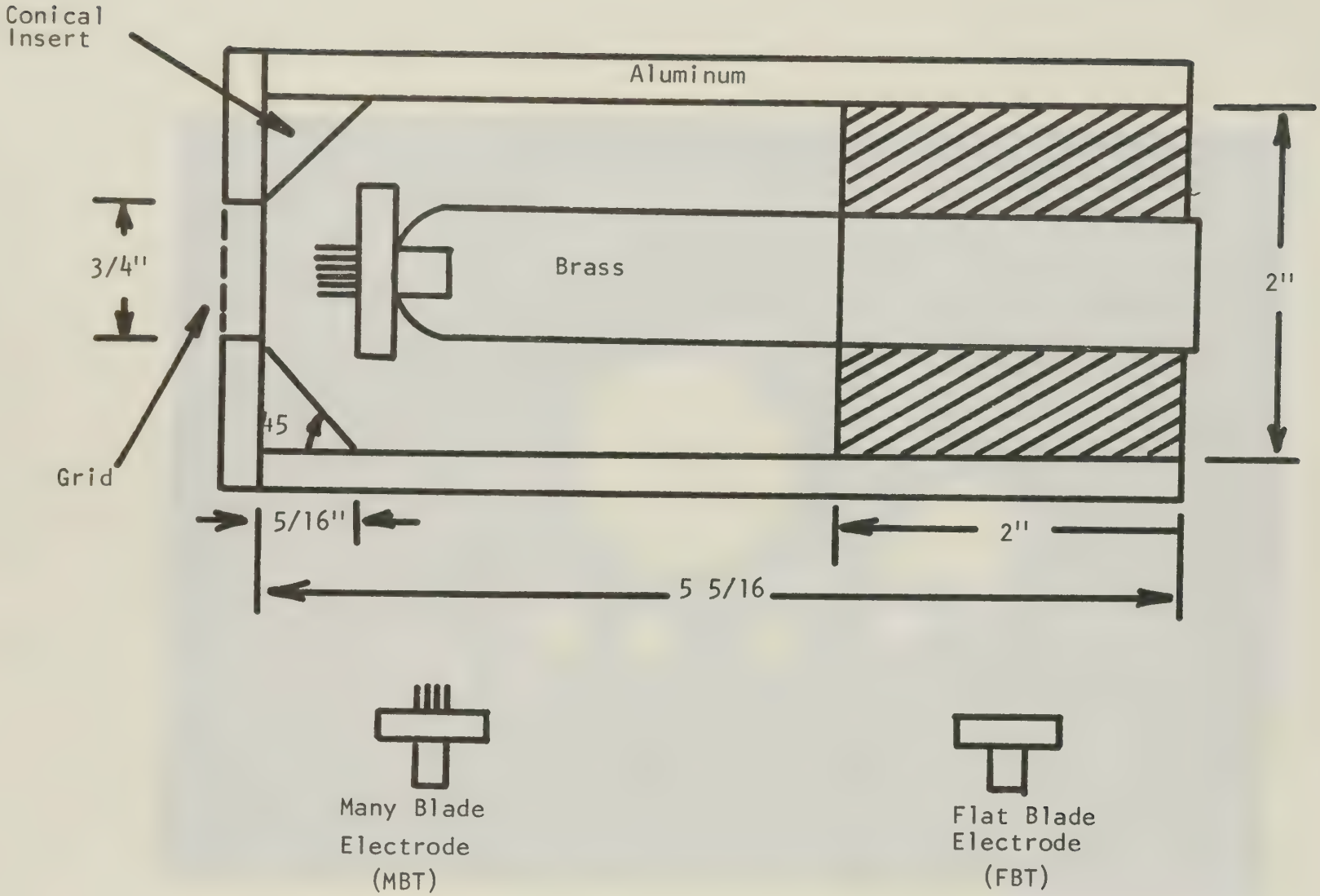

Fig. 4.2 Sketch of Thruster and Components

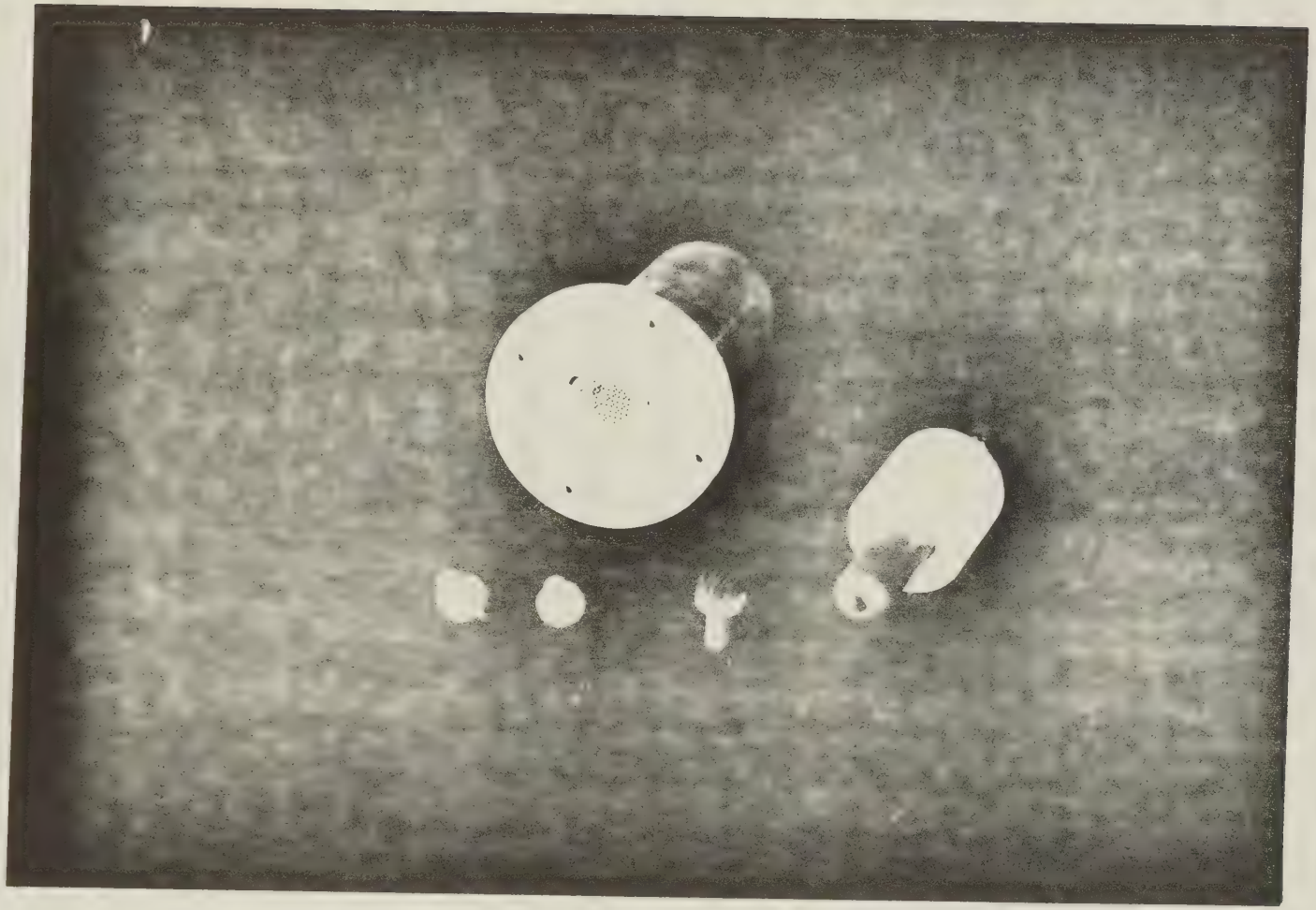

Fig. 4.3 Photograph of Thruster and Components

25 na. and for this reason were not used for TOF tests. Three types of blade electrodes were constructed; a three blade, a six blade and a many blade (17 blades closely packed) type, the latter being used throughout the majority of the TOF tests. The maximum average electric field strength possible without continuous breakdown under vacuum was about 6×10^6 v/m. Average electric field in this case is applied potential divided by interelectrode spacing. The entire thruster was anchored on a plate which moved in a vertical plane for adjustment. The bottom edge of the vertical plane was located on the base plate of the vacuum system.

4.3 Switching Circuitry

The purpose of the switching circuitry was to remove the accelerating voltage from the central electrode in a time very much less than the time of flight of the fastest particle, t_m. Equation (3.7) may be employed to estimate the maximum q/m in the beam. To do this choose $E_s = 10^8$ v/m, $\rho_m = 7.8 \times 10^3$ kg/m^3 and r = 1 micron. An upper limit on q/m is thus about 1 coul/kg. With this information, equations (3.5) and (3.16) may be employed along with the fact that L = 10cm. and V = 14 Kv to find $t_m = 0.1$ msec. Hence a switching time for the high voltage of the order of 1 μsec is necessary. This time was accomplished through the use of a hydrogen thyratron. The entire switching circuit is shown in Fig. 4.4. The hydrogen thyratron was chosen as the high voltage switch because of its low "conducting voltage drop" (about 100 volts) as well as its fast switching ability. The anode of the thyratron was connected directly to the thruster via a high vacuum feedthrough. The 5C22 thyratron was capable of with-

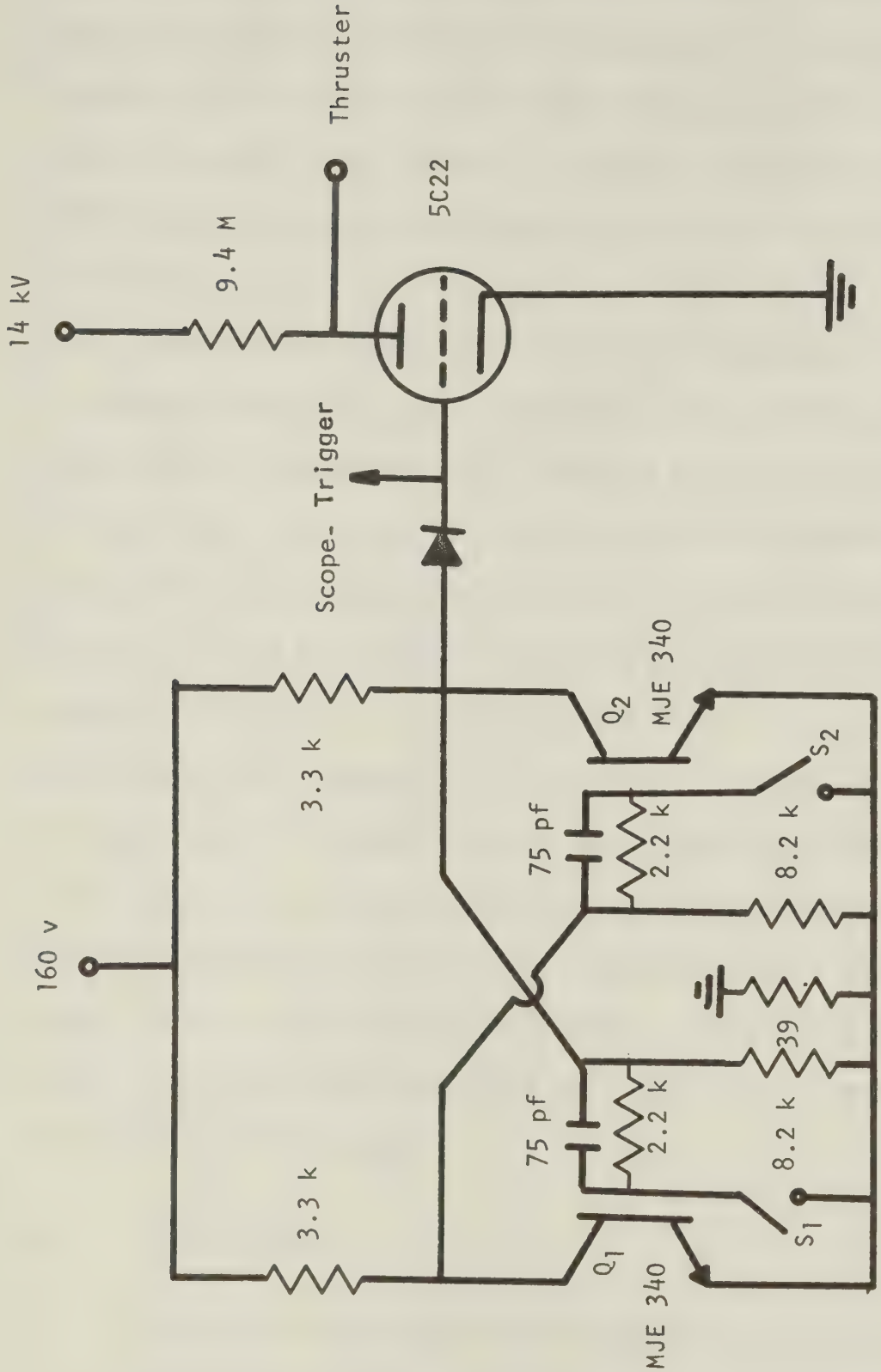

Fig. 4.4 Schematic of Switching Circuit

standing 16 Kv and since the anode resistor was 9.4 MΩ the tube was operating below its so-called holding current. It was driven by a bistable multivibrator as shown which acted as a D.C. switch. The diode in the grid lead was used to protect the driving transistors from reverse voltage spikes appearing at the grid after ionization of the hydrogen.

The circuit operated in the following manner. With switch S_1 closed, transistor Q_2 was saturated, the grid of the thyratron was essentially at ground potential, and the thyratron was thus in the off condition: thus the full potential of 14 Kv appeared across the electrodes of the thruster and particles were accelerated. Opening switch S_1 caused no changes. Switch S_2 was then closed, Q_2 did not conduct and current was supplied to the thyratron. If enough current and voltage were supplied to the thyratron it conducted fully. In this case about 40 ma and 25 volts were found to be necessary. In this fashion the thyratron was found to switch in the order of 1 μsec. The oscilloscope was triggered from the grid and the delay time between grid and anode pulses was found to be in the order of 1 μsec. A ten to one probe attenuated the grid signal to trigger a Tektronix 549 storage oscilloscope.

4.4 The Detector

Since the purpose of these experiments was primarily to develop TOF apparatus more emphasis is placed on the detector than on the thruster. The purpose of the detector was to measure the beam current decay. A sketch of the detector is shown in Fig. 4.5 and a photograph in Fig. 4.6. The detecting plate was fastened to a nylon support and

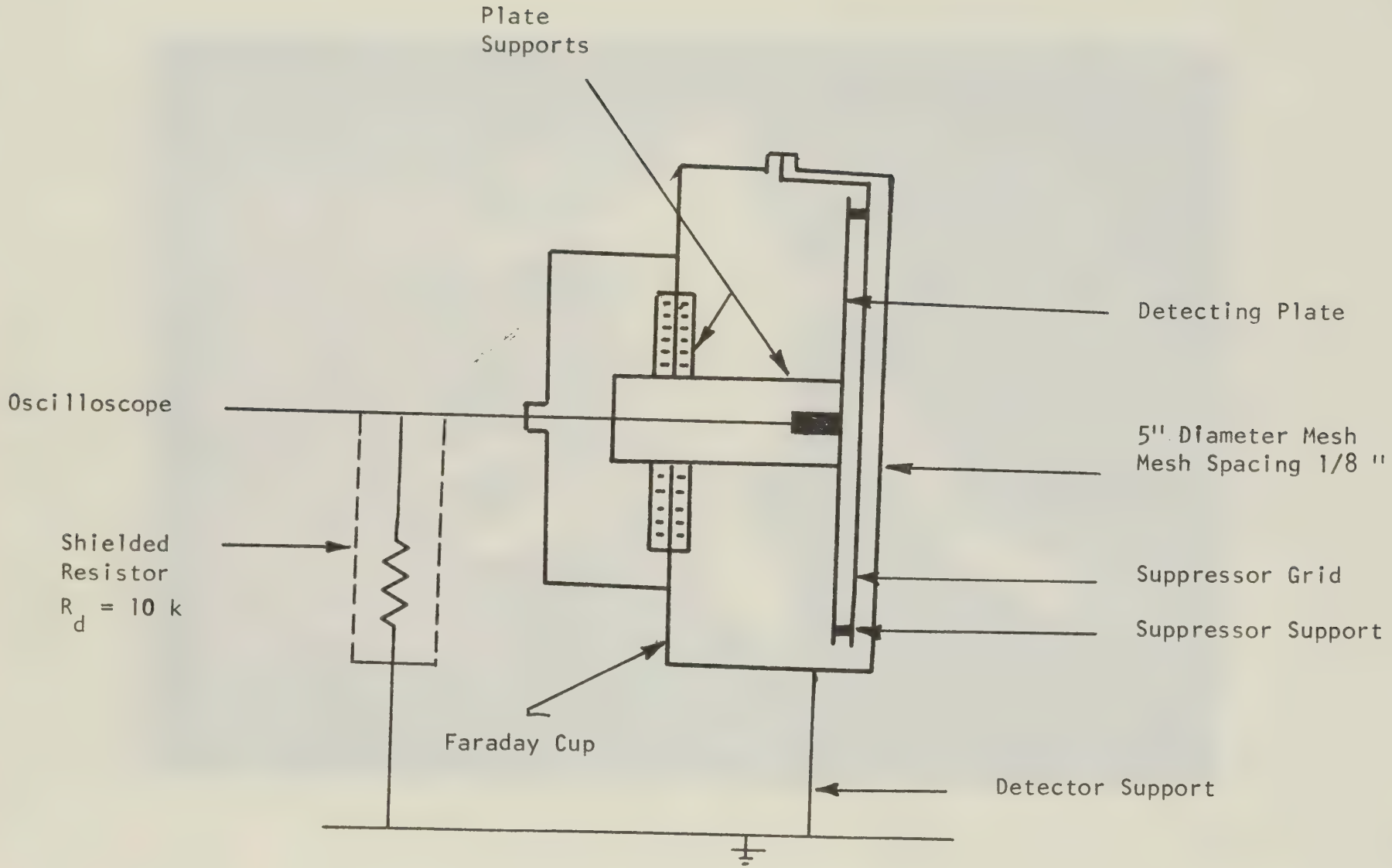

Fig. 4.5 Sketch of Detector

Fig. 4.6 Photograph of Detector

placed inside a Faraday Cup to provide adequate shielding from stray fields. All electrical feedthroughs were coaxial in nature, once more, to shield from stray fields. A suppressor grid was included and was operated at a series of negative potentials to prevent false current readings possibly caused from secondary emission of electrons due to solid particle bombardment. It was found to have no effect however. It is assumed that the reason the suppressor had no effect is that the velocity and hence the energy of the solid particles was not sufficient to cause secondary emission. In contrast, it has been found by other researchers using liquid particles at speeds in excess of 1 km/sec. that a suppressor grid is necessary[130]. The value of the resistor chosen was obtained in the following manner. The capacitance to ground of the detector was measured as 22 pf. The capacitance of the coaxial cable (about five feet in length) linking the oscilloscope to the detector was measured as 173 pf. The capacitance of the oscilloscope was 47 pf. The total capacitance was therefore 242 pf. Naming this capacitance C_{def} and the detecting resistor R_d, the relationship that must be satisfied is

$$R_d C_{def} \ll t_m \qquad (4.1)$$

As stated earlier t_m = 0.1 msec. If C_{def} = 242 pf

$$R_d \ll 400 \text{ K}\Omega$$

Accordingly a value of R_d = 10 kΩ was chosen. The distance L between the detector and the thruster was chosen simply so that t_m could be easily measured on the oscilloscope employed. The value used was L = 10.4 cm yielding a t_m = 0.1 msec. Since the steady state beam current was typically 50 na to 150 na, the maximum voltages produced

across the 10 KΩ resistor ranged from 0.5 mv. to 1.5 mv. Finally, all devices were grounded to a common point thus eliminating any signals due to so-called "ground loops". The results obtained using this method of detection are presented in the following section.

4.5 Presentation and Discussion of Experimental Results

The results obtained during the course of the experiments carried out are presented in Fig. 4.7 to Fig. 4.13. In all cases the accelerating potential was 14 Kv and the propellant consisted of micron sized iron carbonyl spheres. In Fig. 4.7 to Fig. 4.11 the accelerator electrode was of the many blade configuration (MBT) while for the others it was of the flat blade configuration (FBT). It can be seen (as expected) that the maximum charge-to-mass ratio produced by the MBT thruster was higher (by approximately one order of magnitude) than that produced by the FBT thruster. The reason, of course, is that the charging electric field of the MBT device was higher. The data of Fig. 4.7 and Fig. 4.8 represent the most promising results in the sense that the specific impulse was the highest attained in the course of these experiments. Both photographs display the initial flat portion of the trace and the decaying tail. The fact that the corresponding individual parameters vary only slightly attests to the repeatability of individual trials. Approximate values of beam current, thrust and specific impulse, obtained by numerical integration of the trace data, were 140 na., 210 μN and 1.3 sec. respectively. It was noted that any two trials performed under the same conditions yielded the same results at least to within the degree indicated by Fig. 4.7 and Fig. 4.8. The phrase "same conditions" implies such

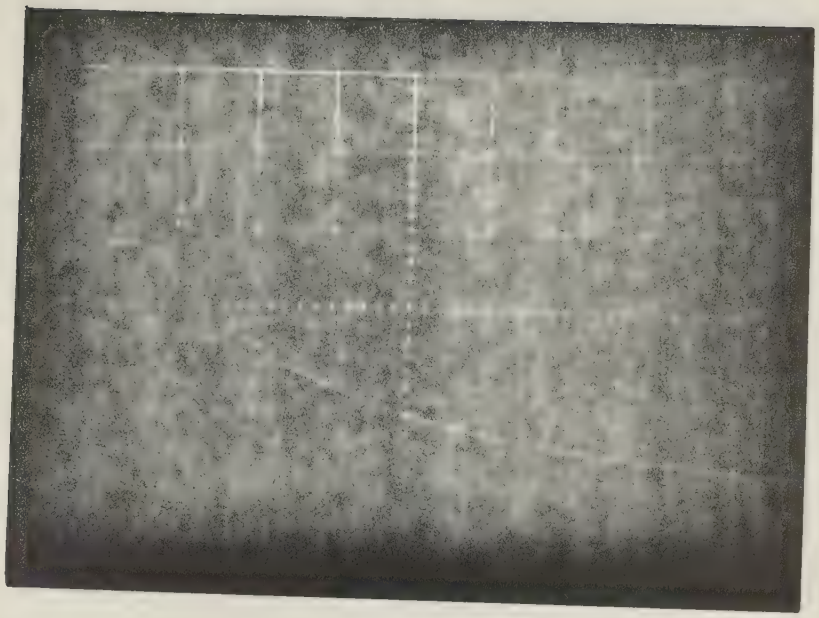

Sensitivity: 0.5 mv/cm 2 ms/cm

Many Bladed Thruster

Propellant: 3 micron iron carbonyl

V = 14 kV

I_o = 140 na

T = 208 μN

$\dot{M}$ = 16.1 x 10^{-6} kg/sec

$\langle u_{ex} \rangle$ = 12.9 m/sec

I_{sp} = 1.32 sec

$\langle \frac{q}{m} \rangle$ = 8.7 x 10^{-3} coul/kg

$\langle \frac{q}{m}^{1/2} \rangle^2$ = 5.95 x 10^{-3} coul/kg

$(\frac{q}{m})_{max}$ = 0.48 coul/kg

η_u = 68 %

Fig. 4.7 Oscillogram of Time of Flight Trace

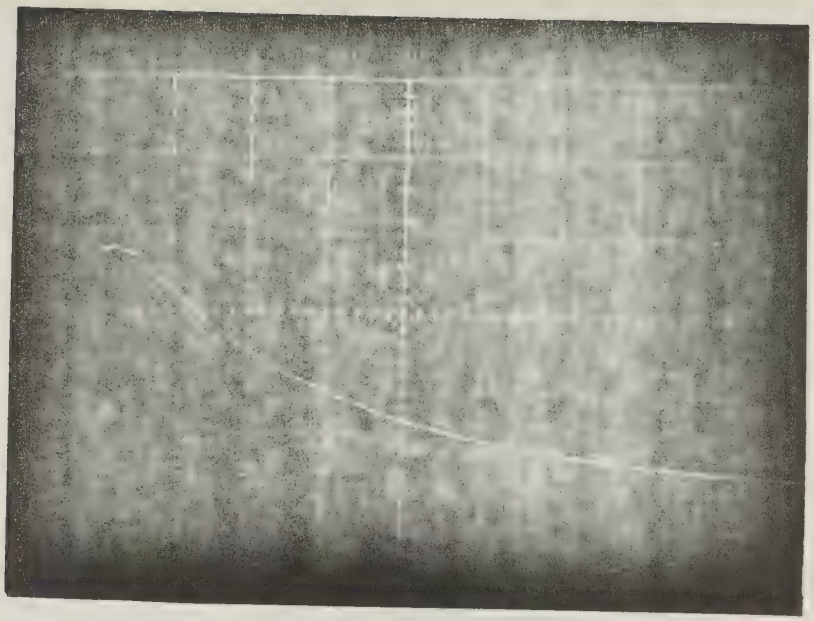

Sensitivity: 0.5 mv/cm 2ms/cm

Many Bladed Thruster

Propellant: 3 micron iron carbonyl

V = 14 kV I_o = 138 na

T = 206 μN $\dot{M} = 16.3 \times 10^{-6}$ kg/sec

$\langle u_{ex} \rangle$ =12.6 m/sec I_{sp} = 1.28 sec

$\left\langle \frac{q}{m} \right\rangle = 8.48 \times 10^{-3}$ coul/kg $\left\langle \frac{q}{m}^{1/2} \right\rangle^2 = 5.67 \times 10^{-3}$ coul/kg

$\left(\frac{q}{m} \right)_{max}$ = 0.60 coul/kg η_u = 67 %

Fig. 4.8 Oscillogram of Time of Flight Trace

factors as the same amount of propellant in each case, the same electrode geometry, photographs taken at the same time into the trial, the same type of propellant.

Fig. 4.10 and Fig. 4.11 indicate thruster operation at a lower beam current. This data was obtained approximately half way through a test run; that is, one half of the fuel had been ejected. Although the current and thrust have decreased from the corresponding quantities of Fig. 4.7, the mass flow rate has not. Consequently, charge-to-mass ratio, velocity and specific impulse have decreased.

In the above four cases, 3 micron diameter particles were utilized as propellant. It is interesting to compare the parameters of a beam composed of 8 micron diameter particles with those of a beam composed of 3 micron diameter particles. Data derived from 8 micron diameter particles is presented in Fig. 4.11. Upon examination of this data it is obvious that the beam current has decreased from that of the three micron powder, the thrust has remained essentially the same, the mass flow rate has increased by almost a factor of two and hence the charge-to-mass ratio has decreased by a factor of four and the specific impulse by a factor of two.

Two further tests were conducted with a flat bladed electrode (FBT) for the sake of comparison with the MBT. The data from these tests is presented in Fig. 4.12 and Fig. 4.13. In both cases the current, charge-to-mass ratio and velocity decreased with respect to the corresponding quantities produced by the MBT device while the thrust, mass flow rate and beam distribution efficiency increased. Of course, the decrease in charge-to-mass ratio is to be expected, since the local charging electric field of the FBT was less than that of the

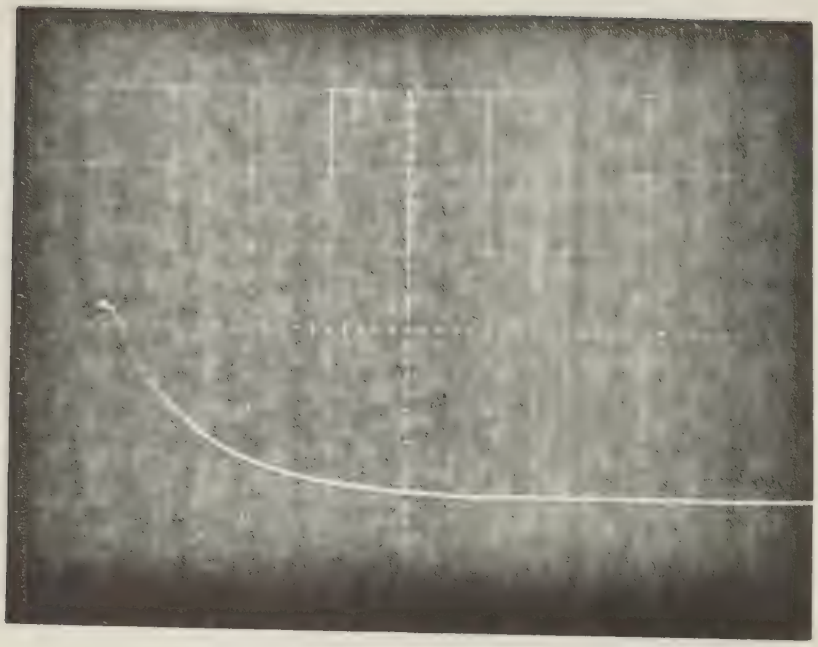

Sensitivity: 0.5 mv/cm 5 ms/cm

Many Bladed Thruster

Propellant: 3 micron iron carbonyl

$V = 14$ kV $I_o = 115$ na

$T = 183$ μN $\dot{M} = 15.9 \times 10^{-6}$ kg/sec

$\langle u_{ex} \rangle = 11.5$ m/sec $I_{sp} = 1.18$ sec

$\left\langle \frac{q}{m} \right\rangle = 7.24 \times 10^{-3}$ coul/kg $\left\langle \frac{q}{m}^{1/2} \right\rangle^2 = 4.73 \times 10^{-3}$ coul/kg

$\left(\frac{q}{m} \right)_{max} = 0.39$ coul/kg $\eta_u = 65$ %

Fig. 4.9 Oscillogram of Time of Flight Trace

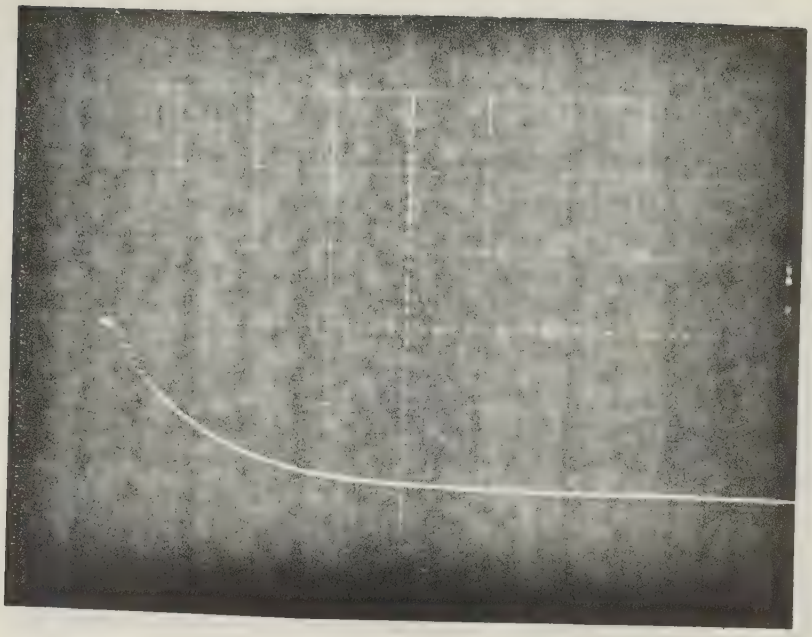

Sensitivity: 0.5 mv/cm 5 ms/cm

Many Bladed Thruster

Propellant: 3 micron iron carbonyl

V = 14 kV I_o = 100 na

T = 164 μN $\dot{M} = 14.7 \times 10^{-6}$ kg/sec

$\langle u_{ex} \rangle$ = 11.1 m/sec I_{sp} = 1.14 sec

$\langle \frac{q}{m} \rangle = 6.8 \times 10^{-3}$ coul/kg $\langle \frac{q}{m}^{1/2} \rangle^2 = 4.4 \times 10^{-3}$ coul/kg

$(\frac{q}{m})_{max}$ = 0.37 coul/kg η_u = 65%

Fig. 4.10 Oscillogram of Time of Flight Trace

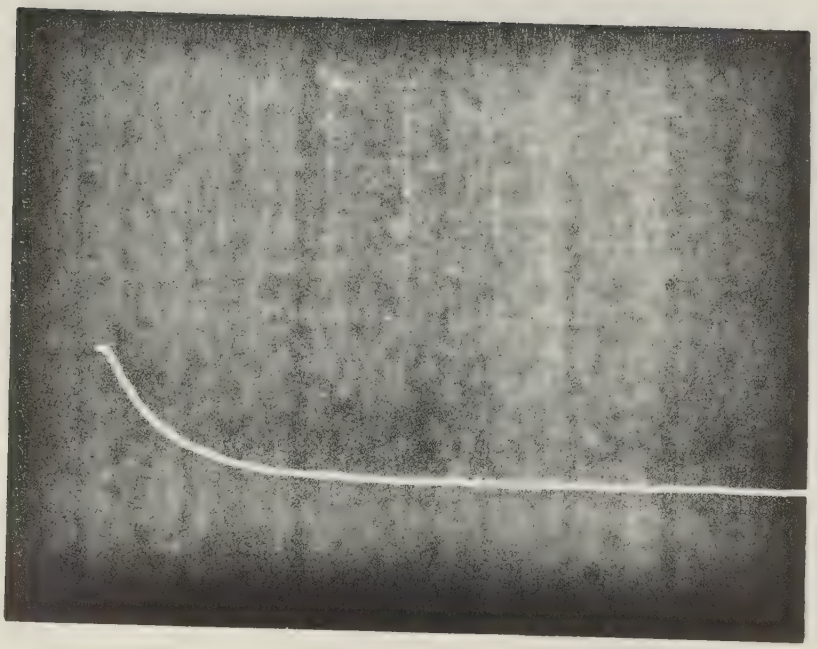

Sensitivity: 0.5 mv/cm 10 ms/cm

Many Bladed Thruster

Propellant: 8 micron iron carbonyl

V = 14 kV

I_o = 80 na

T = 210 μN

$\dot{M}$ = 27.9×10^{-6} kg/sec

$\langle u_{ex} \rangle$ = 7.53 m/sec

I_{sp} = 0.768 sec

$\left\langle \frac{q}{m} \right\rangle = 2.86 \times 10^{-3}$ coul/kg

$\left\langle \frac{q}{m}^{1/2} \right\rangle^2 = 2.02 \times 10^{-3}$ coul/kg

$\left(\frac{q}{m} \right)_{max} = 9.6 \times 10^{-2}$ coul/kg

η_u = 71 %

Fig. 4.11 Oscillogram of Time of Flight Trace

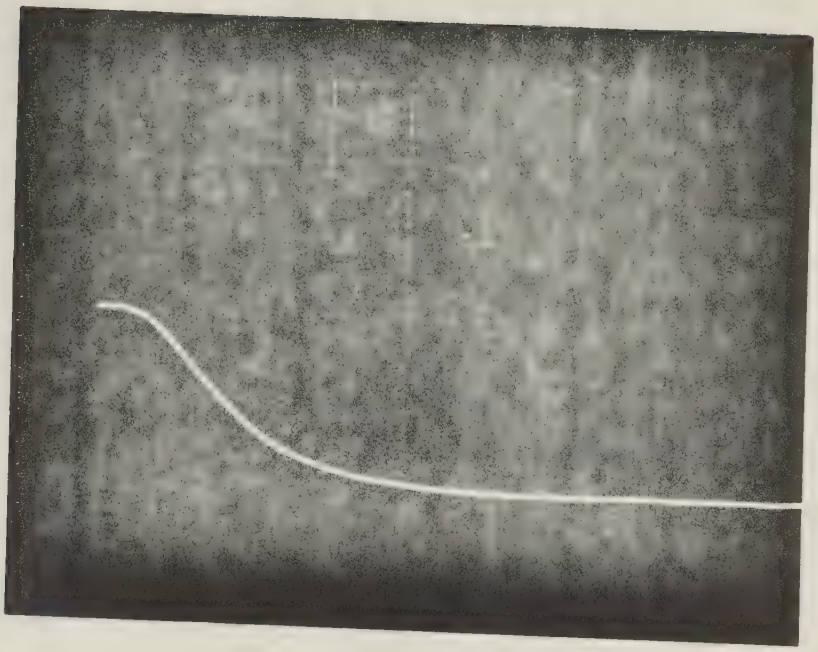

Sensitivity: 0.5 mv/sec 5ms/cm

Flat Bladed Thruster

Propellant: 3 micron iron carbonyl

V = 14 kV I_o = 102 na

T = 234 μN $\dot{M}$ = 22.6×10^{-6} kg/sec

$\langle u_{ex} \rangle$ = 10.5 m/sec I_{sp} = 1.07 sec

$\left\langle \frac{q}{m} \right\rangle = 4.6 \times 10^{-3}$ coul/kg $\left\langle \frac{q}{m}^{1/2} \right\rangle^2 = 3.94 \times 10^{-3}$ coul/kg

$\left(\frac{q}{m} \right)_{max} = 6.18 \times 10^{-2}$ coul/kg η_u = 85 %

Fig. 4.12 Oscillogram of Time of Flight Trace

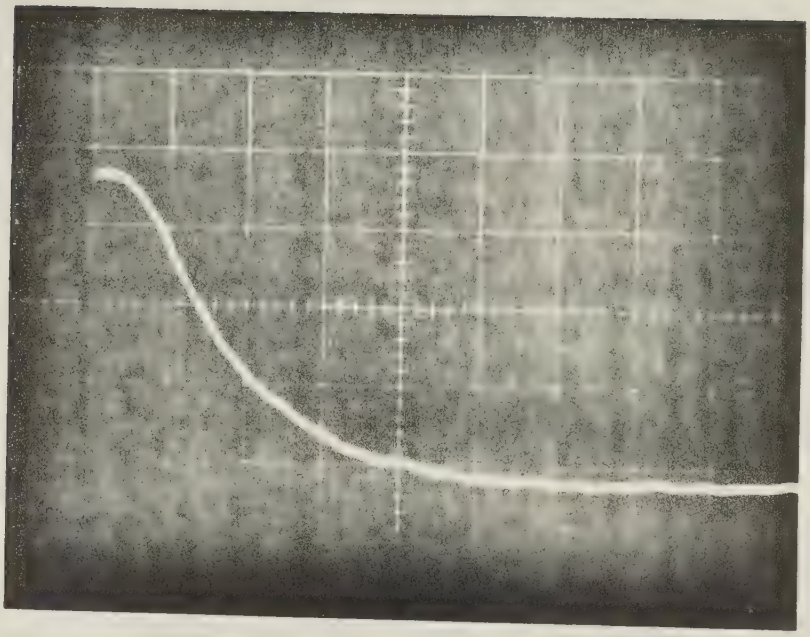

Sensitivity: 0.2 mv/cm 10 ms/cm

Flat Bladed Thruster

Propellant: 10 micron iron carbonyl

V = 14 kV I_o = 74 na

T = 350 μN $\dot{M} = 75 \times 10^{-6}$ kg/sec

$\langle u_{ex} \rangle$ = 4.67 m/sec I_{sp} = 0.48 sec

$\left\langle \frac{q}{m} \right\rangle = 0.99 \times 10^{-3}$ coul/kg $\left\langle \frac{q}{m}^{1/2} \right\rangle^2 = 0.78 \times 10^{-3}$ coul/kg

$\left(\frac{q}{m} \right)_{max} = 2.41 \times 10^{-2}$ coul/kg η_u = 79 %

Fig. 4.13 Oscillogram of Time of Flight Trace

MBT. A further decrease in charge-to-mass ratio was experienced due to the increase in particle diameter as in Fig. 4.13

It is extremely difficult to estimate accurately experimental error involved in this work. The difficulty can be appreciated if one considers the main sources of experimental error. They are the accuracy of the numerical integration, the accuracy attained in measur- the times t_o and t_f and the fact that the dispersive character of the beam does not demand that the distance travelled to the detector by each subbeam be equal. The only true test of experimental error would be a comparison with a direct mechanical measurement of the thrust. Some researchers in liquid colloid propulsion claim agreement within 10% (131).

It is clear from the results presented that the thrusting device leaves much to be desired in so far as the specific impulse is concerned. It has been confirmed that the charge-to-mass ratio and specific impulse increase with decreasing particle radius. It appears that mass flow rate is a function of particle radius. Furthermore, it appears that mass flow rate increases with particle radius resulting in a decrease in specific impulse. Thrust appears to have a weak dependence on particle radius. One might also observe that the beam distribution efficiency is a function of accelerating electrode configuration. Since charge-to-mass ratio is a function of accelerating electrode configuration it is reasonable to expect the same of beam distribution efficiency. Finally, it is worthwhile repeating that the close correlation of the data of Fig. 4.7 and Fig. 4.8 and of Fig. 4.9 and Fig. 4.10 attest to the reliability of the time of flight technique.

5. SUGGESTIONS FOR FUTURE RESEARCH

Suggestions for future research may be presented in the most helpful fashion by considering the following three categories:

i) the thruster

ii) parametric analysis

iii) propellant size and composition

5.1 The Thruster

The purpose of the thruster is to charge individual particles as highly as possible, accelerate them, focus them and guide them to the exit aperture. In order to charge particles as highly as possible it will be necessary to charge them as near to the field ion emission limit as possible. Hence intense local electric fields will be necessary. One method of constructing electrodes capable of producing such intense local electric fields lies in the electro-chemical etching of thin walled metal tubing (0.001 inch wall thickness). Attempts were made to construct electrodes in this manner, however the product was not suitable for use at the time of the writing of this thesis. Thin walled tubing is commercially available from Electronic Space Products, Los Angeles, California. It would appear that commercially available razor blades and needles are not sharp enough to produce desired electric field strengths.

An effective solid particle thruster would, in all probability require a particle feed system. A feed system would allow particles to deagglomerate so that the beam would be comprised of smaller diameter particles having high charge-to-mass ratio and hence high specific

impulse. A sophisticated feed system might employ feedback control. For example, it might be possible to regulate the particle feed rate by monitoring the propellant beam current. The large size of solid particles as compared to ions demands that the methods of focusing and guiding be electrostatic. Literature on the subject is readily available[132],[133].

5.2 Parametric Analysis

In addition to improvements in the thruster, a parametric analysis is essential to the development of a suitable device. Knowledge of the dependence of mass flow rate on beam current would provide the researcher with the thrust per ampere of beam current for a given exhaust velocity. The manner in which all parameters vary with particle radius would be very enlightening. It has been shown that charge-to-mass ratio and specific impulse increase with decreasing particle radius. However, the behavior of thrust, mass flow rate and beam current as a function of particle radius is still unknown. The relationship between the applied electric field necessary to accelerate particles of a given radius will also be interesting. During the experiments carried out, it was observed that in attempting to accelerate particles of different radii, particles with smaller radii required a larger applied electric field to agitate them than did those of larger radii. Parametric tests involving particle radius will not be easy because of the added complication of the interparticle London - Van der Waals forces in the submicron range and the accompanying agglomeration problem.

5.3 Propellant Size and Composition

As indicated in the previous section, propellant size is a very important parameter. As particle size decreases, London - Van der Waals interparticle forces tend to cause agglomeration problems. Obtaining spherical particles in the submicron range is very difficult. In fact, if deagglomeration can be accomplished, hollow particles should prove interesting, as they are capable of providing higher charge-to-mass ratios.

The other important factor influencing particle charging is electrical conductivity. Basic tests performed during the course of the experiments indicated that propellants derived from materials of high electrical conductivity are probably the best. While individual particles of semiconducting or insulating material may be charged highly, it does not follow that large groups of particles of the same material will be highly charged. Finally a detailed study of the physical processes involved in particle charging such as the time and contact area necessary to charge a given particle might lead to improved methods of charging and material selection.

BIBLIOGRAPHY

1. Goddard, Esther C. and Pendray, G.E., editors. The Papers of Robert H. Goddard. Volume 2, p. 690, McGraw Hill Book Co., New York, 1970.

2. Oberth, H. Wege zur Raumschiffahrt. Edwards Brothers Book Co., Ann Arbor, Michigan, 1945.

3. von Braun, W. and Ordway, F.I. History of Rocketry and Space Travel. T.Y. Crowell Co., New York, 1966.

4. Stoiko, M. Soviet Rocketry. Chapter 2, p. 21. Holt, Rinehart and Winston Book Co., New York, 1970.

5. Op. Cit. (2)

6. Seifert, H.S. et al. The Physics of Rockets. American Journal of Physics, Vol. 15, No. 1, Jan.-Feb., 1947.

7. Cybulski, R.J. et al. Results from SERT I Ion Rocket Flight Test. NASA Tn D - 2718, 1965.

8. Hunter, R.E. et al. Cesium Contact Ion Microthruster Experiment Aboard Applications Technology Satellite (ATS) IV. Journal of Spacecraft and Rockets, Vol. 6, No. 3, pp. 368-370, Sept. 1969.

9. Black, W.L. et al. An Electromagnetic Attitude Control System for a Synchronous Satellite. Journal of Spacecraft and Rockets, Vol. 8, No. 7, July 1971.

10. Nieserding, W.C. et al. Comparative In-Flight Thrust Measurements of the SERT II Thruster. Paper 70-1124, AIAA 3rd Electric Propulsion Conference 1970.

11. Goldman, R.G. et al. Description of the SERT II Spacecraft and Mission. Paper 70-1124. AIAA 3rd Electric Propulsion Conference 1970.

12. Kerslake, W.R. et al. Flight and Ground Performance of the SERT II Thruster. Paper 70-1125. AIAA 3rd Electric Propulsion Conference 1970.

13. Rappaport, P. Photovoltaic Power. Journal of Spacecraft and Rockets, Vol. 4, No. 7, July 1967.

14. Shaw, G.A.D. and Falconer, J.C. Space Electric Rocket Test Solar Array Power System. Paper 70-1133. AIAA 3rd Electric Propulsion Conference 1970.

15. Oman, H. High-Voltage Solar Array For Ion Engines. Paper 70-1138. AIAA 8th Electric Propulsion Conference. 1970.

16. Goodyer, E.M. Principles of Spaceflight Propulsion. Chapters 2 and 3. Permgon Press, Toronto, 1970.

17. Hammit, A.G. A Simplified Theory for Chemical Rockets. Astronautica Acta, Vol. 14, No. 1, p. 57.

18. Sutton, G.P. Rocket Propulsion Elements. Chapter 4. John Wiley and Sons, Inc., New York, 1967.

19. Seifert, H.S. editor. Space Technology. Chapter 14. John Wiley and Sons, Inc., New York, 1959.

20. Moeckel, W.E. Propulsion Systems for Manned Exploration of the Solar System. Astronautics and Aeronautics, Vol. 7, August 1969.

21. Cooper, R.S. Prospects for Advanced High-Thrust Nuclear Propulsion. Astronautics and Aeronautics, Vol. 4, Jan. 1966.

22. Bussard, R.W. and De Lauer, R.D. Nuclear Rocket Propulsion. McGraw Hill Book Co., New York, 1958.

23. Op. Cit. (20)

24. Openshaw, P.R. Electric Propulsion Development. The Aeronautical Journal of the Royal Aeronautical Society, Vol. 73, Dec. 1969.

25. Ellion, M.E. et al. Survey of Reaction Control Systems for Synchronous Satellites. Society of Automotive Engineers, Aerospace Systems Conference, 1967.

26. Moletor, J.H. Application of Ion Thrust Motors in Attitude and Position Control of Satellites in Physics and Technology of Ion Motors. Edited by F.E. Marble and J. Surugue. Gordon and Breach Science Publishers, New York, 1966.

27. Boucher, R.A. Electrical Propulsion for Control of Stationary Satellites. Journal of Spacecraft and Rockets, Vol. 1, No. 2, April 1964.

28. Molitor, J.H. and Kaplan, M.K. Optimization of Ion Engine Control Systems for Synchronous Satellites. Journal of Spacecraft and Rockets, Vol. 1, No. 5, Oct. 1964.

29. Loc. cit. (13)

30. Op. cit. (19), Low Thrust Flight, Chapter 9.

31. Op. cit. (19), Low Thrust Flight, Chapter 10.

32. Sears, F.W. Thermodynamics, Chapter 5. Addison Wesley, Resding Massachusetts, U.S.A., 1950.

33. Jahn, R.G. Physics of Electric Propulsion. McGraw Hill Book Co., New York, 1968.

34. Op. cit. (25)

35.. Jackson, F.A. et al. An Operational Electrothermal Propulsion System for Spacecraft Reaction Control, Paper 66-213. AIAA 5th Electric Propulsion Conference, 1966.

36. Murch, C.K. and Krieve, W.F. Electrothermal Thruster Performance with Biowaste Propellants. Paper 70-1161. AIAA 8th Electric Propulsion Conference, 1970.

37. Halbach, C.R. and Yoshida, R.V. Development of a Biowaste Resistojet. Paper 70-1133. AIAA 8th Electric Propulsion Conference, 1970.

38. Wallner, L.E. and Czika, J. Arcjet Thruster for Space Propulsion. NASA TND - 2868. January 1965.

39. Proceedings of the Third Symposium on Advanced Propulsion Concepts. Vol. 1. Gordon and Breach Science Publishers, New York, 1963.

40. Proceedings of the Fourth Symposium on Advanced Propulsion Concepts. Gordon and Breach Science Publishers, New York, 1966.

41. Stuhlinger, E. Electric Propulsion Development. Academic Press, New York, 1963.

42. Kash, S.W. Plasma Acceleration. Stanford University Press. Stanford, California. 1960.

43. Ducati, A.C. et al. Experimental Results in High Specific Impulse Thermionic Acceleration. AIAA Journal, Vol. 2, No. 8. August 1964.

44. Clark, K.E. et al. Quasi-Steady Magnetoplasmadynamic Arc Characteristics. Paper 70-1095. AIAA 8th Electric Propulsion Conference, 1970.

45. Clark, K.E. and Jahn, R.G. The Magnetoplasmadynamic Arcjet Astronautica Acta. Vol. 13, No. 4, 1967.

46. Nerheim, N.M. and Kelly, A.J. A critical Review of the State-of-the-Art of the MPD Thruster. Paper 67-688. AIAA Electric Propulsion and Plasmadynamics Conference, 1967.

47. Bohn, W.L. and Peters, T.H. Activities in the Field of MPD Propulsion in Germany. Paper 69-279. AIAA 7th Electric Propulsion Conference, March 1969.

48. Fanchiotti, A. et al Research Program on Electric Propulsion at the University of Rome. Paper 70-1086. AIAA 8th Electric Propulsion Conference, 1970.

49. Hoell, J.M. et al. Velocity and Thrust Measurements in a Quasi-Steady MPD Thruster. Paper 70-1080. AIAA 8th Electric Propulsion Conference, 1970.

50. Michels, J.C. and Sigman, D.R. Exhaust Characteristics of a Megawatt Nitrogen MPD - Arc Thruster. Paper 70-1081. AIAA 8th Electric Propulsion Conference, 1970.

51. Malliaris, A.C. and John, R.R. OUtstanding Problems Regarding the Feasibility of a Repetitively Pulsed MPD Propulsion System. Paper 70-1093. AIAA 8th Electric Propulsion Conference, 1970.

52. Le Grives, E. French Research on Electric Propulsion: Present Status and Prospects for Development. Journal of Spacecraft and Rockets. Vol. 5, No. 7, July 1968.

53. Ibid (52)

54. Forrester, A.T. and Kuskevics, G. (editors) Ion Propulsion. AIAA Selected Reprints, Vol. III. American Institute of Aeronautics and Astronautics, Special Publications Department.

55. Marble, F.E. and Surugeu, J. Physics and Technology of Ion Motors. Gordon and Breach Science Publishers. New York, 1966.

56. Langmiur, D.B., Stuhlinger, E. and Sellen, J.M. Electrostatic Propulsion. Academic Press. New York, 1961.

57. Stuhlinger, E. Electric Propulsion Development. Academic Press. New York, 1963.

58. Loh, W.H.T. Jet, Rocket, Nuclear, Ion and Electric Propulsion: Theory and Design. Springer-Verlay. New York, 1968.

59. Brewer, G.R. Ion Propulsion. Gordon and Breach Science Publishers. New York, 1970. Chapter 3, p. 61.

60. Ibid (59)

61. Cranberg, L. The Initiation of Electrical Breakdown in Vacuum. Journal of Applied Physics, Vol. 23, No. 5, May 1952.

62. Mickelsen, W.R. and Kaufman, H.R. Status of Electrostatic Thrusters for Space Propulsion. NASA TND - 2172. May 1964.

63. Currie, M.R. and Molitor, J.H. Ion Propulsion: A Key to Space Exploration. IEEF Student Journal, Jan. 1968.

64. Op. Cit. (12)

65. King, H.J. and Poeschel, R.L. A 30-Cm. Diameter, Low Specific Impulse, Hollow Cathode Mercury Thruster. Paper 70-1099. AIAA 8th Electric Propulsion Conference, 1970.

66. Loeb, H.W. State of the Art and Recent Developments of the Radio Frequency Ion Motor. Paper 69-285. AIAA 7th Electric Propulsion Conference, 1969.

67. Loeb, H.W. Les fusees ioniques a radio-frequence. 9th Congres International Aeronautique, June 1969.

68. Loeb, H.W. Recent Works on Radio Frequency Ion Thrusters. Paper 70-1102. AIAA 8th Electric Propulsion Conference, 1970.

69. Ibid (68)

70. Meckel, B.B. High Specific Impulse Thrust by Sputter-Ejection of Neutral Atoms. Astronautica Acta, Vol. 12, No. 3, 1966.

71. Wehner, G.K. Comments on "High Specific Impulse Thrust by Sputter Ejection of Neutral Atoms". Astronautica Acta. Vol. 14. 1968. pp. 65-68.

72. Cheng, S. Sputtering as an Advanced Concept of Space Propulsion. Astronautica Acta, Vol. 12, No. 4, 1966.

73. von Hoerner, S. The General Limits of Space Travel The Search for Extraterrestrial Life. p. 144, W.A. Benjamin, Inc., New York, 1963.

74. Glasstone, S. Sourcebook on Space Sciences. D. Van Nostrand Co., Inc., New York, 1965.

75. Krause, H.G.L. Relatistiche Raketenmechanik. Astronautica Acta, Vol. II, No. 2, p. 30.

76. Sanger, E. Zur Flugmechanik der Photonenraketen. Astronautica Acta, Vol. III, No. 2.

77. Krohn, V.E. Liquid Metal Droplets for Heavy Particle Propulsion. In reference (56) p. 73.

78. Krohn, V.E. Glycerol Droplets for Electrostatic Propulsion. In reference (57) p. 435.

79. Resnick, R. and Halliday, D. Physics for Students of Science and Engineering, Part II, Second Edition, John Wiley and Sons, New York, 1960, Chapter 28.

80. Hendricks, C.D. et al. Photomicrography of Electrically Sprayed Heavy Particles. AIAA Journal, Vol. 2, No. 4, April 1964.

81. Carson, R.S. and Hendricks, C.D. Natural Pulsations in Electrical Spraying of Liquids. AIAA Journal, Vol. 3, No. 6, June 1965.

82. Pfeifer, R.J. and Hendricks, C.D. Parametric Studies of Electrohydrodynamic Spraying. AIAA Jounal, Vol. 6, No. 3, March 1968.

83. Hogan, J.J. Parameters Influencing the Charge-to-Mass Ratio of Electrically Sprayed Liquid Particles. Ph.D. Thesis, University of Illinois, 1964.

84. Beynon, J.C. et al. Present Status of Colloid Microthruster Technology. Paper 67-531, AIAA Electric Propulsion and Plasmadynamics Conference, Sept. 1967.

85. Hunter, R.E. The Quest for Heavy Particle Propulsion. In ref. (39) p. 19.

86. Cohen, E. STL Heavy Particle Propulsion Program. In ref. (39) p. 35.

87. Hendricks, C.D. Physics of Charged Colloidal Particles and the Technology of Their Production. In ref. (45) p. 139.

88. Hendricks, C.D. Colloid Propulsion: State of the Art and Review of Current Research. In ref. (31) p. 91.

89. Hunter, R.E. and Wineland, S.H. Charged Colloid Generation Research. Space Electronics Symposium. Los Angeles, California. May 1965.

90. Hunter, R.E. and Wineland, S.H. Exploration of the Feasibility of an Electrodless Colloid Thruster Concept. Proceedings of the Sixth International Symposium on Space Technology and Science, Tokyo, 1965.

91. Cohen, E. Research on Charged Colloid Generation. APL-TDR 64-75. Wright-Patterson Air Force Base 1964.

92. Gignoux, D. et al. Charged Colloid Generating System for Electric Propulsion. NASA CR-54049. Oct. 1963.

93. Gignoux, D. and Anton, H. Investigation of Charged Colloid Beams for Electrostatic Propulsion. NASA CR-54702. May 1967.

94. Cohen, E. and Huberman, M.N. Research on Charged Particle Electrostatic Thrusters. AFAPL-TR-66-94. Wright Patterson Air Force Base, 1966.

95. Huberman, M.N. and Cohen, E. Research on Charged Particle Electrostatic Thrusters. AFAPL-TR-67-115. Wright Patterson Air Force Base. 1967.

96. Kidd, P.W. Parametric Studies with a Single-Needle Colloid Thruster. Journal of Spacecraft and Rockets, Vol. 5, No. 9. Sept. 1968.

97. Cohen, E. et al. Colloid Thruster Technology. '69 Proceedings of the Eighth International Symposium on Space Technology and Science. Tokyo, 1969.

98. Derel, J. et al Focusing and Deflection of Heavy Charged Particle Beams. AIAA 7th Electric Propulsion Conference. March 1969. Paper AIAA 69-283.

99. Makin, B. and Bright, A.W. Determination of Charge/Mass and Thrust from a Positively Charged Colloidal Beam. AIAA Journal, Vol. 7, No. 10, Oct. 1969.

100. Zafran, S. and Kemp, R.F. Colloid Microthruster Test Stand. Journal of Spacecraft and Rockets, Vol. 6, No. 10. Oct. 1969.

101. Zafran, S. and Beynon, J.C. Colloid Microthruster System Life Test. AIAA 8th Electric Propulsion Conference.

AIAA Paper 70-1110. Sept. 1970.

102. Geis, J.W. and Turner, J.M. Beam Distribution Effects on Colloid Engine Performance. AIAA 3th Electric Propulsion Conference. AIAA Paper 70-1109. Sept. 1970.

103. Huberman, M.N. Measurement of Energy Dissipated in the Electrostatic Spraying Process. Journal of Applied Physics, Vol. 41, No. 2, Feb. 1970.

104. Kidd, P.W. et al. A Comparison of Time-of-Flight and Thrust Stand Data For Two 100 lb Colloid Thrusters. AIAA 8th Electric Propulsion Conference. AIAA Paper 70-1114. Sept. 1970.

105. Stark, K.W. et al. Research and Development in Needle and Slit Colloid Thrusters. NASA - TMX 63426. November 1968.

106. Derel, J. et al. Analytical Study of Colloid Annular Thrusters. AIAA 8th Electric Propulsion Conference. AIAA Paper 70-1113. Sept. 1970.

107. Yahiku, A. et al. Experimental Study of Colloid Annular Thrusters. AIAA 8th Electric Propulsion Conference. AIAA Paper 70-1112. Sept. 1970.

108. Derel, J. et al. Research and Development of a Charged-Particle Bipolar Thruster. AIAA Journal, Vol. 7, No. 3. March 1969.

109. Bunson, W.C. and Herren, P.C. Alternating Current Operation of a Colloid Source. AIAA 5th Propulsion Joint Specialist Conference. AIAA Paper 69-495. June 1969.

110. Cox, A.L. Condensation Colloid Propellants for Electrostatic Propulsion (In ref. 30) p. 53.

111. Norgren, C.T. Onboard Colloidal Particle Generator for Electrostatic Engines. In ref. (47) p. 407.

112. Jamba, D.M. Heavy Particle Source. ARS Electric Propulsion Conference. March 1962. ARS Paper 2399-62.

113. Jamba, D.M. Charging and Removal of Surface-Condensed Particles for Colloid Propulsion. AIAA Electric Propulsion Conference. March 1963. AIAA Paper 63053-63.

114. Norgren, C.T. and Goldin, O.S. Experimental Analysis of the Exhaust Beam from a Colloid Thruster. AIAA

Fourth Electric Propulsion Conference. Sept. 1964. AIAA Paper 64-674.

115. Goldin, D.S. and Norgren, C.T. Thrust Measurements of Colloid Particles as an Indication of Particle Size and Thruster Operation. AIAA Electric Propulsion Conference. March 1963. AIAA Paper 63-050.

116. Singer, S. et al. An Experimental Study of Colloidal Propulsion using Sub-Micron Solid Particles. AIAA Electric Propulsion Conference. March 1963. AIAA Paper 63-052.

117. Harris, S.P. Research on Charged Colloidal Particle Propulsion. AIAA 2nd Aerospace Sciences Meeting. January 1965. AIAA Paper 65-72.

118. Harris, S.P. and Farber, M. Development of a Solid Charged Colloidal Particle Thruster. AIAA Fifth Electric Propulsion Conference. March 1966. AIAA Paper 66-255.

119. Peterson, C.R. Feeding, Deagglomerating and Charging Solid Particles for Colloid Propulsion. Ph.D. Thesis M.I.T. January 1963.

120. Schertler, R.J. and Norgren, C.T. Experimental Investigation of Charging Submicron Carbon Powder for Colloidal Particle Thrusters. NASA TN D-3657. July 1966.

121. Norgren, C.T. et al. Colloid Thruster Beam Analysis: Design and Operation of a Suitable Quadrupole Mass Filter. TN D-3036. 1965.

122. Muller, E.W. Field Desorption. Phys. Rev. Vol. 102, No. 3. pp. 618-624. 1956.

123. Muller, E.W. Direct Observation of Crystal Imperfections by Field Ion Microscopy. pp. 77-99. Interscience Publishers. New York, 1962.

124. Hendricks, C.D. Informal discussion with F.S. Chute and F.E. Vermeulen.

125. Cho, A.Y.H. Contact Charging of Micron Sized Particles in Intense Electric Fields. Journal Appl. Phys., Vol. 35, No. 9. Sept. 1964.

126. Smythe, W.R. Static and Dynamic Electricity. McGraw Hill

Third Edition. New York, 1968. P. 131

127. Ibid (124)

128. Mueller, E.W. and Tsong, T.T. Field Ion Microscopy Principles and Applications. American Elsevier Publishing Company, Inc., New York, 1969. p. 72.

129. Hamaker, H.C. The London-Van der Waals Attraction Between Spherical Particles. Physica IV, No. 10. Nov. 1937. p. 1058.

130. Ibid (105)

131. Kidd, P.W. et al. A Comparison of Time of Flight and Thrust Stand Data for Two 100μlb Colloid Thrusters. Paper 70- 1114. AIAA 8th Electric Propulsion Conference 1970.

132. Kino, G.S. and Harker, K.J. Space Charge Theory for Ion Beams, in reference (41), p. 175.

133. Kirstein, P., Kino, G.S. and Waters, W.E. Space Charge Flow, McGraw Hill, New York, 1967.